Gravitational Camera: A Thought Experiment

Mostafa 'Neo' Mohsenvand*
MIT Media Lab, Massachusetts Institute of Technology, Cambridge, Massachusetts 02139, USA
(Dated: 18 November 2026)

We analyze an idealized gravitational camera: an array of point sensors, each measuring the electric and magnetic parts of the tidal tensor, $\mathcal{E}_{ij}$ and $\mathcal{B}_{ij}$, with arbitrarily small noise, and derive within linearized gravity what it can image in three regimes. In the near zone, imaging is the downward continuation of a harmonic potential; a Wiener-filter analysis gives an angular resolution $\Delta\theta = 4.43/q_c$ with $q_c \simeq \ln \mathrm{SNR}$ and an information content growing as $(\ln \mathrm{SNR})^3$, while positivity of mass gives power-law resolution of sparse scenes. The field at one time fixes only the harmonic moments of the density. The commutator $[Q_h, \dot{Q}_g] = i\hbar \int \rho \, \nabla h \cdot \nabla g \, dV$, realized classically by thermal fluctuations or by the energy an impulsive tide adds, fixes the whole density through Calderón's exponential solutions, whereas a black hole returns only its mass, spin and Hawking temperature. Radiation from slow sources is unresolved. For thermal emission, Hawking's absorption coefficient $\alpha = 16\pi G\eta/c^3$, with η the shear friction at terahertz frequencies, gives the glow of matter; we bound it for any material by a sum rule and evaluate it for real materials and the Earth. Writing one reading as the complex symmetric matrix $\mathcal{W} = \mathcal{E} + i\mathcal{B}$, we show that its ten components are four invariants, an orientation and the velocity of its rest frame; this gives a sensor's own velocity, a test for relative motion, the exact state of a moving mass, the separation of up to four crossing waves, and a one-point test of the speed and polarization of metric waves. The same methods describe a binary from the near zone to the wave zone, the Galaxy at millihertz frequencies, and a primordial graviton background at 0.905 K.

I. INTRODUCTION

Gravitational waves were first detected in 2015 by LIGO, an instrument four kilometres long that reports a single number at each instant. In the language of photography it is a camera with one pixel. This paper takes that language seriously. We suppose that such detectors could be made as small and as sensitive as we please, place one at every pixel of a sensor, and ask what picture results when the sensor is pointed at an ordinary scene: a room, a street, the ground beneath our feet.

The question has an answer because gravity is simple where it is weak. Every form of matter and energy produces it, in proportion to its energy (and, for fast motion and for light, its momentum and stress too) whatever it is made of, and nothing shields it. The same two facts that make gravity so hard to detect make a gravitational camera easy to reason about: we need only the linear theory, and the stress and motion of the matter in view.

Our results are these.

- A pixel measures the *tidal field*, ten numbers at each point (Section II). One component of it, which is what an interferometer reads, cannot tell a passing wave from the pull of a nearby object, and for everyday scenes the pull dominates.
- What the camera sees falls into three regimes, set by how far the source is compared with the wavelength it would radiate (Section III).
- In the near field the camera sees mass itself, moving or still, through any obstacle. Its blur is a fixed fraction of the distance, and improves only with the logarithm of the sensitivity, for clocks and accelerometers as much as for tidal pixels; but mass is never negative, and a scene of a few bodies is measured far more sharply than it can be drawn. A body's steady pull hides its interior; its thermal tremor, at a known temperature, reveals it, and a push from outside does the same at any temperature (Section IV).
- In the waves radiated by moving bodies, a compact body moving slowly is smaller than its own wavelength and appears as a point (Section V).
- In thermal radiation the camera can be as sharp as an infrared camera. Matter is transparent, and glows in proportion to its internal friction and a power of its temperature, up to a limit that a sum rule sets for every material (Section VI).
- Matter cannot act as a useful lens, a mirror or a screen for gravitational waves, so the image must be computed from what the pixels record (Section VII).
- One pixel measures far more than a sensor of light at a point, and a few pixels more still (Section VIII). A pixel's ten numbers are four invariants, the orientation of the field and the velocity of its rest frame, so it reads its own velocity through an unknown scene and detects motion within it whatever its own. It tells whether its field could come from a single round body or a single wave, reads a moving body's position, velocity and mass exactly at any speed, separates up to four waves crossing it (a count that one theorem gives for a field of any spin), ranges a wave source, sees moving bodies where they are now

* mmv@mit.edu

rather than where they were, and reads the speed and all six polarizations of a wave in one reading. Its magnetic part separates a wave from the pull of nearby objects at a fixed cost in noise, and supplies the one scale the electric part lacks, so a single pixel ranges a moving mass; a few pixels side by side measure distance from how the field varies.

- The expected number of gravitons that arrive sets what there is to be seen: a first image, with its budget, and the reason why nothing made of matter could catch it (Section IX); and a summary of what the camera can do that light cannot (Section X).

- On the scale of the sky (Section XI): the field of two black holes in orbit changes, at a sixth of their wavelength, from the pull of two bodies to the waves of one; an explosion is invisible unless it is lopsided, and then leaves space permanently stretched; the Galaxy's centre, hidden from light by dust, is the brightest part of the millihertz sky; and if the Big Bang was ever hot enough to make gravitons in equilibrium, the whole sky glows at 0.905 K, shares the large spots of the microwave background, and has nothing dark on it but black holes.

- What the field outside a body determines of its interior is one subject, gravitational hair (Section XII). The field at one time gives the harmonic part of the body's mass and no more; the field at two times gives all of it, through the same logarithm; and a black hole at rest yields seven numbers to the first measurement and only its temperature to the second. The second measurement can be a tide applied from outside, followed by a weighing: the body's weight alone, read after enough such tides, gives all of its density, which is what remains in classical physics of the holography argued for quantum gravity.

Figure 1 shows where this leads. An observer stands on the night side of the Earth and looks down. In light there is only dark ground. In thermal gravitational radiation the planet is a set of glowing shells, and beyond it, shining straight through, is the core of the Sun.

a. What is already known. The ingredients exist separately. Gravity sensors already map buried structures by their pull [1]; small gravimeters are being made cheap enough to be set out as the pixels of an imager [2, 3], and a patent calls an array of them a gravity camera [4]. The designers of LIGO worked out how strongly a walking person disturbs it [5], and seismologists have recorded the gravitational signal of an earthquake arriving before the shaking [6]. Gravity gradiometry has been proposed for imaging the contents of cargo containers [7] and for locating objects under water [8]. Networks of pulsars are analysed as imaging telescopes for gravitational waves from the distant universe [9], the gravitational radiation of the Sun has been calculated [10, 11], and the tidal field has been visualised around black holes and simple sources [12]. Much of the algebra of a single reading is known in other forms: the frame in which the electric and magnetic parts share their axes, the principal observer, has been built from the curvature's invariants [13]; the cross product of the two parts is the curvature's super-Poynting vector [14]; curvature can be measured operationally with test bodies and clocks [15]; resonant spheres read five components of the tide at one place [16]; and the polarization of a harmonic wave, as a detector of both parts would record it at one place, has been drawn as four points on the sky [17]. What we add is a single account of what an ideal observer of the tidal field would record of ordinary surroundings, followed from the near field to the radiation field and the thermal glow, with the limits of each regime stated.

II. WHAT A PIXEL MEASURES

A freely falling observer feels no gravitational field at their own position. What remains measurable is how the field differs between nearby points: the tidal field. For an observer at rest, with proper time t and coordinates $x^0 = ct$, x^i, it is the symmetric tensor

$$\mathcal{E}_{ij} = c^2 R_{0i0j}, \tag{1}$$

where R is the Riemann curvature tensor, with signature $-+++$ and $R^{\alpha}{}_{\beta\gamma\delta} = \partial_\gamma \Gamma^{\alpha}_{\beta\delta} - \dots$. The factor c^2 gives $\mathcal{E}_{ij}$ the units s^{-2}. Two free particles separated by a small vector ξ^i accelerate relative to one another by

$$\frac{\mathrm{d}^2 \xi^i}{\mathrm{d}t^2} = -\mathcal{E}_{ij}\, \xi^j. \tag{2}$$

Figure 2 shows what this does to a ring of free particles, and Fig. 3 the field around masses and in a wave.

Two limits of Eq. (1) matter here. Close to slowly moving matter, the tidal field is the second derivative of the Newtonian potential Φ:

$$\mathcal{E}_{ij} = \partial_i \partial_j \Phi. \tag{3}$$

For a body of mass M at distance r its size is $2GM/r^3$ along the line to the body. Far from its source, in a gravitational wave of strain h^{TT}_{ij} (in the transverse traceless gauge),

$$\mathcal{E}_{ij} = -\tfrac{1}{2}\, \partial_t^2 h^{\mathrm{TT}}_{ij}. \tag{4}$$

An interferometer such as LIGO reads one component of $\mathcal{E}_{ij}$, integrated twice in time, as the fractional change h in the length of its arms.

Such a detector therefore responds to the ordinary pull of a passing lorry and to a wave from a distant collision, and nothing in its one reading tells them apart. The pull is not small. A person of 70 kg standing one metre away produces $\mathcal{E} \approx 9 \times 10^{-9}\,\mathrm{s}^{-2}$. If they sway by five centimetres once a second, the field changes by $3\,\delta r/r$ of itself, about $1.4 \times 10^{-9}\,\mathrm{s}^{-2}$, which a detector reads as a

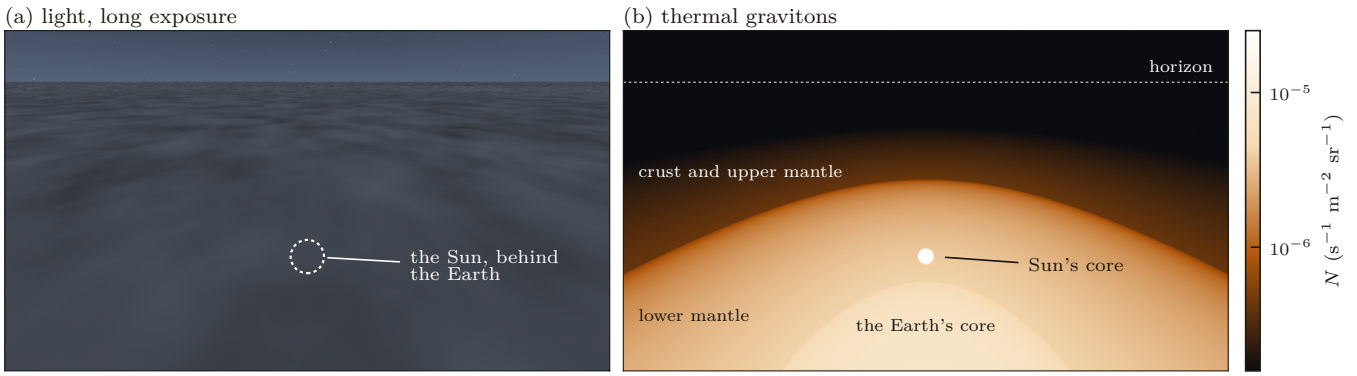


FIG. 1. The Sun at midnight, computed. An observer at latitude 40° north looks north and down, 33° below the horizon, at local midnight, with the same camera, 86° from top to bottom, in both panels. (a) Ordinary light, exposed long enough to show the ground; the dashed circle marks where the Sun lies, behind the planet. (b) Thermal gravitational radiation: the expected number radiance $N(\hat{n})$ of Eq. (69), on a logarithmic scale. The ground is transparent. Lines of sight just below the horizon cross only the crust and upper mantle and are faint; steeper ones cross the hotter lower mantle, and those within 33° of straight down, at the foot of the picture, the core (Fig. 31). The Sun's core, 50° below the horizon, is smaller than a pixel; its flux, under one graviton per square metre per second, is spread over a spot a few pixels across, far brighter than the top of the scale. Section IX gives the model and its assumptions.

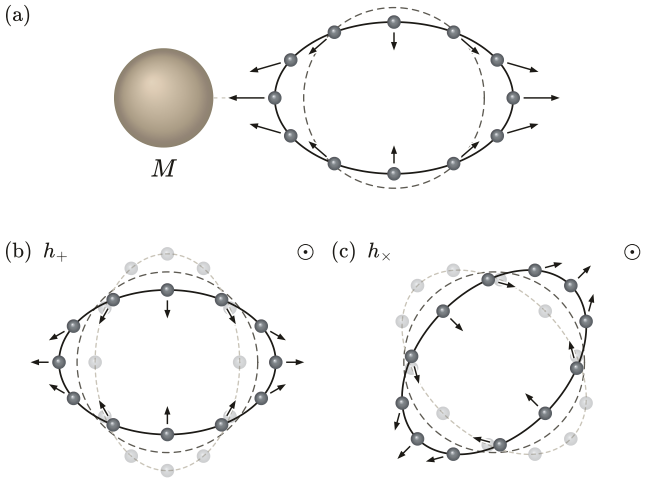


FIG. 2. What a pixel measures: a ring of twelve free test masses, distorted by the tidal field, Eq. (2), with each arrow the displacement of its mass and the dashed circle the ring undisturbed; the distortions are exaggerated. (a) Beside a mass M, the ring is stretched along the line to the mass and squeezed across it, exactly twice as strongly along as across. (b), (c) In a gravitational wave travelling toward the reader (⊙), of polarization h_+ and $h_\times$: the ring is stretched and squeezed equally along two perpendicular directions, which change places every half cycle (the pale ring), and the two polarizations differ by a turn of 45°. The planet's size and distance are schematic. A pixel records the size and orientation of this distortion.

strain $h = 2\,\delta\mathcal{E}/\omega^2 \approx 7 \times 10^{-11}$, where $\omega = 2\pi f$ is the angular frequency, here $2\pi\,\mathrm{s}^{-1}$. The waves LIGO detects have strains near 10^{-21}. This is why people and vehicles must be kept away from its mirrors [5]. The signal that the observatory removes as contamination is the one that a near-field camera records.

An ideal pixel records all of $\mathcal{E}_{ij}$, and also its magnetic counterpart

$$\mathcal{B}_{ij} = \tfrac{1}{2}\, c^2\, \epsilon_{ipq}\, R_{pqj0}, \tag{5}$$

with $\epsilon_{123} = +1$, which describes how the field twists the axes of nearby gyroscopes relative to one another [12]. In vacuum both are symmetric and trace-free, so a pixel yields ten numbers at each instant; with this normalization the two are equal in size in a plane wave, and $\mathcal{B}_{ij}$ is $\mathcal{E}_{ij}$ turned by 45° about the direction of travel. Inside matter the Ricci part of the curvature adds local information that a pixel in vacuum does not see: the trace $\mathrm{tr}\,\mathcal{E} = c^2 R_{00} = 4\pi G\rho$ in the Newtonian limit, and an antisymmetric part of the magnetic tensor, $\mathcal{B}_{[ij]} = -(4\pi G/c)\,\epsilon_{ijk}\,\rho v_k$ for matter of density ρ flowing at velocity $\mathbf{v}$, which points along the flow. The pixel is also assumed not to rotate: a frame turning at angular velocity Ω feels a centrifugal pseudo-tide of order Ω^2, and the Earth's own turning gives $5 \times 10^{-9}\,\mathrm{s}^{-2}$, some thirty thousand times the tide of the Moon, so gyroscopes must hold the frame still. We call an array of such pixels a gravitational camera.

a. What the premise asks. A pixel of this kind is an old idea. The gravitational compass, a cluster of free masses read against one another, was proposed to measure the curvature piece by piece [18, 19]; a sphere with several transducers reads the five numbers of $\mathcal{E}$ at one place [20, 21]; and a detector that reads all of $\mathcal{E}$ has been designed [22]. In the near field the premise asks little more

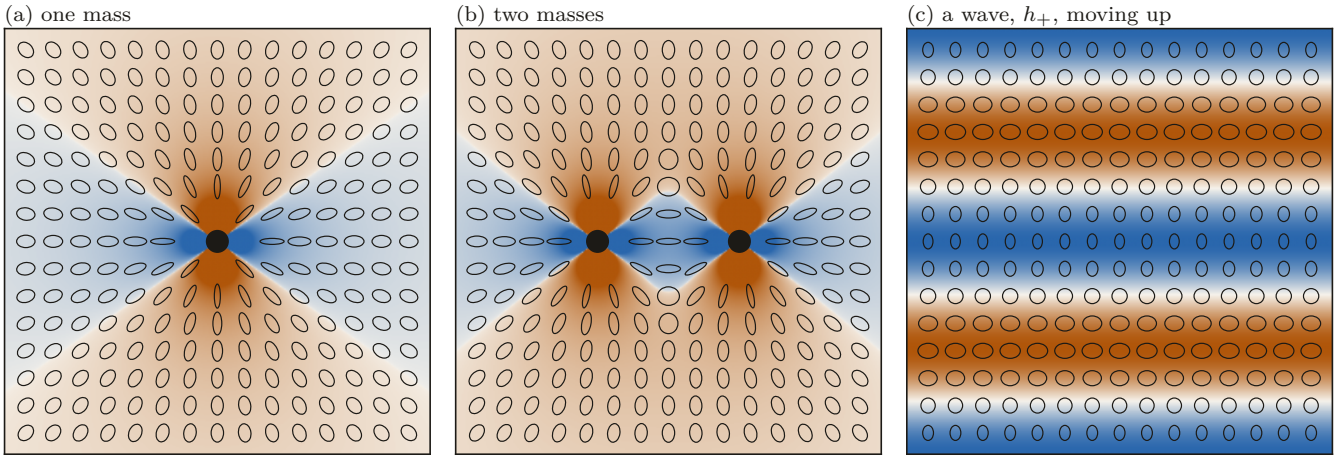


FIG. 3. The tidal field itself. At points of a plane, a small ring of free particles is drawn as the field distorts it (exaggerated, with the strength compressed so that weak regions remain visible), over a map of one component: $\mathcal{E}_{zz}$ (up the page) in (a) and (b), $\mathcal{E}_{xx}$ (across) in (c). Orange marks a stretch along that axis (the component negative, by Eq. (2)), blue a squeeze (positive). (a) One mass: every ring is stretched toward it. (b) Two masses: midway between them the ring is stretched along the line joining them and squeezed across it. (c) A plane wave of polarization h_+ travelling up the page: bands of stretch and squeeze across the direction of travel alternate every half wavelength, and nothing happens along it. A pixel records one such ring, in three dimensions.

than exists. Tides are measured in eotvos, $1\,\mathrm{E} = 10^{-9}\,\mathrm{s}^{-2}$, and the person a metre away is nine of them. An atom gradiometer carried over a buried tunnel reaches 20 E in ten minutes [1]; a superconducting one in the laboratory, 0.02 E in a second [23], a signal-to-noise ratio of five hundred on that person; and a satellite has carried one as sensitive around the Earth [24]. Two free masses of a gram, a centimetre apart and read for a second at the standard quantum limit, would resolve $6 \times 10^{-14}\,\mathrm{s}^{-2}$, a hundred thousand times less than the person's tide. The magnetic part asks more. It can be read by gyroscopes [12], by a gradiometer in motion [25, 26] or by light sent both ways around a loop [27], and in a wave it already enters the response of an interferometer, at first order in the length of its arms over the wavelength [28]; but near slow matter it is smaller than the electric part by v/c. The waves of moving bodies and the thermal glow ask far more again, and the glow asks for something that no matter can supply (Section IX).

b. The Earth's own tide. On the ground the largest tide is the planet's own, $2GM/R^3 = 3.1 \times 10^{-6}\,\mathrm{s}^{-2}$ along the vertical, three hundred times that of the person a metre away. It is steady and known, and it is subtracted, as the empty room is in Section IV: the rooms of this paper are what remains, or rooms in free fall far from any planet. The planet's turning is in the reading too. A pixel at rest on the equator moves with the ground at $\Omega R = 465\,\mathrm{m\,s}^{-1}$, over a planet that turns beneath it, and the two together (Eq. (9) and the spin dipole of Section IV) give it a magnetic part $(3GM\Omega/cR^2)(1 - I/MR^2) = 4.8 \times 10^{-12}\,\mathrm{s}^{-2}$, with I the planet's moment of inertia: seventy thousand times the magnetic part of a person walking past a metre away at $1.4\,\mathrm{m\,s}^{-1}$. This too is steady, and it is a measurement: one pixel on the ground reads I/MR^2, the number that tells a planet with a core from one without (Section IV).

The two parts are best written as one complex matrix, $\mathcal{W} = \mathcal{E} + i\mathcal{B}$, and Section VIII shows how much a single pixel can read from it. The sections in between follow an array of pixels through the regimes in which a camera forms images.

III. THREE REGIMES

What reaches a pixel depends on how the distance r to the source compares with the wavelength $\lambda = c/f$ of the radiation it would emit at frequency f. Inside the *near zone*,

$$r \ll \frac{\lambda}{2\pi} = \frac{c}{2\pi f}, \tag{6}$$

the field is the Newtonian one of Eq. (3), following the source almost instantaneously. Outside it the field is radiation, Eq. (4), falling off as $1/r$. At 1 Hz the near zone reaches to 48,000 km; at 1 kHz, to 48 km. Figure 4 places familiar sources on this map.

Sources of radiation divide again. Bodies in bulk motion radiate at the frequencies at which they move, which are low; hot matter radiates at the frequencies of its molecular motion, which are very high. This gives the three regimes of Table I, taken in turn in the next three sections.

a. Spin, speed and compactness. Almost everything the camera can and cannot do follows from one property of gravity and two small numbers that describe matter.

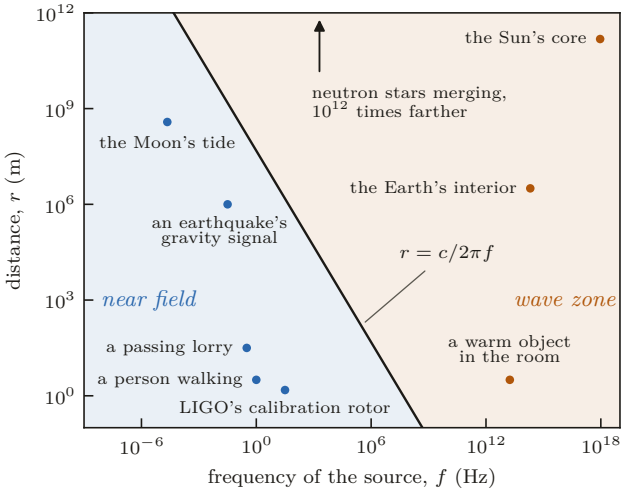


FIG. 4. Where sources lie. The diagonal is the edge of the near zone, Eq. (6), $r = c/2\pi f$. Everything that moves mechanically, from the tides to a calibration rotor beside a LIGO mirror, sits below it and is seen through its changing Newtonian pull. Only radiation at thermal frequencies, far to the right, reaches a nearby camera as waves short enough to form sharp images; thermal sources are placed at the peak of their spectrum, $f = 2.82\,k_B T/h$.

Gravity has spin two: curvature at a point is a symmetric trace-free tensor, and in a wave it is the square $\mathbf{m}\mathbf{m}^T$ of a complex null vector $\mathbf{m}$, where the field of light is the vector itself. This gives the ten numbers of a pixel, the four principal null directions of a reading, the separation of two, three and four waves, the sixty-eight numbers of the sky that one pixel can measure and the spin-two envelope of a sparse array (Section VIII). *Matter is slow*, $v/c \ll 1$: this puts the edge of the near zone, $\lambda/2\pi \sim L/(v/c)$, far beyond any room, makes every compact moving body a point in its own radiation (Section V), and makes the magnetic part of a near field small, so that it is at once a clean channel for waves and a range-finder for moving mass; only thermal motion reaches the frequencies at which the wavelength is shorter than the body. *Matter is tenuous*, its compactness $GM/Rc^2 \ll 1$: this makes it transparent, so that hot matter glows throughout (Section VI), and rules out lenses, mirrors, absorbers and shadows short of a black hole (Section VII), so that images must be computed.

IV. THE NEAR FIELD

In the near zone the camera measures the Newtonian tidal field of the scene as it changes. The field passes through all matter, so no wall can screen a mass from the camera. Its strength is set by mass, so the camera weighs what it sees. And it is present whether or not anything moves, so a perfectly still scene is visible too.

Regime	What the pixel receives	What limits the image
Near field	the changing Newtonian pull of nearby mass	blur grows with distance
Waves from bulk motion	radiation from accelerating bodies	a compact source is an unresolved point
Thermal glow	radiation from molecular motion	almost no gravitons arrive

TABLE I. The three regimes of a gravitational camera.

a. How bright. A body of mean density $\bar\rho$ and radius R at distance r produces a tidal field of magnitude

$$\frac{2GM}{r^3} = \frac{8\pi G}{3}\,\bar\rho\,\theta^3, \qquad \theta = \frac{R}{r}. \tag{7}$$

Tidal brightness is density times the cube of angular size. The Sun and the Moon span the same angle in the sky, and the Moon, being denser, raises the larger tide. A person one metre away spans a far larger angle than either, and outweighs the Moon in the camera's view some fifty thousand times.

b. What the image is. Summing Eq. (3) over all the matter in view, and grouping it by direction, gives the tidal field at the camera as an integral over the sky,

$$\begin{aligned} \mathcal{E}_{ij} &= G\int \mathrm{d}\Omega\,\big(\delta_{ij} - 3\,\hat n_i\hat n_j\big)\,S(\hat n), \\ S(\hat n) &= \int \rho(r\hat n)\,\frac{\mathrm{d}r}{r}. \end{aligned} \tag{8}$$

The quantity S, which we call the *tidal column*, is the mass along a line of sight with each part weighted by the inverse of its distance; Fig. 5 shows where the weighting comes from. The integral starts a short distance $r_{\min}$ from the camera (a quarter of a metre in the scenes of this paper), since matter at the camera itself would make S diverge logarithmically, although not $\mathcal{E}_{ij}$. A single pixel measures only five numbers, the quadrupole of S over the whole sky; an array, by comparing the field from pixel to pixel, measures more.

c. The magnetic picture. Small as it is, the near-field magnetic tensor carries its own picture. To first order in v/c, a mass M in direction $\hat n$ at distance r, moving with velocity $\mathbf{v}$, gives

$$\mathcal{B}_{ij} = \frac{3GM}{c\,r^3}\,\big[\hat n_i(\hat n\times\mathbf{v})_j + \hat n_j(\hat n\times\mathbf{v})_i\big], \tag{9}$$

and grouping matter by direction as in Eq. (8) gives the magnetic counterpart of the sky integral,

$$\begin{aligned} \mathcal{B}_{ij} &= \frac{3G}{c}\int \mathrm{d}\Omega\,\big[\hat n_i(\hat n\times\mathbf{J})_j + \hat n_j(\hat n\times\mathbf{J})_i\big], \\ \mathbf{J}(\hat n) &= \int \rho\,\mathbf{v}(r\hat n)\,\frac{\mathrm{d}r}{r}, \end{aligned} \tag{10}$$

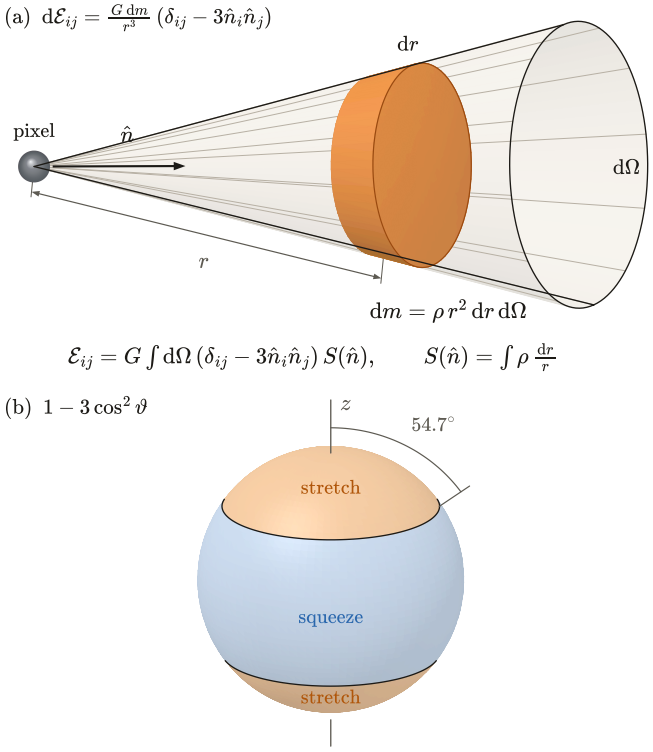


FIG. 5. The sky integral, Eq. (8). (a) A pixel at the apex of a cone of directions $\mathrm{d}\Omega$ about $\hat{n}$. The matter in the cone between r and $r + \mathrm{d}r$, a piece of the cone bounded by two spherical caps (orange), has mass $\mathrm{d}m = \rho\, r^2\, \mathrm{d}r\, \mathrm{d}\Omega$ and adds $G\,\mathrm{d}m\,(\delta_{ij} - 3\hat{n}_i\hat{n}_j)/r^3$ to the tidal field. The r^2 of the volume cancels two of the three powers of $1/r$, so each line of sight contributes its mass weighted by $\mathrm{d}r/r$: the tidal column $S(\hat{n})$. The cone's width and $\mathrm{d}r$ are exaggerated. (b) The sky around the pixel, coloured by the sign of the weight $1 - 3\cos^2\vartheta$ with which one component, $\mathcal{E}_{zz}$, takes matter in each direction: matter in the orange caps, within 54.7° of the z axis ($\cos^2\vartheta > 1/3$), stretches the pixel along z; matter in the blue band squeezes it. The weight averages to zero over the sky, which is why a uniform shell of matter around the camera is invisible to it.

so the magnetic half of the camera images the *current column* $\mathbf{J}$, with the blur law of Eq. (21) below at a signal-to-noise ratio smaller by about v/c. Only motion across the line of sight counts: $\hat{n} \times \mathbf{J}$ removes the radial part, so the magnetic channel is the opposite of a Doppler radar, blind to approach and sensitive to sideways motion. For a single moving mass $|\mathcal{B}|/|\mathcal{E}| = \sqrt{3}\, v_\perp/c$ to first order in v/c, so one reading of one pixel gives the line on which a body lies (the eigenvector of $\mathcal{E}$'s negative eigenvalue, up to its sign) and, from $\mathcal{B}$, its sideways speed; at any speed, the principal null directions of the field give the sideways velocity exactly, Eq. (52) of Section VIII. And outside a spherical body spinning with angular momentum $\mathbf{L}$ the field is exactly that of a spin dipole, $\mathcal{B}_{ij} = -(3G/cr^4)[L_i\hat{n}_j + \hat{n}_i L_j + (\mathbf{L}\cdot\hat{n})(\delta_{ij} - 5\hat{n}_i\hat{n}_j)]$: a hollow shell and a solid ball of equal mass and size spinning at the same rate, whose electric fields are identical everywhere outside them, differ in $\mathcal{B}$ by their moments of inertia, a factor 5/3. At equal angular momentum they are identical outside, and so motion too can hide. A uniform ball of radius $2^{-1/5}R$ turning one way inside a shell of the same density that fills the rest of the sphere out to R and turns the other way at the same rate has no angular momentum, and outside it no magnetic field at all, though all of it moves. For a ball turning at angular velocity $\boldsymbol{\omega}$ about a point $\mathbf{s}$, entered and left by the line of sight at distances $0 < a \le b$, the current column is $\mathbf{J} = \rho\,[(\boldsymbol{\omega}\times\hat{n})(b-a) - (\boldsymbol{\omega}\times\mathbf{s})\ln(b/a)]$. A smooth flywheel looks the same spinning or still, and pulls the same; its current column is a vortex that turns as the wheel turns.

d. What the image cannot show. An array outside the matter it views does not measure S itself, because the field outside a body does not fix the arrangement of mass inside it. A hollow shell and a solid ball of equal mass produce the same field at every point outside both, however close. More generally, adding to a body the density $\delta\rho = \nabla^2\chi/4\pi G$, with χ any smooth function that vanishes outside it, changes the potential by χ and so changes nothing outside [29]; ordinary positive densities $\rho_0 \pm \epsilon\,\delta\rho$ make such pairs out of real matter. The tidal column is therefore a rendering of a known scene, the natural picture of what the camera responds to, and not a quantity the camera could reconstruct uniquely. The near-field images of this paper show S computed from the scene and blurred as described next. Other channels break the ambiguity: the thermal glow shows a shell as a ring; a shell and a ball of equal mass spinning at the same rate differ in $\mathcal{B}_{ij}$ by the ratio of their moments of inertia, 5/3 (*The magnetic picture*, above), though at equal angular momentum they are again alike; and heat, or a tide applied from outside, reveals the rest (*What heat reveals*, below). The camera's position matters too: inside a closed spherical shell it feels no tide from the shell at all, whatever its mass.

e. What the image does show. The ambiguity has an exact shape. For a body whose outside is connected, every density splits in one way only into two parts,

$$\rho = \rho_h + \frac{\nabla^2\chi}{4\pi G}, \tag{11}$$

where ρ_h is harmonic inside the body, $\nabla^2\rho_h = 0$, and χ vanishes on the surface together with its gradient. The field outside fixes ρ_h completely and is blind to the rest [30]. The potential outside is built from the moments $\int \rho\, h\, \mathrm{d}V$ of the density against functions h harmonic in the body (the solid harmonics $r^\ell Y_{\ell m}$ about a point inside), and the second part has none of them, since $\int h\,\nabla^2\chi\,\mathrm{d}V = \int \chi\,\nabla^2 h\,\mathrm{d}V = 0$. It follows that any estimate of the interior that is linear in the data and treats every point inside alike and independently, a white prior as in Eq. (19), is itself harmonic: it is built from the data's own kernels, which are. A harmonic function has no maximum or minimum inside the region where it is harmonic. The least assuming picture of an interior that a camera outside can draw, taking the body's outline from light, therefore

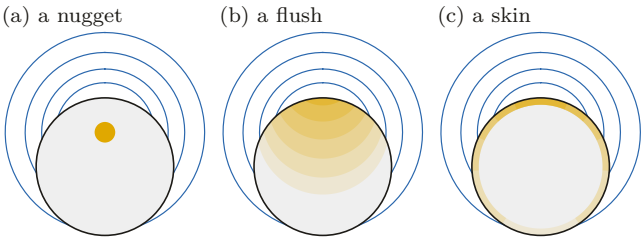


FIG. 6. Same outside, different inside: three steel balls whose fields are identical everywhere outside them. (a) A gold nugget halfway from the centre to the wall. (b) Its harmonic projection, Eq. (12), the least assuming interior that a camera outside could draw, shaded in bands that double in density up to $46\,m/4\pi R^3$ at the near wall. (c) Its balayage: the nugget's mass spread over the surface as a skin, drawn just inside the surface as a band of constant width shaded in the same way, in steps that double in surface density up to $6\,m/4\pi R^2$ over the nugget. Blue: equipotentials of the gold's share of the field, drawn outside each ball (the steel's share is the same in all three and is left out). They are the same in all three, and in (b) and (c) they centre on a nugget that is not there.

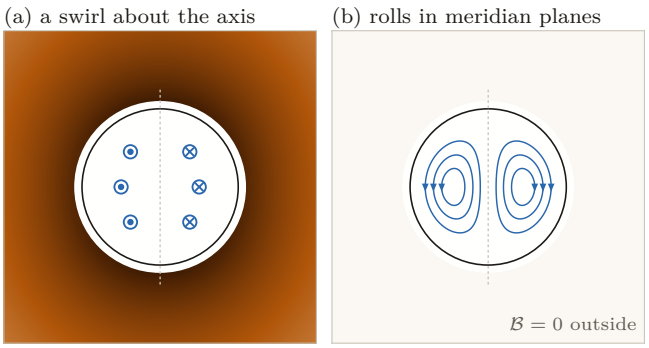


FIG. 7. Silent flows. Inside a ball, (a) a swirl about its axis (in this meridian plane the flow comes out of the page on one side and goes in on the other) and (b) rolls in meridian planes, drawn as stream lines, with the same smooth profile. Outside, the size of the magnetic part of the field of each, computed by the same integration over the ball and shaded over four decades below the swirl's largest value; nothing is computed in the white margin. The swirl shows; the rolls are silent, to the accuracy of the integration, below 10^{-4} of the swirl's field.

has its densest and its lightest points on the surface. It can never show a core. Every round body appears as a uniform ball of its mean density, and the layered Earth, seen from outside in this way, as $5513\,\mathrm{kg\,m^{-3}}$ throughout.

Figure 6 shows three bodies with the same field outside. A steel ball of radius R holds a gold nugget of mass m at the distance s from its centre. The nugget's harmonic projection, the density harmonic in the ball that has the same field outside, is

$$\rho_h = \frac{m}{4\pi R^3}\sum_{\ell=0}^{\infty}(2\ell+1)(2\ell+3)\left(\frac{sr}{R^2}\right)^{\ell}P_\ell(\cos\vartheta), \quad (12)$$

with ϑ the angle from the nugget's direction; the sum is $(3-10t^2+8t^3\cos\vartheta-t^4)/(1-2t\cos\vartheta+t^2)^{5/2}$, with $t=sr/R^2$. For $s=R/2$ it is a flush on the wall nearest the nugget, $46\,m/4\pi R^3$ there, fifteen times the nugget's mass spread evenly, fading toward the far wall, where it dips just below zero, so that only the steel keeps it a real density. Poincaré's balayage sweeps the same mass onto the surface as a skin of surface density $m(R^2-s^2)/4\pi R\,|\mathbf{x}-\mathbf{s}|^3$, thickest over the nugget. At any sensitivity, a camera outside cannot tell the three apart.

f. What breaks the tie. The three differ first in a number that the electric part cannot see, $\int\rho\,r^2\,\mathrm{d}V$, the trace of the second moment of the mass: ms^2, $\frac{3}{5}\,mR^2$ and mR^2 for the nugget, the flush and the skin (r^2 is not harmonic, so by Eq. (11) the field outside carries no trace of it). The moment of inertia contains it, $I_x = \frac{2}{3}\int\rho\,r^2\,\mathrm{d}V + \int\rho\,(r^2/3-x^2)\,\mathrm{d}V$, where the second integral is harmonic and shared. Spun at the same rate about an axis across the line to the nugget, the three therefore differ in angular momentum, and so in the spin dipole of their magnetic fields (*The magnetic picture*, above), by the gold's shares of the moment of inertia, 0.25, 0.48 and $0.75\,mR^2$. The ball and the shell above, with $\int\rho\,r^2\,\mathrm{d}V = \frac{3}{5}MR^2$ and MR^2, are the simplest case. Spin breaks this tie and others of its kind: the magnetic field of a body turning at a known rate holds $\int\rho\,r^2h\,\mathrm{d}V$ for every harmonic h, of which the moment of inertia is the first, and for a round body the only one. Heat breaks them all, as shown below. The thermal glow, which sums along lines instead of reaching out as a potential, would show the nugget as a spot, the flush as a gradient and the skin as a ring, but the glow measures friction and temperature, not mass (Section IX). A pixel inside the matter escapes the ambiguity altogether, because there $\mathrm{tr}\,\mathcal{E} = 4\pi G\rho$ reads the density where the pixel is (Section II).

The magnetic part has a blind spot of the same kind for flows. Outside a body, $\mathcal{B}$ comes from the potential $\int\rho\mathbf{v}\,\mathrm{d}V'/|\mathbf{x}-\mathbf{x}'|$ of its steady flow of mass. If the flow is $\rho\mathbf{v} = \nabla\times\nabla\times\mathbf{V}$, with $\mathbf{V}$ vanishing together with its derivatives at the surface, that potential is a pure gradient outside, and $\mathcal{B}=0$ there. Every confined flow that is the same all round an axis and turns in its meridian planes, such as the simplest convection rolls inside a star or a planet's core, is of this form: it is silent outside, however fast it runs. Of such a flow only the swirl about the axis shows, and only through its harmonic part, of which the spin dipole is the first term. Figure 7 shows the field of both kinds of flow inside a ball, integrated numerically: outside it, the rolls' field vanishes to the accuracy of the integration, while the swirl's does not.

Together the channels go further than any one. For the Earth the glow gives the radius of the core, 3480 km, from the kinks in its brightness (Figs. 31 and 32); the electric part gives the mass; and the magnetic part, with the rate of turning known, gives the moment of inertia, $0.331\,MR^2$, the value the Preliminary Reference Earth Model is built to match [31]. A two-layer Earth with that core, mass

and moment of inertia has a core of 12,500 kg m^{-3} and a mantle of 4150 kg m^{-3}. The reference model's core averages 11,000; the difference is the compression of the mantle under its own weight, which two numbers cannot resolve.

g. What heat reveals. Every warm body trembles, and its trembling has a near field. In classical thermal equilibrium the velocities of the particles of a body are independent of their positions and of one another, with $\langle v_a^2 \rangle = 3k_BT/m_a$, whatever forces hold the body together. Any moment of its mass, $q_h = \sum_a m_a\, h(\mathbf{x}_a)$, therefore changes at a rate whose mean square follows at once:

$$\langle \dot{q}_h\, \dot{q}_g \rangle = k_BT \int \rho\, \nabla h \cdot \nabla g \, \mathrm{d}V. \tag{13}$$

For h harmonic, q_h is one of the moments from which the field outside is built, and the camera reads it; but $\nabla h \cdot \nabla g = \frac{1}{2}\nabla^2(hg)$ is not harmonic beyond the lowest orders, so the right-hand side holds what the static field cannot see. For the multipoles $h = r^\ell Y_{\ell m}$, summed over m,

$$\sum_m \langle |\dot{q}_{\ell m}|^2 \rangle = \frac{\ell(2\ell+1)^2}{4\pi}\, k_BT \int \rho\, r^{2\ell-2}\, \mathrm{d}V. \tag{14}$$

The dipole gives the mass: its tremor is the Brownian motion of the body as a whole. The quadrupole gives $\int \rho\, r^2\, \mathrm{d}V$, the number that told the nugget from its flush and its skin, and the shell from the ball, whose tremors differ by 5/3 whatever their elastic constants and their friction; these set only at which frequencies the tremor lies, not how much of it there is. The octupole gives $\int \rho\, r^4\, \mathrm{d}V$, and so on. For a round body the whole sequence fixes the density at every radius, since a positive distribution on a finite interval is fixed by its moments; for any body, the products $\nabla h \cdot \nabla g$ of harmonic functions reach every Fourier component of the density, as Calderón showed for an inverse problem of the same form [32]. At a known temperature a warm body cannot hide its interior from a camera outside it, though, as in Eq. (21), fine detail is reached only through exponentially small signals. That noise can show what a mean field hides is known for waves: the correlations of the field outside an incoherent source fix its intensity, though a steady source of the same shape could hide [33], and the echoes inside a block of metal have been read from its thermal noise alone [34].

Three conditions apply: the modes that carry the tremor must be classical, $\hbar\omega \ll k_BT$; slow enough to be seen as near field, $\omega r \ll c$; and measured in full. All three hold for a solid, whose smooth moments fall on its lowest modes of vibration. In a lattice ball of 924 masses joined by springs, 85% of the quadrupole's tremor lies at one frequency and 99% below twice it; a shell of the same mass and radius, whose thickness is a third of its radius, trembles 1.22 times as much, the ratio of their second moments, at frequencies more than twice as low (Fig. 8). A steel ball ten centimetres in radius rings in its lowest quadrupole mode near 15 kHz, with 4×10^8 quanta

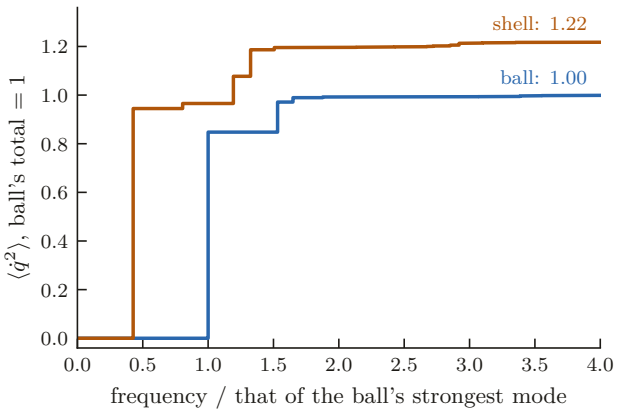


FIG. 8. The thermal tremor of a ball and a shell whose fields outside are identical: lattices of equal masses joined by springs, with the same total mass and radius, the shell's thickness a third of its radius. Each curve adds up, mode by mode in order of frequency, the mean square rate of change of the quadrupole moment, Eq. (14); frequency is in units of the ball's strongest quadrupole mode. The totals are in the ratio of the bodies' second moments, $\int \rho\, r^2\, \mathrm{d}V$, whatever the springs; the shell is softer, and its tremor lies at lower frequencies.

in it at room temperature, and its tremor makes a tide of $3 \times 10^{-25}\,\mathrm{s}^{-2}$ a metre away, where $\omega r/c = 3 \times 10^{-4}$. That mode emits one graviton in 7×10^{17} years. The camera detects the ball's ringing without receiving any of its radiation: the graviton counts that limit the thermal glow (Section VI) say nothing about the near field. Its cost is distance. A quadrupole's tide falls as r^{-5}, so when the tremor is far below the noise, the information gathered about it grows only as the observing time over r^{20}: from 20 cm to a metre costs 10^{14} times as long.

h. What an applied tide reveals. A tide applied from outside reads the same numbers at any temperature. By the fluctuation–dissipation theorem [35] the tremor is the dissipative part of the body's response, and Eq. (13) becomes the inertial sum rule familiar from nuclear physics [36]:

$$\frac{2}{\pi} \int_0^\infty \omega\, \mathrm{Im}\, \chi_h(\omega)\, \mathrm{d}\omega = \int \rho\, |\nabla h|^2\, \mathrm{d}V, \tag{15}$$

where χ_h is the response of q_h to a tide whose potential is $-Fh$. The friction and the stiffness of the body spread the response over frequency but cannot change its total. The static part of the response is the body's tidal Love number [37]: a ball of rigidity μ, density ρ and surface gravity g acquires a quadrupole $\frac{1}{3}k_2R^5/G$ times the applied tide, with $k_2 = \frac{3}{2}/(1 + 19\mu/2\rho gR)$ for a uniform ball; for the steel ball, $k_2 = 4 \times 10^{-16}$. The same compliance sets the static jitter, $\langle \delta q_h^2 \rangle = k_BT\, \chi_h(0)$. Quantum mechanics bounds the jitter between the classical value and that of a single mode at the mean frequency, $\sqrt{A/\chi_h(0)}$ with A the sum of Eq. (15) (Appendix A).

i. A model-independent thermometer. The ratio of tremor to response is the temperature, but only if the push couples to the same quantity that the pixel reads [38]. Surround the pixel with a thin spherical shell of radius a and shift mass around it, changing its surface density by $\delta\sigma = -15f\,\hat{n}\cdot D\cdot\hat{n}/4\pi a^4$, for a fixed trace-free tensor D and an amplitude f. Its interaction with any matter outside the shell is exactly $-f\,D:\mathcal{E}$, with $\mathcal{E}$ the field of that matter at the pixel and $D:\mathcal{E} = D_{ij}\mathcal{E}_{ij}$, so it pushes on precisely the combination $y = D:\mathcal{E}$ that the pixel reads. Then

$$T = \frac{\omega\, S_{yy}(\omega)}{2k_B \operatorname{Im}\chi_{yy}(\omega)}, \tag{16}$$

where S_{yy} is the spectrum of the reading and χ_{yy} its response to f, and every unknown about the body, its modes, their shapes and how each shows at the pixel, cancels. The shell's own field at the pixel, $6GfD/a^5$, is in phase with f and adds nothing to $\operatorname{Im}\chi_{yy}$. A body not in equilibrium reads as an average of its temperatures, weighted by where it dissipates.

j. How sharp. The space between scene and camera is empty, so the potential there obeys Laplace's equation. Consider a pattern in the scene that repeats across the line of sight with wavenumber k, at depth z from the sensor. Laplace's equation forces it to fade with height as

$$\Phi \propto \cos(kx)\, e^{-kz}: \tag{17}$$

fine detail dies away before it reaches the camera, and coarse detail survives. To reconstruct the scene the camera must multiply each pattern by e^{kz}, and its noise with it. If the largest features are recorded with signal-to-noise ratio SNR, patterns with $e^{kz} > \mathrm{SNR}$ are lost in the noise, and detail finer than about $\pi z/\ln\mathrm{SNR}$ cannot be recovered.

The estimate can be made exact. Let a flat array at distance z from a sheet of sources with surface density σ record the tidal field along its normal with white noise of spectral density N_0. With $\Phi = -GM/r$ the normal component above a mass is negative, a stretch, so we record $d = -\mathcal{E}_{zz}$. In Fourier space across the array the data are

$$\hat{d}(\mathbf{k}) = 2\pi G\, k\, e^{-kz}\,\hat{\sigma}(\mathbf{k}) + \hat{n}(\mathbf{k}), \tag{18}$$

and the factor k says that a uniform sheet is invisible: its pull is the same at every pixel and at every height, so it has no tidal field at all. Define the signal-to-noise ratio as the peak field of a point mass m, $2Gm/z^3$, over the noise of the field averaged across a patch of side z, $\sqrt{N_0}/z$: so $\mathrm{SNR} = 2Gm/(z^2\sqrt{N_0})$. Each Fourier component of a point mass then stands above its own noise by $s = \pi\,\mathrm{SNR}\; kz\, e^{-kz}$, and the best linear reconstruction (the Wiener filter, with a sheet of independent point masses m as its prior, one per area z^2, whose spectrum is $S_\sigma = m^2/z^2$) keeps it with weight

$$H(k) = \frac{s^2}{1+s^2}, \qquad s = \pi\,\mathrm{SNR}\; kz\, e^{-kz}. \tag{19}$$

SNR	q_c	array	row	two points	$\pi/\ln\mathrm{SNR}$
10^3	10.4	24.0°	20.7°	24.5°	26.1°
10^6	17.8	14.1°	12.1°	14.6°	13.0°
10^{10}	27.5	9.2°	7.9°	9.5°	7.8°
10^{20}	51.1	5.0°	4.2°	5.1°	3.9°
10^{30}	74.5	3.4°	2.9°	3.5°	2.6°
10^{60}	144.3	1.8°	1.5°	1.8°	1.3°

TABLE II. Blur of the near-field image. "Array": full width at half maximum of the reconstructed image of a point, for a flat array, Eq. (21). "Row": the same for a single row of sensors over a two-dimensional scene. "Two points": the smallest separation at which two equal point masses show a dip between them in the array's image (Sparrow's criterion); as for any image formed in amplitude, this slightly exceeds the full width. The last column is the first estimate.

H vanishes for a uniform scene, $k \to 0$, is close to one for patterns from $kz \approx 1/\pi\mathrm{SNR}$ to a little below $kz = q_c$, where it falls through one half:

$$q_c\, e^{-q_c} = \frac{1}{\pi\,\mathrm{SNR}}, \qquad q_c \approx L + \ln L, \quad L = \ln(\pi\,\mathrm{SNR}) \tag{20}$$

(10.1 against the exact 10.4 at $\mathrm{SNR} = 10^3$). The image of a point is therefore close to the diffraction pattern of a round pupil of radius q_c/z, $2J_1(x)/x$ with $x = q_c r/z$ and J_1 the Bessel function. The full width at half maximum of this image, an amplitude and not its square, as an angle seen from the array, is

$$\Delta\theta = \frac{4.43}{q_c} \tag{21}$$

to within four per cent for every $\mathrm{SNR} \geq 100$ (for a single row of sensors over a two-dimensional scene, $3.79/q_c$; the scene is then made of line masses perpendicular to the row, and the potential obeys Laplace's equation in two dimensions). Table II gives values computed without approximation, and Fig. 9 shows the law.

For an array at least as wide as the scene is deep, the angular blur does not depend on distance or on the size of the array, only, through q_c, on the logarithm of its sensitivity. A signal-to-noise ratio of a thousand gives 24°; a million, 14°; 10^{30}, still 3.4°. To match the sharpness of the human eye, one arcminute, would take a signal-to-noise ratio near 10^{6600}. The first estimate $\pi/\ln\mathrm{SNR}$ is of the right size everywhere, but it runs sharp at high sensitivity, because the image of a point is wider than π/q_c. Figure 10 shows the reconstruction of two masses, and the near-field images of this paper are blurred by Eq. (21). The same logarithmic limit is long familiar wherever fields that obey Laplace's equation are continued back toward their sources: in geophysics, where gravity and magnetic surveys are continued downward [39, 40], and in near-field acoustic holography [41].

k. A flown gradiometer. The law can be read off an instrument that exists. The satellite GOCE carried a gradiometer around the Earth for four years at a height of

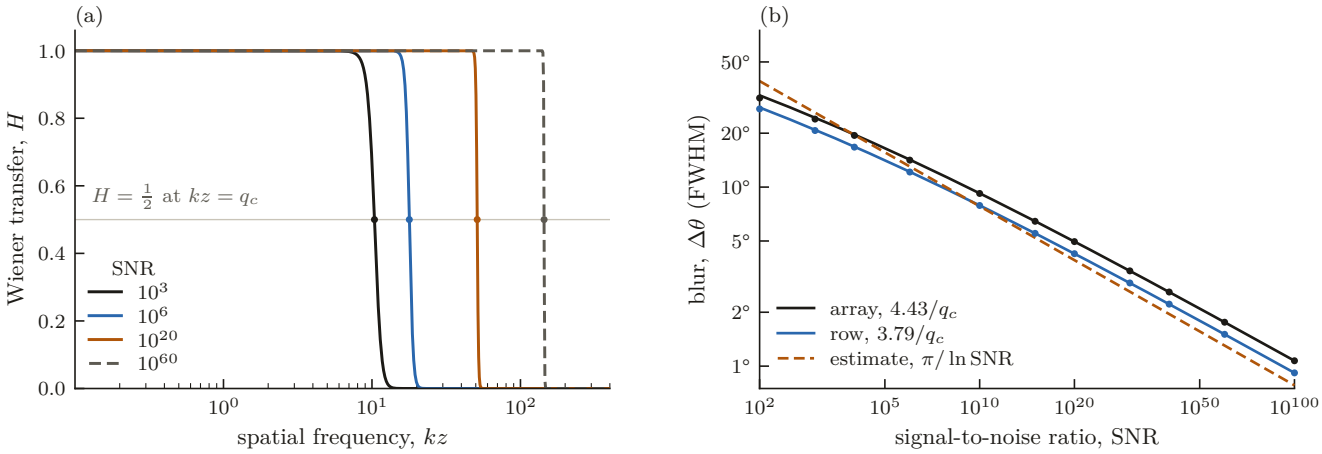


FIG. 9. The exact near-field resolution law. (a) The Wiener filter H of Eq. (19) against spatial frequency, for four signal-to-noise ratios: patterns coarser than $kz = q_c$ are kept almost whole, finer ones are lost. Dots mark $H = \frac{1}{2}$ at q_c, Eq. (20). Raising the sensitivity from 10^6 to 10^{60} moves the cutoff only from 18 to 144. (b) The resulting blur, the full width at half maximum of the image of a point, for a flat array ($4.43/q_c$) and a single row ($3.79/q_c$), with values computed directly (dots) and the first estimate $\pi/\ln\mathrm{SNR}$ (dashed).

$z = 254\,\mathrm{km}$, reading the tide to between 0.01 and 0.02 E in a second [24]. Its final map of the Earth's field runs out of signal between spherical harmonic degrees $\ell = 280$ and 300 [42, 43], where the pattern on the ground has wavenumber $k = \ell/R$, so that kz is between 11 and 12. Equation (20) reads that cut-off as a signal-to-noise ratio of two to four thousand, and Eq. (21) gives the blur: 21° to 23°, a hundred kilometres on the ground seen from two and a half times as high, which is about what the mission was designed to resolve. Four years of the most sensitive gradiometer yet flown correspond to the first row of Table II.

l. Other gravitational sensors. Nothing here depends on reading curvature. Pixels linked into one array could compare clocks, reading the potential itself, or accelerometers, reading its gradient. Over a sheet their kernels go as $q^{-1}e^{-q}$ and e^{-q}, where the tidal camera's goes as $q\,e^{-q}$, and Eq. (20) becomes $q^p e^{-q} = 1/\pi\mathrm{SNR}$ with $p = -1$, 0 and 1. At $\mathrm{SNR} = 10^3$ the cut-offs are 6.2, 8.1 and 10.4; at 10^{20}, 43.4, 47.2 and 51.1. They differ by about the logarithm of q_c, and the definition of SNR shifts each by a similar amount. The blur belongs to Laplace's equation, which every static gravitational field obeys in empty space, not to the detector.

m. A small camera. A camera much smaller than its distance from the scene does worse. Inside a camera of width D, the part of the field that varies over the sky with angular degree ℓ changes across the camera by a factor $(D/2r)^{\ell-2}$ relative to the quadrupole, for a source at distance r. Detail of degree ℓ therefore needs $\mathrm{SNR} \gtrsim (2r/D)^{\ell-2}$, and

$$\ell_{\max} \approx 2 + \frac{\ln \mathrm{SNR}}{\ln(2r/D)}, \qquad \Delta\theta \approx \frac{\pi}{\ell_{\max}}. \tag{22}$$

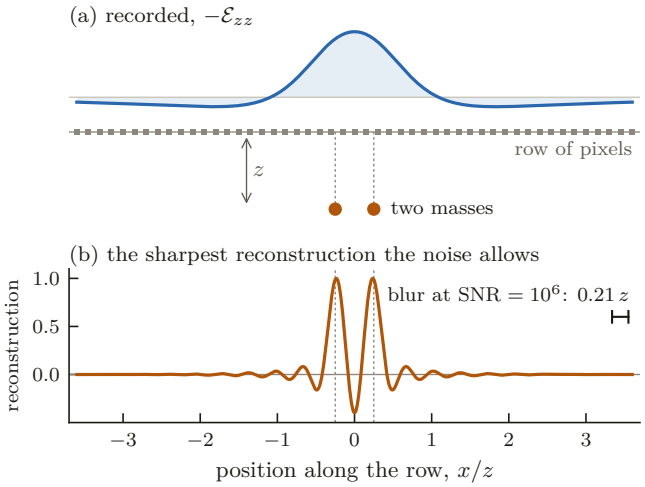


FIG. 10. The near-field blur, for a row of pixels over a two-dimensional scene: two line masses a distance $z/2$ apart at depth z, recorded with signal-to-noise ratio 10^6. (a) The geometry, to scale, and what the pixels record: $\mathcal{E}_{zz}$ along the row, a single smooth bump. (b) The best reconstruction of the masses that the noise allows, the Wiener filter of Eq. (19); its ripples are the price of discarding the detail that noise has swamped. The bar is the blur, $0.21\,z$.

A camera ten centimetres across, looking at a lorry fifteen metres away with $\mathrm{SNR} = 10^6$, sees detail of about 40°, not 14°. A single pixel, $D \to 0$, sees the quadrupole alone. Widening the camera helps logarithmically until it is about as wide as the scene is deep; beyond that, Eq. (21) applies.

n. The precision of a simple scene. The blur limits what can be drawn of an arbitrary scene, not how precisely

a simple one can be measured. If the scene is known to hold a single point mass at depth z, an infinite plane recording $\mathcal{E}_{zz}$ with the noise above determines its position to within $\sqrt{2/5}\,z/\mathcal{R}$ across and $z/\mathcal{R}$ in depth, and its mass to within $\sqrt{5}/\mathcal{R}$ of itself, where $\mathcal{R} = (\sqrt{3\pi}/4)\,\mathrm{SNR}$ is the signal-to-noise ratio of the whole field pattern (the Cramér–Rao bounds with position and mass estimated jointly). At one metre and $\mathrm{SNR} = 10^3$ the mass is placed to within a millimetre, while its image is 24° wide. Two equal masses, by contrast, can be told from one only when they are farther apart than about $z/\sqrt{\mathcal{R}}$, because the difference they make grows as the square of their separation. What limits the image is the variety of scenes allowed, not the precision of the data.

o. A worked case. The locked safe (Fig. 11) shows both sides of this. Panels (e) and (f) of that figure show the field of the two safes itself and what a row of pixels at the camera records of it, before any image is computed: readings of a few times $10^{-9}\,\mathrm{s}^{-2}$, of which the gold is a tenth. The empty room and the two safes are known and subtracted; what remains is 324 kg of gold, in one safe or the other, 3.5 m in front of the camera. A square array a metre across, of 11×11 pixels, reads the five components of $\mathcal{E}$ with white noise set by the SNR above for this mass at this depth. Asked only which safe holds the gold, the data answer quickly: the two possibilities give readings 1.8 standard deviations apart at $\mathrm{SNR} = 10$, so the camera is wrong 18% of the time, and $\mathrm{SNR} = 34$ makes it wrong once in a thousand. Some questions it cannot answer at any sensitivity: a sphere of gold and a point of the same mass give identical readings, as Newton showed. Others need more than it has: the bar's shape departs from a point's by only 0.6 standard deviations at $\mathrm{SNR} = 10^3$. Asked instead for an image that assumes little beyond mass lying in the plane of the safes, the same data weigh the contents of a safe only to within ±730 kg at $\mathrm{SNR} = 10^3$: the image cannot say where the gold is. The array is a small camera in the sense of Eq. (22), whose blur of about 33° is wider than the two metres between the safes, and a broad layer of mass has no tidal field at all. Appendix A gives the details, and the effect of tilting the array, which matters only through where its pixels are.

p. The positivity of mass. One fact is missing from that image: mass is never negative. A Gaussian image allows a cell to hold minus five hundred kilograms of gold beside one holding plus five hundred, and the near field cannot see the difference; that is where its large errors hide. Requiring every cell's mass to be positive, and assuming nothing else, the same data at $\mathrm{SNR} = 10^3$ put 316 ± 20 kg in the right-hand safe (the mean and spread over noise) and almost nothing in the left; at $\mathrm{SNR} = 10^4$, 328 ± 1 kg, the small excess being the cost of modelling a bar as a grid of points. This is the mathematics of super-resolution of positive sources [44, 45]: a scene made of a few compact masses is resolved down to separations that shrink as a power of the sensitivity, as for the two masses above, not as its logarithm. The logarithmic law of Eq. (21) is the limit for a scene crowded with mass; for an empty room holding a few objects, which is most of the scenes of this paper, positivity is the camera's most powerful prior, and it is one that the electrostatic analogue, whose charges have two signs, does not have.

q. Zeros of the shear above two buried masses. One exact feature survives the blur. Above two equal masses d apart, buried at any depth z greater than $\frac{\sqrt{3}}{2}d$, the shear of the tidal field in the plane of the array, $(\mathcal{E}_{xx} - \mathcal{E}_{yy}) + 2i\,\mathcal{E}_{xy}$, vanishes at exactly two points, on the perpendicular bisector of the pair (turned 90° from the line joining the masses) and exactly d apart, whatever the depth: with the masses at $x = \pm d/2$, on the bisector $x = 0$ the term $\mathcal{E}_{xy}$ vanishes by symmetry and $\mathcal{E}_{xx} - \mathcal{E}_{yy}$ is proportional to $y^2 - d^2/4$. Shallower than $\frac{\sqrt{3}}{2}d$, four more zeros appear off the bisector. The separation of the two zeros gives d directly, with no reconstruction (Fig. 12). Noise places each to within about $z^2/6\mathcal{R}d$, so they separate two masses once d exceeds about $z/\sqrt{6\mathcal{R}}$: the limit of *The precision of a simple scene*, above, now reached by inspection. For unequal masses the zeros move with depth, and their separation gives d only approximately.

r. Limits on sensitivity. The premise of arbitrary sensitivity eventually meets the rest of physics. A heuristic argument, not a theorem: a camera that fits within the distance z to the scene, without becoming a black hole, has a mass below $zc^2/2G$, so its energy of interaction with a source of mass M_s is below about $M_s c^2$. If quantum mechanics then limits how quickly the camera's state can become distinguishable to a rate set by that energy, as it does for a fixed coupling and a single measurement task, over a time τ we would have $\mathrm{SNR} \lesssim M_s c^2 \tau/\hbar$, with G and z cancelling. For a person watched for the age of the universe this is about 10^{70}, a blur of 1.5°. On this estimate no near-field camera could draw a face; making the estimate rigorous needs the coupling, the resources and the discrimination task to be stated exactly. The estimate is generous in another way: a camera of mass $zc^2/2G$ three metres away would pull on the person with 10^{15} times the Earth's gravity. Asking it to pull no harder than the Earth does lowers its mass, and the ceiling, by fifteen orders of magnitude, to 7×10^{54}, and widens the blur only from 1.5° to 1.9°.

Quantum mechanics sets a sharper limit when the scene is itself quantum. Hold a mass m behind a wall in a superposition of two places a distance d apart. The centre of mass of an isolated system cannot move, so the two branches differ in their quadrupole, about md^2, and a camera that read it before light from the place where the superposition is undone could arrive would learn which way the mass went faster than causality allows. The resolution of exactly this thought experiment [46, 47] is that the vacuum fluctuations of the field forbid localizing any probe to better than about a Planck length, which limits what a camera can learn in a given time, and that whenever it could learn enough, undoing the superposition radiates gravitons that carry the information away. A perfect camera is therefore a perfect source of decoherence:

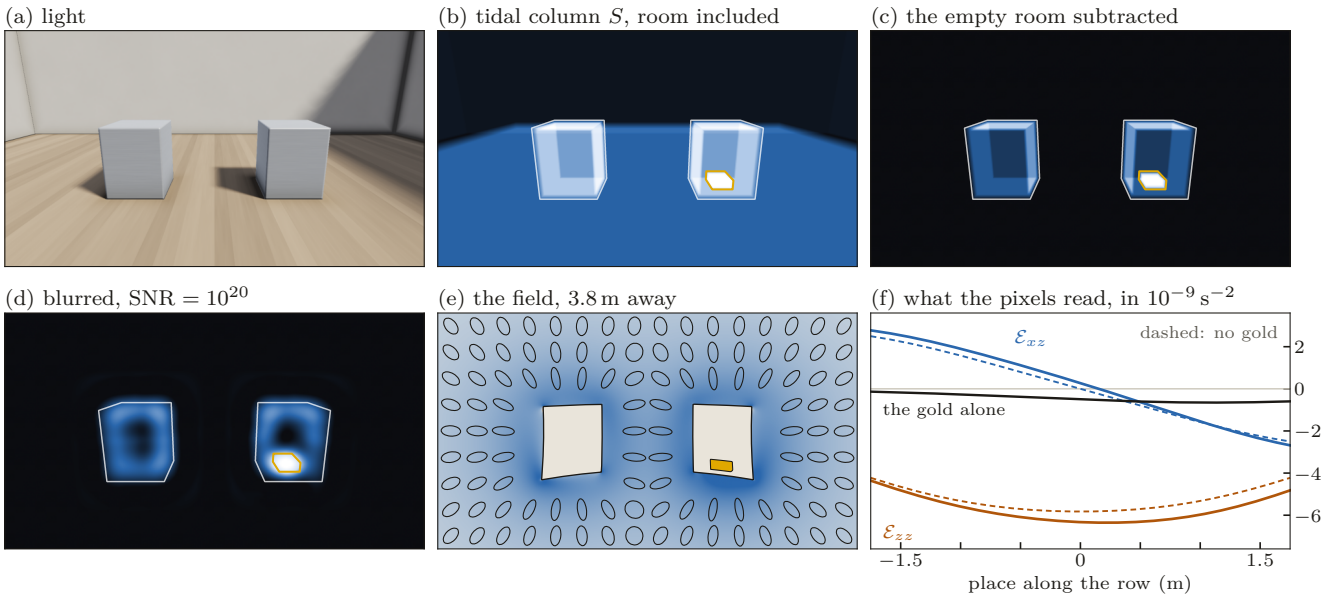


FIG. 11. The locked safe, computed. Two identical steel safes 3.5 m away; the right-hand one holds 324 kg of gold. (a) Ordinary light, from the same camera. (b) The tidal column $S(\hat{n})$ of Eq. (8), exact, with the floor and walls of the room included; white lines mark the outlines that light shows, and the yellow line the gold, which it does not. (c) The same with the empty room, which is known, subtracted. (d) Panel (c) blurred by the point spread of the Wiener reconstruction at a signal-to-noise ratio of 10^{20}, Eq. (21): the gold still stands out through the steel. Blurring S in this way treats the scene as if it lay at a single depth; it shows what an array as wide as the scene is deep could resolve, not a reconstruction from simulated data (*A worked case*, in the text). Panels (b)–(d) share one scale. (e) The tidal field of the two safes on a sphere 3.8 m about the camera, which passes through the middle of each, seen from the same camera, drawn as in Fig. 3: rings of free particles across the line of sight as the field distorts them (exaggerated, the strength compressed), over a map of the component along the line of sight, blue for squeeze and orange for stretch. Where the sphere cuts the safes it is drawn grey, and where it cuts the gold, yellow. (f) What the pixels read: two components of the tensor along a row of pixels 3.5 m long at the camera, with the gold (solid) and without it (dashed), and the gold's own part (black), at most 6.5×10^{-10} s^{-2}. These curves, with noise, are all that an image of the scene is computed from.

its picture of a quantum object through a wall ends the object's superposition.

s. The information in a near-field image. The resolution law says how fine the detail of a near-field image can be. A different question, the one Shannon asked of a telegraph line [48], is how much the image can say: how many bits the data carry about the scene. Equation (18) answers it with no further assumption. Each Fourier component of the scene reaches the array as a signal in additive Gaussian noise, standing above it by the ratio s of Eq. (19), and components with different $\mathbf{k}$ are independent. A real signal in Gaussian noise with power ratio s^2 carries at most $\frac{1}{2}\log_2(1+s^2)$ bits, a bound reached when the signal is itself Gaussian, and a scene of area A has $A\,\mathrm{d}^2k/(2\pi)^2$ real components in each d^2k. Per area z^2 of the scene, with $q = kz$, the data therefore hold

$$C = \frac{1}{4\pi}\int_0^\infty q\,\log_2\!\left(1+\pi^2\mathrm{SNR}^2 q^2 e^{-2q}\right)\mathrm{d}q \qquad (23)$$

bits about any scene with the spectrum of the prior of Eq. (19), and a scene made of point masses carries somewhat less. Where $s > 1$, which is for q between about $1/\pi\mathrm{SNR}$ and q_c, the logarithm is close to $2\log_2 s$; elsewhere it is small. Integrating $2q\log_2 s$ over that range, with $\ln(\pi\mathrm{SNR}) = q_c - \ln q_c$ from Eq. (20), gives

$$C \approx \frac{q_c^3/3 - q_c^2/2}{4\pi\ln 2} \qquad (24)$$

to within three per cent for $\mathrm{SNR} \geq 10^3$ and half a per cent beyond 10^{10}.

The two terms have a plain reading. The patterns that survive the noise are the components with $q < q_c$, and there are $q_c^2/4\pi$ of them per area z^2; the rest of Eq. (24) is the number of bits each carries on average, $(q_c/3 - \frac{1}{2})/\ln 2$, the mean of $2\log_2 s$ over them. Greater sensitivity gives both more patterns and more bits in each, so with $q_c \approx \ln\mathrm{SNR}$ the information grows, eventually, as $(\ln\mathrm{SNR})^3/12\pi\ln 2$: as the cube of the logarithm of the sensitivity. At $\mathrm{SNR} = 10^3$ a near-field picture holds 38 bits per area z^2, about nine patterns of four bits each. At 10^6 it holds 200 bits; at 10^{30}, 1.6×10^4. At the heuristic ceiling of the previous paragraph, a person watched for the age of the universe, it holds 1.8×10^5 bits, some 22 kilobytes, spread over 2,200 patterns of 80 bits each: about the size of a thumbnail photograph,

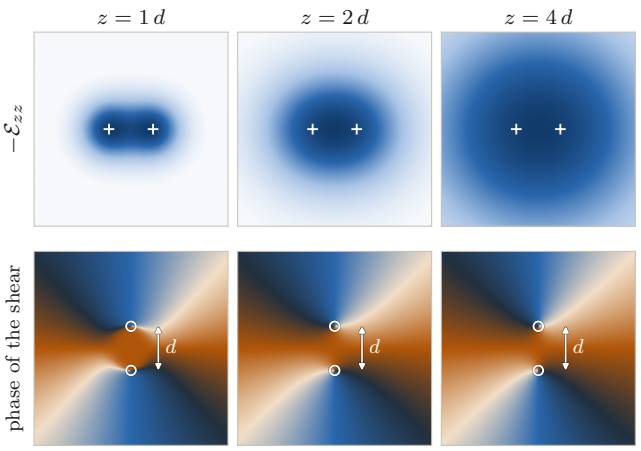


FIG. 12. The zeros of the shear above two buried masses. Two equal masses d apart (crosses) lie at depth z below the plane of a camera; each panel spans $4.4\,d$ of that plane. Top: the ordinary near-field picture, $-\mathcal{E}_{zz}$, which blurs into one as z grows. Bottom: the phase of the shear in the plane, $(\mathcal{E}_{xx} - \mathcal{E}_{yy}) + 2i\,\mathcal{E}_{xy}$, which turns once around each of two zeros (circles). The zeros lie on the perpendicular bisector of the pair, exactly d apart at every depth greater than $\frac{\sqrt{3}}{2}d$.

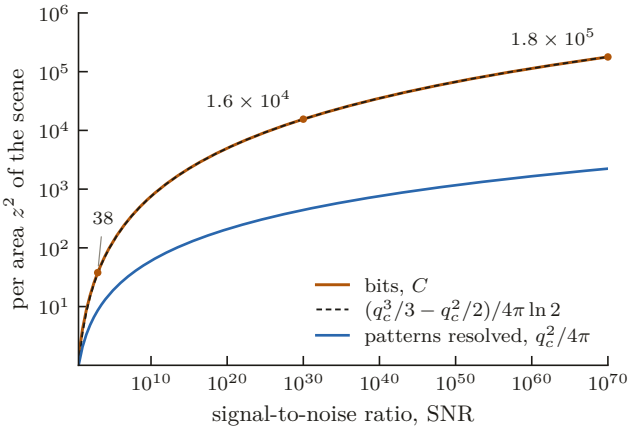


FIG. 13. The information in a near-field picture, per area z^2 of the scene, against the signal-to-noise ratio. Orange: the bits the data carry about the scene, Eq. (23). Dashed: the closed form of Eq. (24), which lies on it. Blue: the number of independent patterns resolved, $q_c^2/4\pi$. Raising the sensitivity by sixty-seven orders of magnitude, from 10^3 to 10^{70}, raises the information only from 38 bits to 1.8×10^5, about 22 kilobytes.

after sixty-seven orders of magnitude more sensitivity (Fig. 13). This is also why a blurred image and a precise measurement are compatible. The data hold few bits, and a scene known to be simple spends them all on a few numbers.

The camera's other channels scale differently, and the comparison shows what is peculiar to the near field. A wave camera of width D at wavelength λ resolves about $(D/\lambda)^2$ directions in each steradian, and each carries about $\log_2 \mathrm{SNR}$ bits: the aperture fixes the number of patterns, and sensitivity adds bits only in proportion to its logarithm. In the near field there is no aperture to fix the number of patterns; sensitivity sets it through e^{-kz}, and that is why the power is three rather than one. A single pixel, at the other extreme, is limited by geometry rather than noise: from a sky of many overlapping sources it learns twenty-five numbers of its brightness, sixty-eight with polarization, however sensitive it is (Section VIII). And the thermal glow, recorded by counting gravitons, is limited by their number: N gravitons over M resolution cells carry at most about $N \log_2 M$ bits. A camera a metre square looking down at the Earth for a year counts about 1,800 of them in the model of Section IX, so its picture of the planet's interior holds a few kilobytes at any reasonable resolution.

The logarithmic limit is the central result for the whole subject. The near field is where everyday things are visible, and it can never be sharp. Sharp images need waves.

V. WAVES FROM MOVING BODIES

Outside the near zone a source of mass quadrupole moment $Q_{ij}(t)$ produces the strain

$$h_{ij}^{\mathrm{TT}}(t, r) = \frac{2G}{c^4 r}\, \ddot{Q}_{ij}^{\mathrm{TT}}\left(t - \frac{r}{c}\right), \tag{25}$$

and radiates the power $P = (G/5c^5)\,\langle \dddot{Q}_{ij}\, \dddot{Q}_{ij} \rangle$. For two masses m a distance d apart, turning about their centre at angular velocity Ω,

$$P = \frac{8}{5}\,\frac{G m^2 d^4\, \Omega^6}{c^5}. \tag{26}$$

Two one-kilogram masses a metre apart, spun sixteen times a second, radiate 4.5×10^{-41} W: one graviton every fifteen years.

a. A compact body is a point. The waves of Eq. (26) have twice the rotation frequency, so their wavelength is $\lambda = \pi c/\Omega$, while the masses move at $v = \Omega d/2$. Hence

$$\frac{\lambda}{d} = \frac{\pi}{2}\,\frac{c}{v}, \tag{27}$$

and the same holds, up to a factor of order one, for any body whose parts move at speed v through distances comparable with its size. The wavelength then exceeds the body by the factor by which light outruns it. No aperture can resolve an object much smaller than the wavelength it is seen by, so a compact, slowly moving body is a point in its own radiation. The exceptions are sources whose motion is small compared with their size: a large body vibrating with small amplitude, or many small sources driven in step, can be larger than its wavelength and show a form (Eq. (28) below).

b. A source larger than its wave. Far from any source, of whatever size and speed, the wave is

$$h_{ij}^{\mathrm{TT}}(\omega, R\hat{n}) = \frac{4G}{c^4 R}\, e^{i\omega R/c}\, \Lambda_{ij,kl}(\hat{n})\, \tilde{T}_{kl}\!\left(\omega, \frac{\omega \hat{n}}{c}\right), \quad (28)$$

with Λ the transverse traceless projection and $\tilde{T}_{kl}(\omega, \mathbf{k}) = \int T_{kl}\, e^{i\omega t - i\mathbf{k}\cdot\mathbf{x}}\, \mathrm{d}t\, \mathrm{d}^3x$: each direction carries one Fourier component of the stress, on the sphere $|\mathbf{k}| = \omega/c$. A camera at distance R whose aperture D spans the directions within D/R of the source reads a cap of that sphere, and so sees the source with detail $\lambda R/D$, as any aperture does. A compact source is the point $\mathbf{k} \to 0$, Eq. (25). The simplest source larger than its wave is many compact ones driven in step, such as the generators of a continental power grid, which turn together over distances greater than the 3000 km wavelength of their waves. Its wave is that of one rotor times the sum $\sum_s e^{-i\phi_s - i\omega\hat{n}\cdot\mathbf{x}_s/c}$ over their positions and phases. Close together they add their amplitudes, and N rotors radiate N^2 times the power of one; far apart they add their powers, N times. Such a source does show its form, but the camera must undo, for each point of the source, the delays from that point, not those of a plane wave, because an aperture wide enough to resolve it lies in its Fresnel zone, $D^2 \gg \lambda R$; and two sources in step are separated only once $D \gtrsim 1.4\,\lambda R/s$ for a separation s, against about $\lambda R/s$ for sources that are not, the familiar penalty of imaging in coherent light.

c. The polarization of an unresolved source. The radiation is not the same in all directions, and it is polarized (Fig. 14). Along the axis of rotation it is strongest and circularly polarized, with the handedness of the rotation; in the plane of rotation it is eight times weaker and linearly polarized. From the polarization alone, a camera can read the axis and sense of a rotor it cannot resolve.

d. The sense of turning. Let the rotor's angular velocity make the angle ι with the direction from the rotor to the camera. At twice the rotation frequency the two polarizations of its wave have amplitudes

$$h_+ = A\,\frac{1+\cos^2\iota}{2}, \qquad h_\times = A\cos\iota, \qquad A = \frac{4G\,\Delta I\,\Omega^2}{c^4 r}, \quad (29)$$

a quarter of a cycle apart, $h_+(t) = h_+ \cos 2\Omega t'$ and $h_\times(t) = h_\times \sin 2\Omega t'$ with $t' = t - r/c$, measured on axes across the line of sight one of which lies along the projection of the spin (on axes turned by an angle ψ the two mix as a spin-2 pair, while I and V below do not change), where ΔI is the difference between the two principal moments of inertia in the plane of rotation ($md^2/2$ for the pair of Eq. (26)). The pattern of stretching that passes over the camera therefore turns, and the share of the signal that is circularly polarized, the ratio of the Stokes parameters V and I,

$$\frac{V}{I} = \frac{2\,h_+ h_\times}{h_+^2 + h_\times^2}, \quad (30)$$

is positive when that pattern turns anticlockwise as the camera sees it, which is the sense in which the rotor itself appears to turn. It is $+1$ seen along the spin ($\iota = 0$, the rotor turning anticlockwise as seen), -1 seen against it, and zero edge-on. The camera reads the sense of rotation from the sign of V and the tilt of the axis from its size, without resolving the rotor at all (Fig. 15).

e. What does not radiate. The source of the wave field is the part of the stress that is transverse to the line of sight and has no trace. Steady motion in a straight line radiates nothing: its quadrupole grows, but with a constant second derivative, and only a change in that radiates. Nor does anything that keeps spherical symmetry, however violently it pulsates, or a wheel turning steadily about its axis of symmetry, whose arrangement of mass does not change. And a pressure that is the same in all directions is pure trace: it is removed exactly by the projection in Eq. (25), a statement we have verified numerically. The camera sees shear and lopsided motion, not pressure.

Because everyday speeds are so far below that of light, these effects cannot be shown at human scale. A pair of balls turning once a second radiates waves 150,000 km long, and a room is deep inside their near zone. Figure 16 is therefore drawn with the speed of light, and of gravity with it, set to twenty centimetres a second. The waves are then ten centimetres long, an array a metre and a half across resolves them to 4°, and each rotor appears as a spot. The change rescales the wavelength for display and nothing else; it is not a consistent world. The balls of the figure move at 1.4 m/s, seven times faster than the slowed light, where Eq. (26) would not hold. Brightness is shown on a relative scale, and the polarization is that of Eq. (30), which does not depend on the speed of light: what the spot's colour says about the sense of turning is the same at any speed.

VI. THE THERMAL GLOW

Sharp images need wavelengths shorter than the scene, and the only motion in ordinary matter fast enough is thermal. At room temperature it radiates at wavelengths of tens of micrometres, the same as thermal infrared light, so a gravitational camera working there could be as sharp as an infrared one.

a. Absorption. A gravitational wave crossing a medium shears it at the rate $\frac{1}{2}\dot{h}_{ij}$. A medium of shear viscosity η resists with a stress $-\eta\,\dot{h}_{ij}$, which acts back on the wave as a source. The wave equation becomes

$$\ddot{h}_{ij} + \frac{16\pi G\,\eta}{c^2}\,\dot{h}_{ij} - c^2\nabla^2 h_{ij} = 0, \quad (31)$$

so the wave's energy decays at the rate $16\pi G\eta/c^2$, the result found by Hawking [49]. Per unit length this is an absorption coefficient

$$\alpha = \frac{16\pi G\,\eta}{c^3}. \quad (32)$$

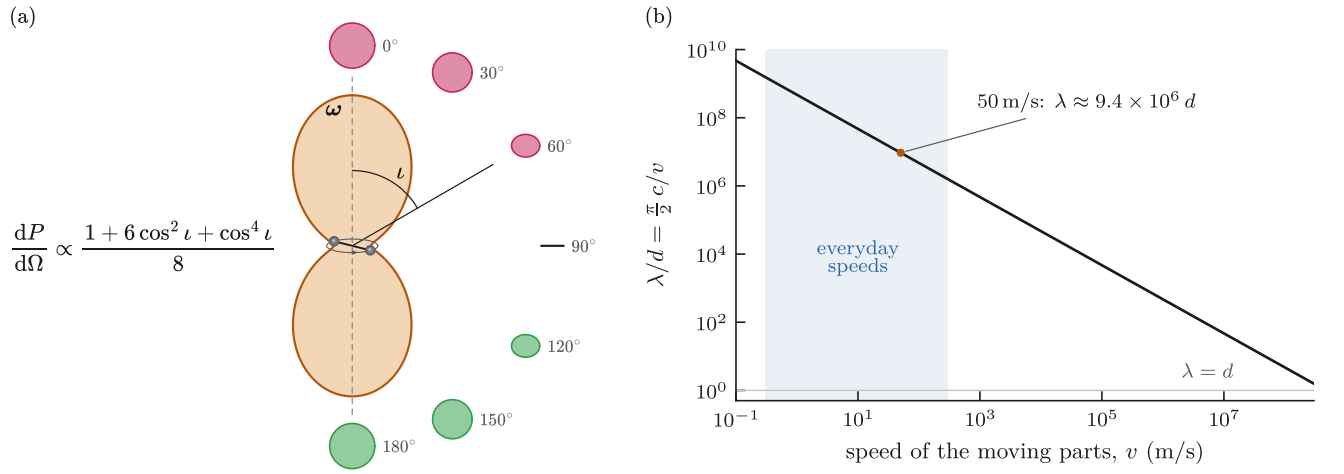


FIG. 14. Radiation from a spinning pair of masses. (a) The power sent in each direction, $(1 + 6\cos^2\iota + \cos^4\iota)/8$, against the angle ι from the spin $\boldsymbol{\omega}$, drawn as a curve in a plane containing the spin: strongest along the axis and eight times weaker in the plane of the orbit. Around it, at every 30°, the polarization an observer there sees, face on: an ellipse with semi-axes in proportion to $(1 + \cos^2\iota)/2$ and $|\cos\iota|$, filled magenta where the pattern of stretching turns anticlockwise as that observer sees it ($V/I > 0$) and green where it turns clockwise, as in Fig. 16, and as strongly as its circular share $|V/I|$ (Eq. (30)); in the plane of the orbit the wave is linearly polarized (a line). The pair at the centre is schematic. (b) The wavelength over the size of the source, Eq. (27), against the speed of its moving parts: for anything moving at everyday speeds the wavelength is millions of times the size of the body.

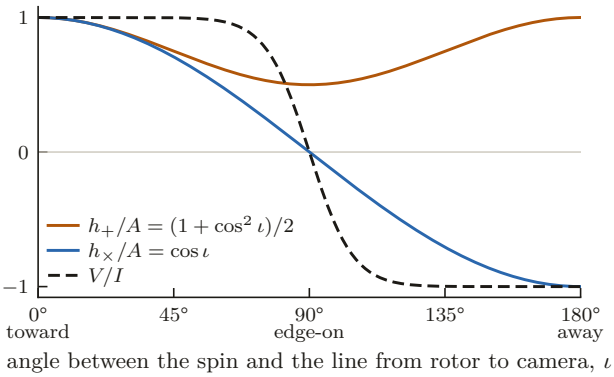


FIG. 15. The wave of a rotor seen from different directions: the amplitudes of its two polarizations, Eq. (29), and its circular share V/I, Eq. (30), against the angle ι between the spin and the direction of the camera. V/I is ± 1 along the axis and changes sign edge-on, where the wave is linearly polarized: its sign gives the sense of rotation, its size the tilt.

Here η is the friction at the frequency of the wave; a viscosity measured by stirring says little about a material's response at the 10^{13} cycles a second of heat, as we discuss below. For water's everyday viscosity, $\alpha \approx 10^{-37}\,\mathrm{m}^{-1}$: a wave would cross nearly 10^{21} light-years of water before losing much of its energy.

b. Emission. A medium that absorbs must also emit. With the Planck radiance $B_\omega(T) = \hbar\omega^3/[4\pi^3c^2(e^{\hbar\omega/k_BT} - 1)]$, summed over the two polarizations, Kirchhoff's law gives the power radiated per unit volume, solid angle and frequency,

$$j_\omega = \alpha(\omega)\, B_\omega(T), \tag{33}$$

where α is the net absorption coefficient, absorption less stimulated emission, and j_ω the spontaneous emission. The same expression follows directly from the thermal fluctuations of shear stress in a viscous fluid, with the stress correlator taken in the unsymmetrized (Wightman) order that the fluctuation–dissipation theorem relates to $\mathrm{Re}\,\eta$. For long wavelengths it is the known result that a thermal plasma radiates gravitational waves in proportion to its shear viscosity [50], and the same law has been applied to the non-relativistic plasma inside the Sun, as one part of its gravitational spectrum [10]. What we add is its application to the solids and liquids around us, whose friction at the frequencies of heat is not that of a plasma.

For the image this means the following.

- *Matter is transparent.* With α so small, nothing absorbs or scatters. A pixel receives the sum of the glow of everything along its line of sight (Fig. 17), and there are no shadows. Against a background of radiance I_{bg}, a body of optical depth τ changes what a pixel receives by $(B_\omega - I_{\mathrm{bg}})(1 - e^{-\tau})$, which for ordinary matter is its own glow, τB_ω, less a negligible dimming of what lies behind.

- *Brightness is temperature times high-frequency friction.* What sets a material's glow is how strongly it resists being sheared at the frequencies of heat, which can be very different from its everyday viscosity (see *Friction at the frequencies of heat*, below).

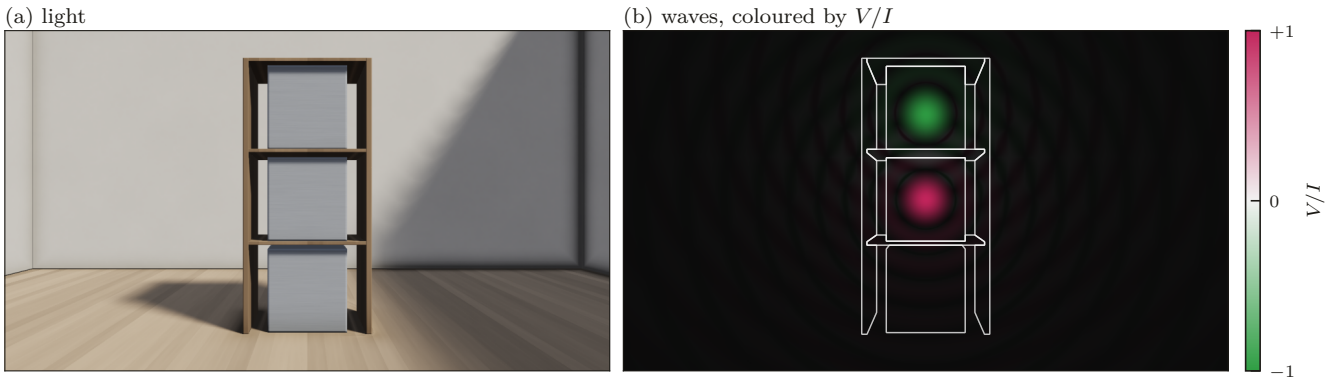


FIG. 16. Which way it turns, computed with the speed of light set to 20 cm/s, so that the waves are 10 cm long and an array 1.5 m wide can resolve the boxes. Three sealed steel boxes on a shelf; in the top and middle ones a pair of balls turns once a second, in opposite senses, and the bottom pair is still. (a) Ordinary light, from the same camera: the boxes are sealed and look the same. (b) The waves: each turning pair is an Airy spot, Eq. (43), and the still pair is dark; the colour is the circular share V/I of Eq. (30), magenta where the pattern of stretching turns anticlockwise as the camera sees it and green where it turns clockwise. At the true speed of light the waves are 1.5×10^8 m long and nothing is resolved, but the polarization still gives the sense of turning.

- *The glow is faint.* A person radiates about 10^{-36} W this way: one graviton in two hundred million years.

Figure 18 shows the transparency at work. Two closed steel furnaces hold the same block of iron, one at room temperature and one at 1500 K. They look the same and, to within the mass of their heat ($\Delta U/c^2$, about 10^{-11} kg per megajoule [51]), weigh the same, so neither light nor the near field can tell them apart at any ordinary sensitivity; the hot iron glows through the steel. If the friction depended neither on frequency nor on temperature, the number of gravitons emitted would grow as T^3 and the hot block would outshine the cold one more than a hundredfold; the next paragraph explains why, for a material whose stresses simply relax, this is an upper estimate.

c. Friction at the frequencies of heat. Equation (32) holds when the wave is slower than the processes that produce viscosity. At the frequencies of heat that is rarely so, and η must be replaced by the dissipative part of the material's shear response at the frequency of the wave, the real part of its dynamic viscosity, $\operatorname{Re}\eta(\omega)$ [52]. A simple model shows how much this matters. A liquid whose stresses relax in a time τ (Maxwell's model) has

$$\operatorname{Re}\eta(\omega) = \frac{\eta_0}{1+\omega^2\tau^2}, \tag{34}$$

so its everyday viscosity η_0 survives only below $\omega \approx 1/\tau$. Above it the friction falls as $\eta_0/(\omega\tau)^2 = G_\infty^2/\eta_0\omega^2$, where $G_\infty = \eta_0/\tau$ is the liquid's stiffness against sudden shear: at a given stiffness, the more viscous liquid glows the less. Honey is viscous because its molecules rearrange slowly; at the frequencies of heat that rearrangement is frozen, and honey need not outshine water at all. In dense matter the friction at those frequencies comes from much faster processes. A wave's wavenumber is about 10^{-5} of that of a sound wave of the same frequency, so

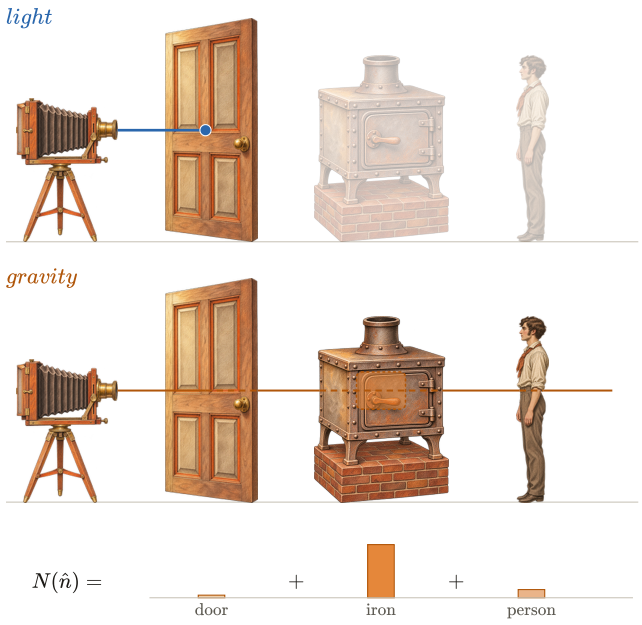


FIG. 17. Two ways of forming a picture. A camera's line of sight passes through a closed door, a closed iron furnace with a hot iron block inside, and a person. In light it ends where it meets the door's face (the dot): a pixel reports one point. Gravitational radiation passes through everything, so the line runs on, dashed where a body hides it, and the hot block shows through the furnace's walls. The pixel reports the sum along the whole line, Eq. (69): each body k adds its number emissivity $j_{N,k}$ times the length ℓ_k of the line inside it, shown below for illustrative values in which the hot iron is far the brightest and the door, crossed only through its thickness, adds little. The objects are illustrations, and their sizes are chosen so that one level line crosses the middle of each.

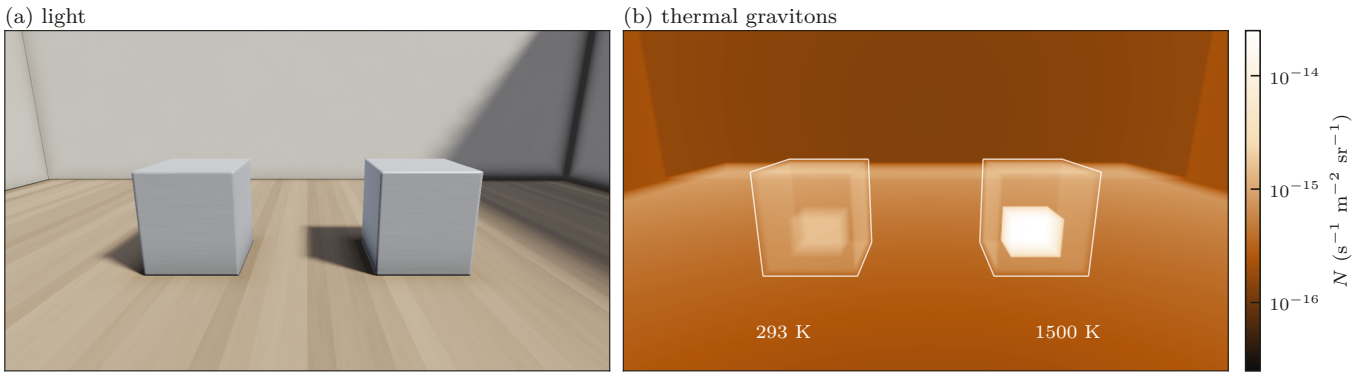


FIG. 18. The closed furnace, computed. Two closed steel furnaces hold the same block of iron, one at 293 K and one at 1500 K. (a) Ordinary light: the two are identical. (b) The expected thermal number radiance, Eq. (69), from the same camera, on a logarithmic scale, with the outlines that light shows. Both blocks show through their steel, since the air about them does not glow, and the hot one is sixteen times the brighter through its middle (twenty-two without the glow of the floor behind them). The room itself glows faintly, brightest where a line of sight crosses the floor at a slant. Iron and steel have the friction of iron in Table III, falling as $1/T$ in the hot block; silica glass stands for the concrete and the plaster.

it shears a material uniformly and cannot make a single sound quantum inside it, which is why a lossless solid absorbs only at its surface. By the fluctuation–dissipation theorem $\operatorname{Re}\eta(\omega)$ is the spectrum of the material's stress at zero wavenumber, and causality fixes its integral [53]:

$$\frac{2}{\pi}\int_0^\infty \operatorname{Re}\eta(\omega)\,\mathrm{d}\omega = G_\infty - G_0, \tag{35}$$

the part of the stiffness against shear that relaxes. Here G_∞ resists a shear too fast for the atoms and the free electrons to follow, and G_0 a slow one; for Maxwell's model the integral is G_∞. At the frequencies of heat the friction is roughly the stiffness that relaxes there divided by the band over which it does so (Table III, Fig. 19).

Free electrons. In a metal a shear deforms the electrons' Fermi sphere, and collisions relax it in a time τ: $\operatorname{Re}\eta = \frac{1}{5}nmv_F^2\,\tau/(1+\omega^2\tau^2)$, with n the density of conduction electrons, m their mass and v_F their Fermi speed. Its integral in Eq. (35), the weight of the channel, is $\frac{2}{5}nE_F$ with E_F the Fermi energy, 38 GPa in copper, and with its collision time, 2.5×10^{-14} s [54], $\omega\tau$ is about one at the frequencies of heat, where the electrons dissipate most: whatever τ, the friction cannot exceed $\frac{1}{10}\,nmv_F^2/\omega$. For iron, whose electrons are not free, we give that bound: an envelope over every collision time, not the spectrum of any one metal.

Driven vibrations. In a crystal with two atoms in its cell a uniform shear pushes one set of atoms against the other [55], and so drives the optical vibration seen in Raman scattering; single-phonon absorption of high-frequency waves has been computed for crystal detectors [56]. Silicon glows in a line at 520 cm^{-1} (15.6 THz), where its friction, 0.03 Pa s, is thirty times the placeholder, a constant friction of 10^{-3} Pa s used here for comparison. The line's weight is the stiffness the shear loses when the atoms relax, $M\omega_0^2\zeta_K^2/8a = 30$ GPa, with M the atomic mass, ω_0 the line, a the cubic lattice constant and $\zeta_K =$ 0.54 Kleinman's parameter. Only three of a wave's five shears drive the line, so averaged over directions its weight is 18 GPa. The line's glow is therefore polarized, and its brightness depends on the direction of view in the crystal: seen along a cube edge it is fully linearly polarized; along a face diagonal, 5/4 as bright and 60% polarized; along a body diagonal, 4/3 as bright and unpolarized. A thermal image of a crystal shows how it is oriented. In a glass, disorder lets a uniform shear drive every vibration [57, 58]; in silica the weight is about the shear modulus [59], spread over the band below 27 THz. In water the stretching of hydrogen bonds near 8 THz and the rocking of the molecules carry it [60]: the friction there, 2×10^{-4} Pa s, is a third of the steady viscosity of the same model of water, 7×10^{-4} Pa s.

Pairs of phonons. Even in a harmonic crystal the uniform part of the stress is quadratic in the atoms' displacements $\mathbf{u}$: integrated over the volume it is $\frac{1}{2}\,\mathrm{d}^2/\mathrm{d}t^2\sum mu_xu_y$, summed over the atoms, which oscillates at sums of two phonon frequencies. A wave thus makes and unmakes pairs of phonons of opposite momentum, up to twice the highest phonon frequency. This weak channel, of classical weight $2nk_BT$ with n the number of atoms per volume, about a gigapascal at room temperature (the values of Table III keep the quantum occupations, which matter for diamond, whose Debye temperature is 2200 K), is the only one in an insulating crystal with one atom in its cell; anharmonicity changes it by a factor of order one, and it makes an eighth of diamond's glow. Akhiezer's damping of sound, the relaxation of the thermal phonons in a time τ, puts a similar weight near zero frequency; at a frequency ω its tail is smaller than the pair band by about $\omega_D\tau\,(\omega/\omega_D)^4$, with $\omega_D\tau$ a thermal phonon's quality factor.

At room temperature these materials glow at one to sixty per cent of the placeholder's power (Table III): 10^{-3} Pa s is an upper estimate, and 10^{-4} Pa s is typical.

Material	Source of friction	η_{eff}	P/V	$\bar{E}/k_BT$
Copper	electrons	1.3	2.8	1.4
Iron	electrons (bound)	≤ 6	≤ 12	1.5
Silicon	Raman line	1.6	3.4	2.6
Diamond	Raman line, pairs	0.12	0.25	6.4
Silica glass	all vibrations	2.3	4.8	2.1
Water	hydrogen bonds	0.54	1.1	1.7
Placeholder		10	21	2.70

TABLE III. The thermal glow of real materials at 293 K: what dissipates a uniform shear at the frequencies of heat; η_{eff}, the constant friction that would give the same power, in 10^{-4} Pa s; the power per volume, $4\pi\int j_\omega\,\mathrm{d}\omega$, in $10^{-35}\,\mathrm{W\,m^{-3}}$; and the mean energy of the gravitons. Copper: one conduction electron per atom at its lattice constant [62], with the collision time of its conductivity [54]. Iron: its volume per atom [63] and two conduction electrons per atom. Silicon and diamond: lattice constants, elastic constants and Kleinman's parameters as compiled by [55], Raman lines and widths from [55, 64, 65], each line counted for three of the five shears, its share averaged over directions. Silica: the simulated glass of [58, 59]. Water: the simulated spectrum of [60]. The pair bands use the Debye temperatures of copper and of steel [61], and those of silicon and diamond that follow from their elastic constants.

In every solid larger than 30 nm the volume outshines the glow of a lossless surface, Eq. (37) below. A person, taken as 70 litres of water at 310 K, radiates 9×10^{-37} W: one graviton in 2×10^8 years. Metals and water glow redder than a constant friction would; silicon glows in its line, and diamond, whose line lies in the Wien tail, glows bluer. The spectrum of the glow therefore records a material's mechanical losses, a kind of gravitational colour, and with a frequency-dependent friction the number emissivity must be computed as $j_N=\int\alpha(\omega)\,B_\omega\,\mathrm{d}\omega/\hbar\omega$ rather than by dividing the power by $2.70\,k_BT$. When a metal's collision rate is proportional to temperature, as it is above the Debye temperature [61], $\omega\tau$ at the peak of the glow stays fixed and the friction falls as $1/T$, so the power grows as T^3 and the number of gravitons as T^2: by this estimate the hot iron of Fig. 18 sends about 25 times as many gravitons as the cold, not more than a hundred.

These estimates hold to about a factor of two: the Drude form ignores that the collision rate depends on frequency once $\hbar\omega$ exceeds the phonon energies, Debye's spectrum smooths the peaks of the real one, the glass's weight assumes that shear relaxes as uniaxial strain does in simulation [59], and the water spectrum comes from a classical simulation of rigid molecules [60]. Quartz, with many atoms in its cell, should be driven like the glass [58], and with it most rock; soft tissue should glow like water.

d. A bound on the glow. The sum rule caps the glow of every material. Its friction is positive and its integral fixed by Eq. (35), so a relaxing stiffness $\Delta\mu=G_\infty-G_0$ emits the most when all of it sits where the Planck spectrum peaks:

$$\frac{P}{V}\leq 11.37\,\frac{G\,\Delta\mu\,(k_BT)^3}{\hbar^2c^5},\qquad \frac{\dot N}{V}\leq 5.18\,\frac{G\,\Delta\mu\,(k_BT)^2}{\hbar^2c^5},\tag{36}$$

the constants being eight times the largest values of $x^3/(e^x-1)$, at $x=\hbar\omega/k_BT=2.82$, and of $x^2/(e^x-1)$, at $x=1.59$. At room temperature 30 GPa radiates at most $5.6\times10^{-35}\,\mathrm{W\,m^{-3}}$. Silicon, whose line lies close to the best frequency, reaches 98% of the power its own weight allows; silica 69%, water 40%, copper 39%, and diamond, whose line is in the Wien tail, 16%. The same weight limits absorption: the optical depth of a path of length L, integrated over frequency, is $8\pi^2GL\,\Delta\mu/c^3$, which for a metre of 30 GPa is $6\times10^{-24}\,\mathrm{s^{-1}}$, so no material is opaque over any band of useful width (Section VII). It is the rule by which the cross-section of a resonant bar, integrated over frequency, depends only on its mass and the speed of sound in it [66]. And the placeholder friction is not a material at high temperature: to glow as brightly as 10^{-3} Pa s, a material needs 110 GPa of relaxing stiffness at room temperature and 2.1 TPa at 5500 K, several times the shear stiffness of diamond (Section IX).

Temperature cannot be read from the glow alone: a different temperature with a different friction spectrum gives the same j_ω, so a thermal gravitational image measures temperature only when the material's response is known from elsewhere.

e. Volume and surface emission. Thermal radiation from the vibrations of a solid has been calculated before [67–69]; for an elastic sphere without internal damping its strength was found to grow with the sphere's surface, not its volume. Which channel wins should depend on how far a sound wave travels before it is damped: where that distance is much shorter than the body, as in most solids at room temperature, the volume emission of Eq. (33) should dominate, while a cold, pure crystal might glow at its surface. Both can be computed. In an elastic body without loss a wave is absorbed only where the stiffness changes, at the surface, where it launches sound [70]; for a sphere below its Debye temperature the thermal glow that follows is [69]

$$L_S=4\pi R^2\,\frac{\pi^2}{24}\Big(1+\frac{3c_T}{2c_L}\Big)\frac{G\rho\,c_T^3\,(k_BT)^2}{\hbar c^5},\tag{37}$$

with c_T and c_L the speeds of shear and compressional sound. By Kirchhoff's law this is the glow of a surface that absorbs the fraction $\pi^2(1+3c_T/2c_L)\,G\rho c_T^3/c^3\omega^2$ of a wave, which is Dyson's absorption with its constant. Friction inside, $\mathrm{Re}\,\eta=\rho c_T^2/\omega Q$ for sound of quality factor Q, makes the volume glow by Eq. (33); since this friction falls as $1/\omega$, the power grows as T^3 rather than T^4, with $L_V=V\,32\zeta(3)\,G\rho c_T^2(k_BT)^3/\pi c^5Q\hbar^2$, and

$$\frac{L_V}{L_S}=\frac{256\,\zeta(3)}{\pi^3\,(1+3c_T/2c_L)}\,\frac{R}{\ell_s},\tag{38}$$

where $\ell_s=Q\hbar c_T/k_BT$ is the distance a thermal phonon travels before it is damped; the prefactor is 5.5 for steel.

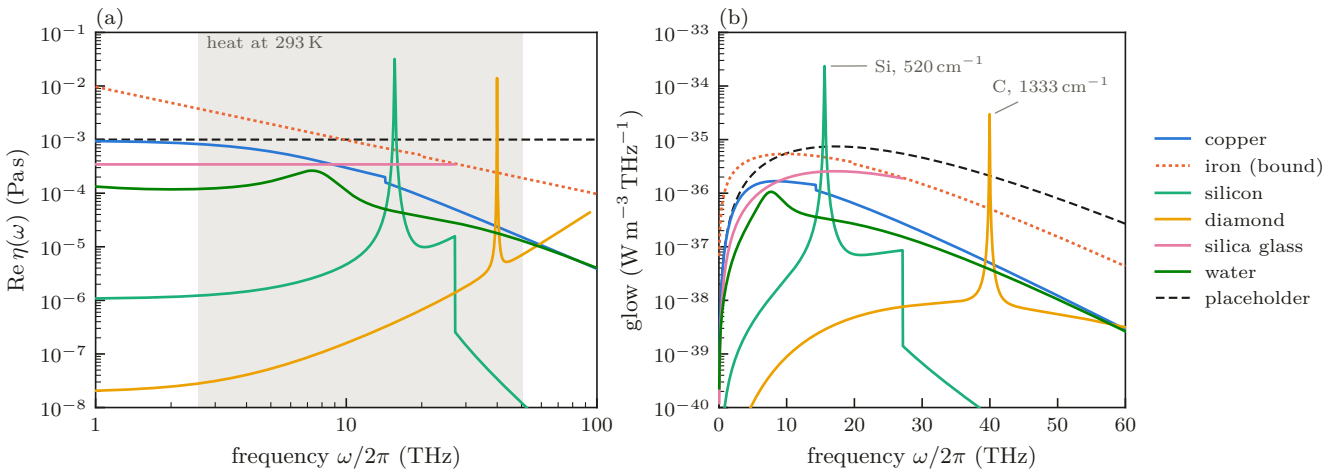


FIG. 19. The friction and the glow of real materials. (a) The friction against a uniform shear, $\mathrm{Re}\,\eta(\omega)$, of the materials of Table III at 293 K; the shaded band is where the Planck radiance exceeds a tenth of its peak. Copper and iron (dotted: the bound for free electrons) relax their electrons; silicon and diamond have lines at their Raman frequencies, drawn as damped oscillators of the measured widths whose far wings are not modelled; the steps are where pair bands end; silica glass is spread evenly over its band; water's friction rises where its hydrogen bonds stretch. (b) The glow they send, $4\pi j_\omega$ per unit of frequency, Eq. (33), with the placeholder's for comparison.

Thermal phonons in solids at room temperature travel nanometres, so ordinary bodies glow through their volume: a steel ball of radius 10 cm at room temperature glows 10^{-46} W from its surface and, with $Q \approx 10$ for its thermal phonons, 7×10^8 times more from its volume. A pure crystal cooled until its phonons cross it glows at its surface, in proportion to T^2 rather than T^3, as Dehnen, Romero and Schäfer found.

VII. A CAMERA WITHOUT A LENS

a. The optical constants of matter. The gravitational field of matter of density ρ changes the speed of a gravitational wave of angular frequency ω by the fraction [71]

$$n - 1 = \frac{2\pi G\rho}{\omega^2}, \tag{39}$$

where n is the refractive index; for steel at 1 kHz this is 10^{-13}, and it falls as the square of the frequency. The matter's own response adds less still: stiffness changes the square of the wave number by the fraction $16\pi G\mu/c^2\omega^2$, for a shear modulus μ [72], and matter without stiffness, free to move with the wave, responds only through the spread of its velocities, a fraction of order $(v/c)^2$ as large [73]. A steel lens a metre thick would bring such a wave to a focus only some 10^{13} metres away, beyond the orbit of Pluto; and since the wave is three hundred kilometres long, a lens able to act on it at all would have to be far larger. Reflection needs stiffness: a steel wall, however thick, reflects the amplitude $4\pi G\mu/c^2\omega^2 = 2 \times 10^{-23}$ of a kilohertz wave, and 4×10^{-46} of its energy. Absorption is weaker still (Section VI).

A mass does bend passing waves by its gravity, exactly as it bends light, by the angle $4GM/bc^2$ for a ray passing at distance b. Used as a lens, the Earth has a focal length of fifteen thousand times the distance to the Sun, and a focal ratio near 2×10^8. In each case the strength of the effect is set by the same number, the compactness $\mathcal{C} = GM/Rc^2$ of the body, which is 7×10^{-10} for the Earth and of order one only for a black hole. For a uniform body of radius R, whose shear sound travels at c_T with quality factor Q, crossed by a wave of reduced wavelength $\bar\lambda = c/\omega$,

$$\Delta\phi = 3\,\mathcal{C}\,\frac{\bar\lambda}{R}, \qquad |r| = 3\,\mathcal{C}\Big(\frac{c_T}{c}\Big)^2\Big(\frac{\bar\lambda}{R}\Big)^2,$$
$$\tau = \frac{24\,\mathcal{C}}{Q}\Big(\frac{c_T}{c}\Big)^2\frac{\bar\lambda}{R}, \qquad N = \frac{1}{8\,\mathcal{C}}\,: \tag{40}$$

the phase by which the body's field delays the wave, Eq. (39); the amplitude its stiffness reflects; its optical depth from internal friction, Eq. (32) with $\mathrm{Re}\,\eta = \rho c_T^2/\omega Q$; and its focal ratio as a gravitational lens, Eq. (41) below. After $\mathcal{C}$, every factor is below one for ordinary matter at the wavelengths a body of its size could act on: sound is slower than light, and a body smaller than the wavelength diffracts the wave instead of bending, reflecting or shadowing it. So no body much less compact than a black hole provides useful broadband optics. Parts of this are known. Press found that a gravitational mirror larger than its own Schwarzschild radius needs $\mu > \rho c^2$ or $\eta\omega > \rho c^2$, which for stiffness means shear sound faster than light [72]; Smolin wrote the absorption of an elastic body of length L [70] as $(GM/Lc^2)(\lambda/L)^2(c_T/c)^3$, every factor again below one, and concluded that no stable matter absorbs or confines gravitational radiation over a

broad band [74, 75]; and Loeb bounded the dissipation in bound systems [76]. Eq. (40) puts refraction and focusing beside reflection and absorption, and absorption inside a body beside that at its surface. The qualifications "useful" and "broadband" are necessary. A weak lens still focuses if one waits far enough behind it: the transparent Sun brings gravitational waves passing through its interior to a focus beyond 23.5 AU [77]. And a narrow resonance can absorb strongly in a narrow band: stars may absorb at their oscillation frequencies [78]. Across a broad band, and for anything we could build, the optical depth of ordinary matter is negligible, and only black holes cast shadows; a rapidly spinning one even reflects some waves with gain [79].

b. A black hole as the lens. For focusing, the argument comes down to one condition. A lens of radius R that brings rays to a focus at the distance f must bend its edge ray by R/f, and gravity bends it by $2r_s/R$, where $r_s = 2GM/c^2$ for the mass M inside that ray. So

$$\frac{r_s}{R} = \frac{1}{4N} \tag{41}$$

for a lens of focal ratio $N = f/2R$. A pocket lens at $f/10$, five centimetres in radius, would need eleven times the mass of the Moon inside it, seven billion times the density of an atomic nucleus. Nothing short of a black hole is compact enough, so to see what a lens would do for the camera, we put a black hole in front of it.

The natural choice is the hole of Section XI that is as warm as the sky, 1.36×10^{23} kg at 0.905 K: lighter holes are hotter and evaporate, and this one is in balance with the graviton sky. (It is colder than the microwave sky and gains from it, though by less than a part in 10^{51} of its mass each second; and like every such balance, this one is unstable.) Its Schwarzschild radius is 0.2 mm. Diffraction limits it as it limits the Sun: it focuses only waves shorter than about $4\pi r_s = 2.5$ mm, frequencies above 120 GHz. That excludes every wave from moving bodies (focusing a kilohertz wave would take a lens of eight solar masses) but admits the whole thermal glow, whose wavelengths are microns. A point mass has no single focus: rays passing at the distance b cross the axis at $b^2/2r_s$, so a camera on the axis at the distance d collects the rays near the Einstein radius $b_E = \sqrt{2r_s d}$, from a patch of sky $\sqrt{2r_s/d}$ in angular radius.

Where would the camera be? At a metre the ring is 1.2° in radius, but the tide is $2 \times 10^{13}\,\mathrm{s}^{-2}$, enough to tear the camera apart. It falls to a bearable $1\,\mathrm{s}^{-2}$ only 26 km away (Fig. 20). There the ring is 25″ in radius, the rays that reach the camera pass 3.25 m from the hole, and the hole pulls with 1340 times the Earth's gravity. The camera cannot stand still. It must orbit, at 19 km/s, once every nine seconds, while its axis sweeps a circle on the sky, so that any patch of sky is in focus for a third of a millisecond per turn. A detector 10 cm across on the axis ($a = 5$ cm) gathers, from a source behind the hole, the rays through an annulus of about one square metre, $\pi a\sqrt{a^2 + 4b_E^2}$ for a detector of radius a: 130 times its own area. That is an

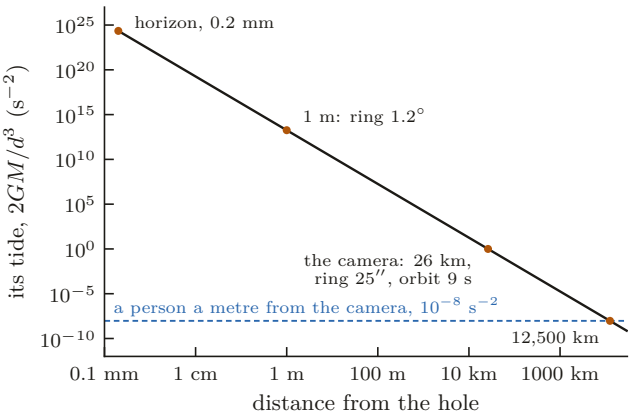


FIG. 20. A black hole as the camera's lens. The tide of the hole that is as warm as the sky (1.36×10^{23} kg, Schwarzschild radius 0.2 mm), the one lens compact enough to focus the thermal glow, against the distance from it. The camera has to sit where the tide is bearable, $1\,\mathrm{s}^{-2}$ at 26 km, where the Einstein ring is 25″ in radius and the camera must orbit the hole every nine seconds. Even there the hole's tide is 10^8 times that of a person a metre from the camera (dashed), and it stays larger until the camera is 12,500 km away.

average over fringes a few centimetres apart, well within the peak gain on the axis that diffraction allows at a wavelength of 10 μm, $\pi w = 4\pi^2 r_s/\lambda = 800$ (Section XI). A hole of two lunar masses does the work of a dish a little over a metre across. Meanwhile it blinds the near field: its tide exceeds that of a person standing a metre from the camera until the camera is 12,500 km away.

c. What a lens would add. Classically, nothing that an ideal array lacks. The array of Eq. (42) records the field and does by computation what any lens does, and a converter of gravitons into photons a metre across, placed before ordinary optics (Section IX), would gather as much as the hole. What a lens does add, like any device that combines the field before detecting it, is quantum: for radiation that holds 10^{-30} gravitons in each mode, combining before detection is what lets a camera count gravitons instead of recording noise (Section IX). And no lens of any kind could sharpen the near field, whose blur is Laplace's equation, Eq. (17). In electromagnetism a slab of negative permittivity restores the fading detail [80], because matter holds charges of both signs and polarizes strongly. Matter answers a tide only by deforming, which adds to the field a fraction of order $G\rho/\omega_0^2$, with ω_0 the frequency at which the material rings: the same small number as Eq. (39). A response of order one would take a material so soft against its own weight that it is unstable to collapse, which for steel means a slab some ten thousand kilometres thick, whose own pull would then fill the image.

d. The computed image. The camera does not need optics, because its pixels record more than a light sensor does. A light sensor registers only the energy that arrives.

A gravitational pixel registers the field itself, with its phase. Waves from a direction $\hat{n}$ (pointing toward their source) reach different pixels at different times, a pixel at $\mathbf{x}_p$ earlier by $\hat{n}\cdot\mathbf{x}_p/c$ the farther it lies toward the source, and the image is made by undoing those delays and adding:

$$I(\hat{n}) = \Big\langle \sum_{ij} \Big| \sum_{p} \Lambda_{ij,kl}(\hat{n})\, \mathcal{E}_{kl}\big(\mathbf{x}_p,\ t - \hat{n}\cdot\mathbf{x}_p/c\big) \Big|^2 \Big\rangle, \quad (42)$$

where $\mathbf{x}_p$ is the position of pixel p and $\Lambda(\hat{n})$ keeps the part of the tensor transverse to $\hat{n}$ and free of trace, the part a wave from that direction can carry. Waves from the chosen direction add in step; waves from elsewhere cancel. This is how arrays of radio telescopes form images, and it is what a lens does with glass. The magnetic records add something a scalar antenna lacks: for a wave from $\hat{n}$, $\epsilon_{ipq}\hat{n}_p\mathcal{B}_{qj} = \mathcal{E}_{ij}$, while for a wave from $-\hat{n}$ the same combination is $-\mathcal{E}_{ij}$, so summing $\frac{1}{2}(\mathcal{E}_{ij} + \epsilon_{ipq}\hat{n}_p\mathcal{B}_{qj})$ in place of $\mathcal{E}_{ij}$ keeps the first and cancels the second, and even a flat array can tell front from back. The sharpness is that of any aperture of width D,

$$\Delta\theta \approx \frac{\lambda}{D}, \quad (43)$$

shown in Fig. 21. The pixels need not all exist at once if the source is steady: one pixel carried across the aperture synthesizes it, as a radar synthesizes an aperture with one moving antenna, for the near field and for pairs of stars that orbit for millions of years. Thermal radiation, whose phase wanders within $\hbar/k_BT$, about $3\times10^{-14}\,$s at room temperature, needs every pixel at the same moment. In the near field there are no delays to undo, and the image is instead obtained by the inversion of Section IV.

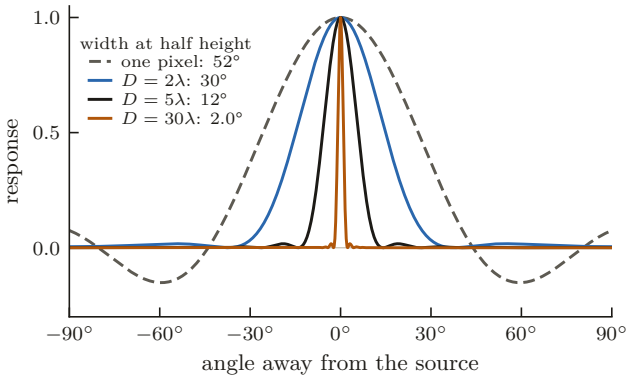


FIG. 21. How sharply a camera can tell directions apart: the response to a single distant source as the computed image is steered away from it, with the width of each curve at half height. For arrays 2, 5 and 30 wavelengths wide the curve is the power of Eq. (42), the pattern of a round aperture. For a single pixel it is instead the best linear estimate of the sky from the pixel's data, its projection onto the spherical harmonics of degree four and below; being an estimate rather than a power, it can be negative, as it is sixty degrees off. Either way a single pixel's view of the sky is blurred over some fifty degrees, and an array sharpens in proportion to its width in wavelengths, Eq. (43).

VIII. ONE PIXEL, SPARSE ARRAYS AND DEPTH

A wave of light or of gravity reaching a point is described by four numbers: two for its direction and two for the strengths of its two polarizations. A sensor of light at a point records six, the electric and magnetic fields; a gravitational pixel records ten, Eqs. (1) and (5). A detector that reads one component cannot tell a wave from the pull of a passing lorry (Section II), and even the whole electric part cannot find a wave beneath an unknown pull. With all ten numbers a pixel can, by the shape of the field and by its magnetic part, and a handful of pixels can do more. This section shows what the six extra numbers give, then what a few pixels add. Most of it follows from writing the ten numbers as one object.

a. One complex matrix. In vacuum $\mathcal{E}$ and $\mathcal{B}$ are real, symmetric and trace-free. Together they form the complex symmetric trace-free matrix

$$\mathcal{W} = \mathcal{E} + i\,\mathcal{B}, \quad (44)$$

five complex numbers. Two facts make this the natural form.

First, observers transform $\mathcal{W}$ by rotations of three-dimensional space with complex angles. A pixel turned by a rotation R reads $R^T\mathcal{W}R$. A pixel moving with rapidity η along a unit vector $\hat{u}$ (speed $c\tanh\eta$) reads $\Lambda\,\mathcal{W}\Lambda^T$ with $\Lambda = \exp(-i\eta\,\hat{u}\cdot\mathbf{L})$ (a scene moving along $\hat{u}$ is seen through Λ^{-1}), where $(L_k)_{ij} = -\epsilon_{kij}$ generates rotations: a change of velocity is a rotation by an imaginary angle. (The restricted Lorentz group is isomorphic to the group of complex rotations, $SO(3,\mathbb{C})$; for the curvature this is the content of Petrov's and Penrose's classifications [81, 82].) The eigenvalues of $\mathcal{W}$, and with them

$$I = \operatorname{tr}\mathcal{W}^2, \qquad J = \operatorname{tr}\mathcal{W}^3, \quad (45)$$

are therefore the same for every observer at that point, however turned and however moving.

Second, the $\mathcal{W}$ of a plane wave is the square of a vector. For a wave travelling along $\hat{k}$, let $\mathbf{e}_1, \mathbf{e}_2$ span the plane across it with $\mathbf{e}_1\times\mathbf{e}_2 = \hat{k}$, and let $\mathbf{m} = (\mathbf{e}_1 + i\mathbf{e}_2)/\sqrt{2}$, a complex vector with $\mathbf{m}\cdot\mathbf{m} = 0$. Since $\mathcal{B}_{ij} = \epsilon_{ipq}\hat{k}_p\mathcal{E}_{qj}$ in the wave, and $\hat{k}\times\mathbf{m} = -i\mathbf{m}$,

$$\mathcal{W} = 2(\mathcal{E}_+ - i\mathcal{E}_\times)\,\mathbf{m}\mathbf{m}^T, \quad (46)$$

where $\mathcal{E}_+$ and $\mathcal{E}_\times$ are the wave's two polarizations, so that a wave's $\mathcal{W}$ has rank one. Conversely the direction of travel is read from $\mathbf{m}$ as $\hat{k} = \operatorname{Re}(i\,\mathbf{m}\times\mathbf{m}^*)/|\mathbf{m}|^2$, which for one wave of any polarization is the gravitational counterpart of the Poynting vector, the normalized super-Poynting vector of the curvature [14]:

$$\hat{n}_i = -\frac{\epsilon_{ijk}\,\mathcal{E}_{jl}\,\mathcal{B}_{kl}}{\mathcal{E}_{ab}\,\mathcal{E}_{ab}}, \quad (47)$$

with $\hat{n} = -\hat{k}$ pointing from the pixel back to the source. The same construction for light gives $\mathbf{E} + ic\mathbf{B} = a\,\mathbf{m}$, a vector rather than a square; the difference between the two, a square against a single power, is the difference between spin two and spin one, and it is the source of almost everything below. Matter neither reflects nor absorbs gravitational waves (Section VII), so none of what follows is spoiled by echoes, as direction finding with radio or sound is indoors.

b. Principal null directions. Every reading has four directions of its own. Writing a complex null vector by its stereographic coordinate z on the sky, $\mathbf{m}(z) = (1 - z^2,\, i(1 + z^2),\, -2z)$, the quartic equation

$$\mathbf{m}(z)^T\, \mathcal{W}\, \mathbf{m}(z) = 0 \tag{48}$$

has four roots, four points on the sphere of directions around the pixel: the principal null directions of the field [82], which for a state of spin two are its Majorana stars [17] (Fig. 22). For one plane wave all four coincide on its direction of travel. For one body at rest they fall in two pairs, on the line to the body and opposite it. Where two or more bodies pull, they are four distinct points. The same distinctions can be read without solving anything, from the invariants: a repeated eigenvalue, the mark of a single body, makes $1 - 6J^2/I^3$ vanish, and a single wave makes $\mathcal{W}$ itself a square, $\mathcal{W}^2 = 0$ (Petrov's types D and N). Neither condition is quite enough alone: $I^3 = 6J^2$ also allows type II, a body with a wave running along the line to it, which is told from type D by $(\mathcal{W} - w)(\mathcal{W} + 2w) = 0$ with $w = -J/I$ the repeated eigenvalue, positive for a single body; and $I = J = 0$ also allows type III. One reading therefore tells whether the field could be that of one round body, whether it is a pure wave, or whether it needs more. The type describes the field, not the objects: two masses on one line through the pixel also give type D, and one body that is not round gives type I. Nor can one instant tell every pull from every wave: two waves running in opposite directions can match, at one event, the tide of two masses at rest, and only a record over time, or over space, tells them apart. The quantity $1 - 6J^2/I^3$ vanishes for a single moving body, and is 0.55 for the two masses of Fig. 22. Light at a point has two principal null directions, not four: its $\mathbf{E} + ic\mathbf{B}$ has only one complex invariant. Any field of light that is not a pure wave has two separate null directions, as a single charge has, so one point of light cannot tell one source from several.

c. Shape. A plane wave stretches and squeezes only across its direction of travel, so its tidal tensor has one vanishing eigenvalue and $\det \mathcal{E} = 0$. The field of a single mass has eigenvalues in the ratio $-2 : 1 : 1$, and its determinant is never zero. One reading of one pixel therefore distinguishes a single wave from a single mass. The test is for an isolated source: the fields of several masses, or of several waves, add, and their sum can have either form.

d. The magnetic part. In a wave the magnetic tidal tensor is as large as the electric one; it is the same pattern turned by 45° about the direction of travel. Near slowly moving matter it is smaller by the ratio of the matter's speed to that of light,

$$\frac{|\mathcal{B}|}{|\mathcal{E}|} = 1 \quad \text{(wave)}, \qquad \frac{|\mathcal{B}|}{|\mathcal{E}|} \sim \frac{v}{c} \quad \text{(near field)}, \tag{49}$$

where $|\mathcal{E}|^2 = \mathcal{E}_{ij}\mathcal{E}_{ij}$ (the Frobenius norm) and likewise for $\mathcal{B}$, and v is the speed of the matter. At a distance r from a compact source of size L, the magnetic part of the field that changes is smaller than its electric part by about $(v/c)(r/L)$, that is, by kr at the frequency of the change: more than v/c, but still far below one in the near zone. Averaged over time, the first holds for any mixture of waves from independent sources, so the magnetic part is a detector of radiation that the pull of nearby objects hardly touches. Coherent waves are an exception: in a standing wave the magnetic part vanishes where the electric part is largest.

e. Ten numbers: four invariants, three angles, three velocities. A reading whose eigenvalues are distinct can be written

$$\mathcal{W} = P\, \mathrm{diag}(w_1, w_2, w_3)\, P^T, \qquad P = R_0\, e^{iK_0}, \tag{50}$$

with P a complex rotation ($P^T P = 1$), split into a real rotation R_0 and an imaginary one. The three complex eigenvalues, which sum to zero, are four numbers no observer can change. The rotation R_0 gives three angles, the orientation of the field's own axes. The imaginary part, $e^{2iK_0} = P^\dagger P$, gives three more: the velocity of the one frame in which $\mathcal{E}$ and $\mathcal{B}$ share their axes, the field's own rest frame (the principal observer of Ref. [13]; for a field of type I it is unique, and it is the rest frame of matter only for a stationary source).

For a scene of masses at rest, $\mathcal{B} = 0$ in the scene's frame, so its eigenvalues are real; a pixel moving through it at any speed still finds real eigenvalues, and finds in P the velocity of the scene relative to itself. The pixel therefore determines its own velocity through an unknown room, at any speed, with no map of the room (Fig. 23). To first order in the speed, in the principal axes of $\mathcal{E}$ with eigenvalues λ_a,

$$\mathcal{B}_{bc} = \frac{v_a}{c}\,(\lambda_c - \lambda_b) \quad ((a,b,c) \text{ cyclic}), \qquad \mathcal{B}_{aa} = 0, \tag{51}$$

so a pixel whose readings carry white noise σ on each component (in the orthonormal basis of the paragraph *How precisely*) reads each component of its velocity to within $c\,\sigma/(\sqrt{2}\,|\lambda_b - \lambda_c|)$. A pixel that reads the tide of a room, $10^{-8}\,\mathrm{s}^{-2}$ near a person, to one part in 10^8, reads its own speed to about two metres per second.

The converse is a test for relative motion within the scene. A pixel moving through a static scene, however fast, always finds real eigenvalues. If they are complex, something in the scene moves relative to the rest of it, or turns; the pixel's own motion cannot make them so (Fig. 23). The phase of the eigenvalues measures turning. Outside a spinning body of mass M and angular momentum $J_s = Mca$, the eigenvalues are proportional

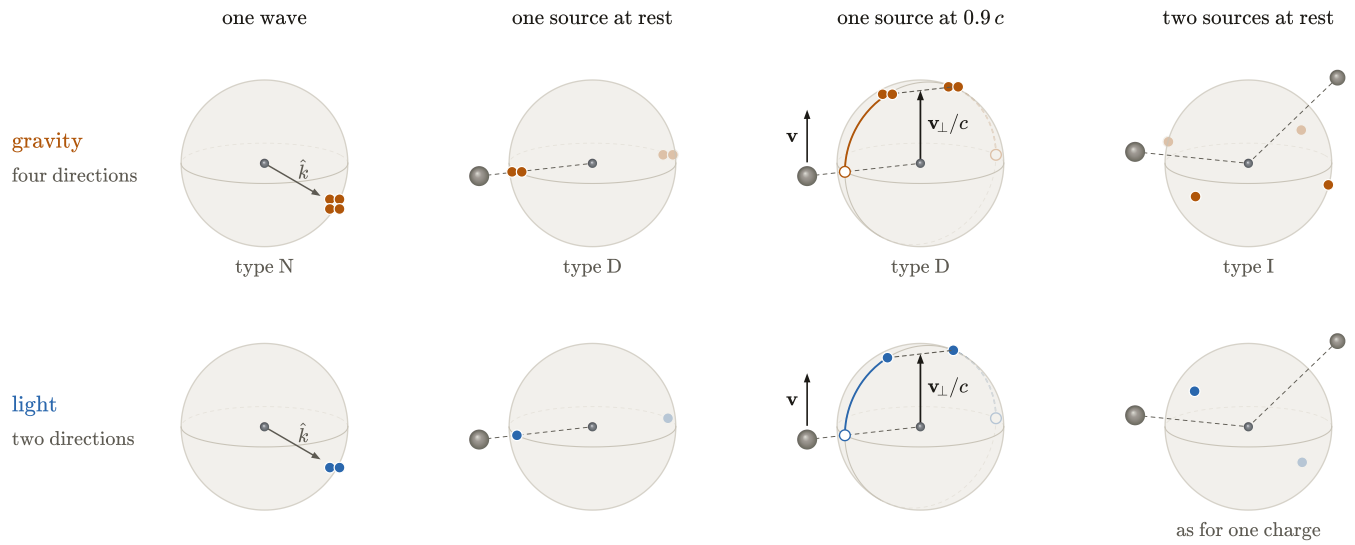


FIG. 22. The principal null directions of a field, the solutions of Eq. (48), on the sky around one pixel (each disc), for gravity (top) and light (bottom). Coincident directions are drawn as touching dots, so that every sky of gravity holds four and every sky of light two; faint dots and dashed lines lie on the far side. One wave puts all of them on its direction of travel $\hat{k}$. One source at rest, a mass or a charge, puts them in two groups on the line through it. Moving across that line at $0.9\,c$, the source folds both groups toward its velocity, along the paths drawn from their places at rest (open circles), and the midpoint of the two, as a vector, is its velocity across the line to where it is now, $\mathbf{v}_\perp/c$, Eq. (52). Two masses at rest give four separate directions (Petrov type I), so they could not be one body; two charges give light's two directions again, at the ends of the line of force, as one charge would.

to $(r - ia\cos\vartheta)^{-3}$, as in Kerr's solution [83], so their phase, $3a\cos\vartheta/r$ for $a \ll r$, reads the spin along the line of sight; for the Earth seen from above a pole it is 1.5×10^{-6}. A pixel resting on the Earth shows both effects. At a pole it does not move, and its eigenvalues have that phase. On the equator the planet turns across the pixel's line to its centre, and to first order in the speeds the eigenvalues stay real, while the velocity read from $\mathcal{W}$ is $(1 - I/MR^2)\,\Omega R = 311\,\mathrm{m\,s^{-1}}$, the speed of the ground less the share that the planet's own turning takes back (Section II).

Light cannot do this. Its field at a point has only two invariants, $\mathbf{E}^2 - c^2\mathbf{B}^2$ and $\mathbf{E}\cdot\mathbf{B}$, and in the frame where $\mathbf{E}$ is parallel to $\mathbf{B}$ a boost along their common axis and a turn about it change nothing. A sensor of light reads at most two components of its own velocity. A single body does the same to gravity's field (type D): coming straight at the pixel, even at $0.3\,c$, it shows no $\mathcal{B}$ at all, and its radial speed is unreadable. Two bodies, or one that is not round, remove the blind spot.

f. The state of a moving body. The four principal null directions of a single body moving at any speed are its two pairs, displaced by aberration toward its direction of motion. Their midpoint, as a vector, is exactly its velocity across the line of sight (Fig. 22):

$$\tfrac{1}{2}\,(\hat{p}_+ + \hat{p}_-) = \frac{\mathbf{v}_\perp}{c}, \tag{52}$$

with $\hat{p}_\pm$ the directions of the two pairs and $\mathbf{v}_\perp$ the velocity across the line from the body to the pixel (Appendix B). The ratio $|\mathcal{B}|/|\mathcal{E}| = \sqrt{3}\,v_\perp/c$ of Section IV is its first-order form. Half their difference points along the line to where the body is now, $\frac{1}{2}(\hat{p}_+ - \hat{p}_-) = \pm(1 - v_\perp^2/c^2)^{1/2}\,\hat{n}$. With the rate of change of the reading, one pixel then has the whole state of the body. The line turns toward the sideways velocity at the rate $v_\perp/r$, which gives the distance and the sign of $\hat{n}$; the repeated eigenvalue of $\mathcal{W}$ is $w = GM/R_*^3$, with R_* the distance in the body's rest frame, $R_*^2 = \gamma^2(r^2 - |\mathbf{v}\times\mathbf{r}|^2/c^2)$ and $\gamma = (1 - v^2/c^2)^{-1/2}$, in which $\mathbf{v}\times\mathbf{r}$ does not change. So

$$r = \frac{v_\perp}{|\dot{\hat{n}}|}, \qquad \dot{r} = -\frac{r}{3}\Big(1 - \frac{v_\perp^2}{c^2}\Big)\frac{\dot{w}}{w}, \qquad M = \frac{w\,\gamma^3 r^3}{G}\Big(1 - \frac{v_\perp^2}{c^2}\Big)^{3/2}\!: \tag{53}$$

position, velocity and rest mass, seven numbers, exactly at any speed (and, as everywhere in this paper, to first order in GM/rc^2). Equation (66) below is the first-order form of the distance. A body coming straight on shows no sideways velocity and cannot be ranged (below), but because its tide $\mathcal{E}_\parallel$ along the line to it grows as r^{-3}, the pixel reads when it will arrive,

$$-\frac{r}{\dot{r}} = \frac{3\,\mathcal{E}_\parallel}{\dot{\mathcal{E}}_\parallel}, \qquad \frac{\mathcal{E}_\parallel\,\ddot{\mathcal{E}}_\parallel}{\dot{\mathcal{E}}_\parallel^2} = \frac{4}{3} - \frac{r\ddot{r}}{3\dot{r}^2}, \tag{54}$$

and from the second ratio whether it is coasting (4/3), braking or driven.

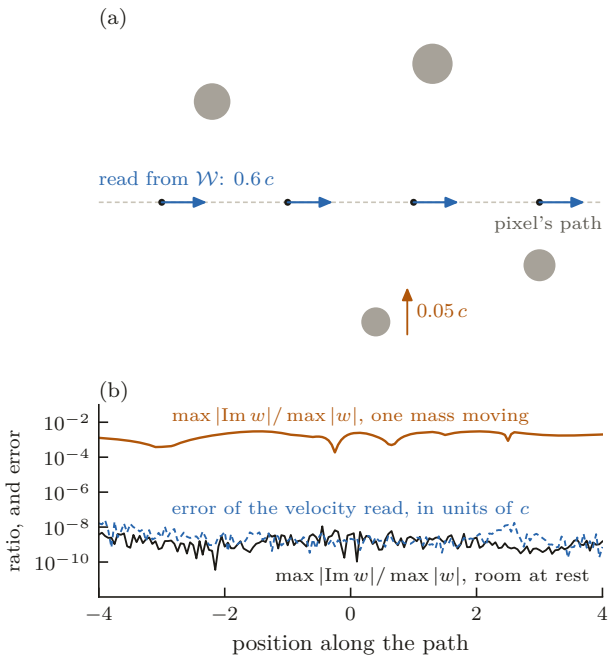


FIG. 23. A pixel's own velocity, and a test for motion in the scene. (a) A pixel crosses a room of four masses unknown to it at $0.6\,c$ (seen from above, in the room's frame), and at every point reads its own velocity from $\mathcal{W}$ alone, Eq. (50) (arrows). (b) Along the path: the error of the velocity read (dashed), and the ratio $\max|\mathrm{Im}\,w|/\max|w|$ over the eigenvalues w of $\mathcal{W}$, which is zero for the room at rest, however fast the pixel moves, to the accuracy of the computation, 10^{-8} here, and is not when one mass crosses the room at $0.05\,c$. Computed from the exact field of uniformly moving masses.

g. Separating waves at one point. Several waves crossing a pixel at once add their matrices, and the algebra of squares lets one pixel separate them.

At one instant, two waves give $\mathcal{W} = c_1\mathbf{m}_1\mathbf{m}_1^T + c_2\mathbf{m}_2\mathbf{m}_2^T$, of rank two, so $\det\mathcal{W} = 0$: two real conditions that tell two crossing waves from the pull of a mass, whose $\det\mathcal{W} = -2(GM/r^3)^3$. The vector $\mathbf{v}$ with $\mathcal{W}\mathbf{v} = 0$ is $\mathbf{m}_1 \times \mathbf{m}_2$; the null vectors orthogonal to it are the roots of one quadratic, and they are $\mathbf{m}_1$ and $\mathbf{m}_2$, which give both directions and then both amplitudes. This is Sylvester's theorem on sums of two fourth powers [84] in the language of the sky. Light cannot do it at all: a single wave already uses four of its six numbers.

At one frequency, three waves can be separated. Writing the reading as $\mathcal{W}(t) = \mathcal{W}_+e^{-i\omega t} + \mathcal{W}_-e^{i\omega t}$ (since $\mathcal{W}$ is complex, $\mathcal{W}_-$ is not the conjugate of $\mathcal{W}_+$), both parts are sums over the same three squares, $\mathcal{W}_\pm = \sum_a \alpha_a^\pm\,\mathbf{m}_a\mathbf{m}_a^T$, and

$$\det(\mathcal{W}_+ - \lambda\,\mathcal{W}_-) = \det[\mathbf{m}_1,\mathbf{m}_2,\mathbf{m}_3]^2\prod_{a=1}^{3}(\alpha_a^+ - \lambda\,\alpha_a^-). \tag{55}$$

Its three roots give the ratios $\lambda_a = \alpha_a^+/\alpha_a^-$, which must be distinct (two face-on binaries turning the same way share one; any three distinct directions give $\det[\mathbf{m}_1,\mathbf{m}_2,\mathbf{m}_3] \neq 0$); at each, one wave drops out, the null vector of what remains is the cross product of the other two $\mathbf{m}$, and cross products of those give all three directions. For a circular binary seen at inclination ι, $|\lambda| = \tan^{\pm4}(\iota/2)$, so the roots also give the three inclinations. Three binaries in one frequency bin, which a single interferometer cannot tell apart, are three separate directions to one pixel.

Over time, four waves can be separated. If the waves come from fixed directions but carry any waveforms at all, the readings span a subspace of the five-dimensional space of matrices; for four waves whose waveforms are linearly independent it is four-dimensional, and there is one matrix A with $\mathrm{tr}(A\mathcal{W}) = 0$ for every reading. Each wave's $\mathbf{m}$ then lies on two conics,

$$\mathbf{m}^T A\,\mathbf{m} = 0, \qquad \mathbf{m}\cdot\mathbf{m} = 0, \tag{56}$$

and two conics meet in four points: the four directions (Fig. 24). For light the same argument gives two.

All three cases are one theorem. In the coordinates of Eq. (48), the five numbers of a reading are the moments $y_j = \sum_a c_a z_a^j$, $j = 0,\dots,4$, of the waves' amplitudes c_a over their directions z_a, so separating waves is Prony's problem of finding the nodes of a sum of powers [85]: the matrix y_{j+k}, stacked over the snapshots, has the polynomial with roots z_a as its null vector, and when its rank equals the number of waves that polynomial is unique. For a point sensor of a field of spin s, with $2s+1$ moments in each of L independent snapshots, this gives generically

$$N_{\max} = \left\lfloor \frac{L(2s+1)}{L+1} \right\rfloor \tag{57}$$

waves, and no more: s at one instant, $\lfloor 2(2s+1)/3 \rfloor$ at one frequency (whose two parts $\mathcal{W}_\pm$ are two snapshots) and $2s$ from a long enough history. For light that is 1, 2 and 2; for gravity, 2, 3 and 4; a field of spin four would separate six waves at one frequency, not five. Bounds of this kind are established for electromagnetic and acoustic vector sensors, where they depend on what is assumed of the sources' polarization [86, 87]. Generic is a real condition: snapshots whose amplitudes are all proportional, or related through the directions themselves, add nothing, and the rank of the moment matrix tells when that has happened. With noise of 10^{-4} of the signal on every component, four waves with random waveforms are located to 10^{-4} radian from three hundred readings.

Uncorrelated sources can be separated from second moments alone. In the frequency domain the two helicities occupy separate halves of the ten numbers, and the brightness and the circular polarization of the sources give two five-by-five matrices built from the same five steering vectors; when the sources' circular fractions differ, diagonalizing one in the frame that whitens the other separates five sources in closed form, with their directions, brightnesses and circular fractions.

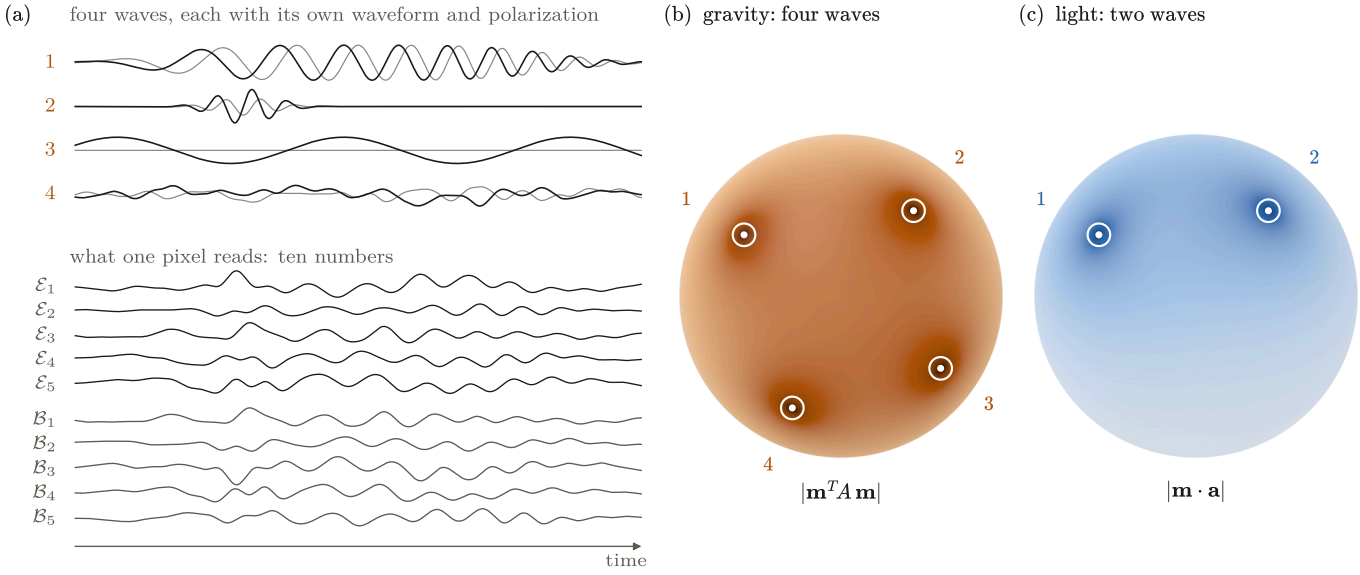


FIG. 24. One pixel, four waves. (a) Four plane waves arrive from four fixed directions, each with its own waveform and polarization (strong and faint lines; the third is linearly polarized, and its faint line is flat), and one pixel reads the ten numbers of $\mathcal{E}$ and $\mathcal{B}$ while all four pass. (b) From the readings alone: the matrix A with $\mathrm{tr}(A\mathcal{W}) = 0$ for every reading, and, on the sky toward the sources, the size of $\mathbf{m}^T A\,\mathbf{m}$, shaded over two and a half decades. It vanishes at exactly four points, Eq. (56): the zeros found from the readings (dots) fall on the four sources (rings). (c) Light from the first two sources, the same way: its readings $\mathbf{E} + i\mathbf{cB}$ span a plane, the vector $\mathbf{a}$ orthogonal to it gives $\mathbf{m}\cdot\mathbf{a}$, and that vanishes at the two sources; a third wave of light would fill all six of its numbers and leave nothing to find.

h. Lensed images at one point. The count assumes the waves overlap in time and frequency. The images of a chirping binary seen through a lens do not. A galaxy splits it into two or four images about an arcsecond apart, whose arrival times differ by hours to months; at any moment each image is at a different stage of the same chirp, and so at a different frequency. In each cell of time and frequency the pixel then reads a single wave, and places it to within $1/\rho$ radian at the signal-to-noise ratio ρ of that image. An arcsecond needs $\rho \approx 2\times 10^5$ at one point, where resolving the images by the width of an aperture would need, at 100 Hz, an array four astronomical units across. From one pixel's noiseless record, two images of a chirp an arcsecond apart and half a second out of step are each placed to two per cent of their separation; with noise the limit is $1/\rho$. Images that overlap in frequency, as a lens of a steady source makes them, are instead a Prony problem whose conditioning falls as a power of their separation.

i. What one pixel sees of the sky. For a sky full of independent sources overlapping in frequency, what a pixel can learn at each frequency is its ten-by-ten spectral matrix, one hundred real numbers. Split by helicity, it holds three blocks: the brightness I and the circular polarization V of the sky in two five-by-five Hermitian blocks, and the linear polarization in a complex symmetric one. The brightness enters through the kernel

$$\sum_{A=+,\times} e^A_{ij}\, e^A_{kl} = P_{ik}P_{jl} + P_{il}P_{jk} - P_{ij}P_{kl}, \qquad P_{ij} = \delta_{ij} - \hat{n}_i\hat{n}_j, \tag{58}$$

(for polarization tensors with $e^A_{ij}e^A_{ij} = 2$), a polynomial of degree four in the components of $\hat{n}$, so the pixel sees the spherical harmonics of I of degree four and below, twenty-five numbers; it sees as many of V, and eighteen of the linear polarization, which carries spin weight four and enters only at degree four. That is

$$25 + 25 + 18 = 68 \tag{59}$$

numbers of the sky, all independent; the other thirty-two of the hundred vanish for any sky of gravitational waves and are checks against sensor noise or anything else. The brightness and the circular polarization never mix at one pixel: one lies in the real part of the spectral matrix, the other in its imaginary part. (They mix in the cross-correlation of two separated detectors [88, 89], through the phase between them.) The same count for a point sensor of a transverse field of spin $s \geq 1$, with two helicities, gives $2(2s+1)^2 + 2(4s+1)$: 28 of 36 for light. Sound, a pressure and a velocity, has one longitudinal polarization and is counted separately: 9 of 16 (Fig. 25).

One of the sixty-eight numbers is the handedness of the whole sky. An isotropic sky of brightness I and net circular polarization V puts exactly $(V/I)\langle\mathcal{E}\cdot\mathcal{E}^*\rangle$ into the imaginary part of $\langle\mathcal{E}\cdot\mathcal{B}^*\rangle$, so one pixel measures whether the sky is chiral, which a single planar interferometer cannot [90].

Not every spectral matrix is a sky. Within one helicity, a sky of independent waves gives $C = \int p(\hat{n})\,\mathbf{v}(\hat{n})\mathbf{v}(\hat{n})^\dagger\,\mathrm{d}\Omega$ with $p \geq 0$ and $\mathbf{v}$ the unit five-vector of a wave from $\hat{n}$, and such matrices fill only part of the positive ones. For

$\mathbf{u}$ the five-vector of $\mathrm{diag}(1,-1,0)/\sqrt{2}$, every wave has $|\mathbf{u}^\dagger\mathbf{v}|^2 \le \frac{1}{2}$, so every sky obeys

$$\mathbf{u}^\dagger C\,\mathbf{u} \le \tfrac{1}{2}\,\mathrm{tr}\,C, \tag{60}$$

while $C = \mathbf{u}\mathbf{u}^\dagger$, positive and of unit trace, reaches one. It is made by two waves along $+\hat{z}$ and $-\hat{z}$ locked in phase, a standing wave. Violating a bound of this kind rejects the picture of independent waves (the cause may be coherence, a near field or a miscalibration), the same convex geometry that tells classical mixtures of spin states from others [91].

The rest of the sky is invisible to second moments. The twelve corners of a regular icosahedron form a spherical design of degree five: they average every polynomial of degree five or less exactly as the whole sphere does [92]. Twelve equal, unpolarized, independent sources at those corners therefore give a pixel exactly the second moments of a uniform sky, while six at the corners of an octahedron, a design of degree three only, do not. Sources that are not Gaussian say more: the fourth moments of the pixel are kernels of degree eight, which no icosahedron averages. Two pixels a wavelength apart tell the two skies apart as well, because their cross-correlation carries the phase $e^{i\omega\hat{n}\cdot\Delta\mathbf{x}/c}$, which no finite design averages exactly.

j. Ranging a wave source. A single plane wave has no distance. The field of a real source at distance r is not quite a plane wave: it carries terms falling as $1/r^2$, $1/r^3$ and beyond, organized by how they turn about the line of sight [93], and a pixel sees them. At one instant the departure of the oscillating part of $\mathcal{W}$ from rank one, the ratio of its second singular value to its first (the singular values $s_1 \ge s_2 \ge s_3$ being the square roots of the eigenvalues of $\mathcal{W}^\dagger\mathcal{W}$, not the eigenvalues of $\mathcal{W}$, which all vanish for a wave), is

$$\frac{s_2}{s_1} = \frac{C(\iota,\theta)}{(kr)^2} + O\big((kr)^{-3}\big), \tag{61}$$

not $1/kr$: the first correction, $\mathbf{m}\,\delta\mathbf{m}^T + \delta\mathbf{m}\,\mathbf{m}^T$ with $\delta\mathbf{m} \propto \hat{k}$, equals $(\mathbf{m}+\delta\mathbf{m})(\mathbf{m}+\delta\mathbf{m})^T$ to that order, and only tilts the apparent $\mathbf{m}$, which at one instant cannot be told from a tilt of the source. The oscillating part is read at one instant from $\dot{\mathcal{W}}$, which holds none of the static tide of the pair's mass, $(c/v)^2$ times larger than the departure. For two masses turning in a circle, seen at inclination ι and wave phase θ,

$$\begin{aligned} C &= \frac{2\sin^2\iota\,\sqrt{A^2+B^2}}{D}, \qquad B = 2\cos\iota\,\sin\theta\cos\theta, \\ A &= (1-3\cos^2\iota)\cos^2\theta - 4\cos^2\iota\,\sin^2\theta, \\ D &= (1+\cos^2\iota)^2\cos^2\theta + 4\cos^2\iota\,\sin^2\theta, \end{aligned} \tag{62}$$

which is 2 seen edge on (except at the phases where the wave itself passes through zero) and, at the phases $\theta = 0$ and π, vanishes at the angle $\cos^2\iota = 1/3$. Over a cycle more can be done. The two frequency parts $\mathcal{W}_\pm$ (the parts at $e^{\mp i\omega t}$, whose amplitudes go as $\cos^4(\iota/2)$ and $\sin^4(\iota/2)$) depart from rank one by $2\tan^{\pm 2}(\iota/2)/(kr)^2$, both with the same s_2, so that $kr = [2\sqrt{s_1(\mathcal{W}_+)s_1(\mathcal{W}_-)}/s_2(\mathcal{W}_+)]^{1/2}$ needs no knowledge of the inclination. And the first-order tilt, invisible at one instant, differs between the two helicities: the directions read from the two parts differ by

$$\Delta\theta_\pm = \frac{8\,|\cot\iota|}{kr}. \tag{63}$$

Equation (63) holds while $\tan^2(\iota/2)$ and $\cot^2(\iota/2)$ both exceed $1/kr$; near face-on the weaker helicity's amplitude falls as $\tan^4(\iota/2)$, so its direction, not the formula, limits the range, and a full fit over distance, inclination and orientation gives the best inclination. A difference of directions measured at signal-to-noise ratio ρ ranges the source out to kr of order ρ, where the rank departure reaches only kr of order $\sqrt{\rho}$. A source seen at $\rho = 10^3$ can be ranged out to several hundred reduced wavelengths: at 100 Hz, a few hundred thousand kilometres. Equations (62) and (63) agree with the exact field of a turning pair to within a few per cent at $kr = 80$, except near $\cos^2\iota = 1/3$ where C itself vanishes, and 0.5 per cent at $kr = 200$ for $\iota \gtrsim 15°$ (Fig. 26).

k. The absence of gravitational aberration. The field of a body moving uniformly is its static field carried along, so it depends on where the body is now. The stretch axis of $\mathcal{E}$ points at the body's present position, at any speed, while its light shows its position a light-travel time ago, displaced by the aberration angle, about $v_\perp/c$ (Fig. 27). Near two masses in orbit the changing part of the field is Newton's field of their present positions to order $(kr)^2$, while their retarded positions would be off by kr itself: at $kr = 0.1$, a tenth to half of a per cent, depending on direction, against ten per cent. The first-order retardation cancels because mass and momentum are conserved. The gravitational Sun is therefore 20.5″ ahead of the optical Sun along its yearly path across the sky. Laplace took the absence of gravitational aberration to mean that gravity travels far faster than light. General relativity, in which gravity travels at the speed of light, predicts the same absence at this order, through this cancellation [94]. A camera that sees mass sees it on its own slice of simultaneity. When a body changes its motion, the field goes on pointing at where it would have been until the news, travelling at the speed of light as a wave, arrives.

l. Tests of general relativity from one reading. Other theories of gravity allow up to six polarizations, and waves that travel at other speeds [95]. For any plane wave of the metric, of any polarization and phase speed v_p, the second Bianchi identity gives, with no field equations assumed,

$$\mathcal{B}_{ij} = \frac{c}{v_p}\,\epsilon_{ipq}\hat{k}_p\,\mathcal{E}_{qj}. \tag{64}$$

So one reading of $\mathcal{E}$ (now with a trace, six numbers) and $\mathcal{B}$ (with an antisymmetric part, eight) gives the direction, the phase speed, all six polarizations, and five checks that they belong to one wave. Summing $\mathbf{e}_j \times \mathbf{b}_j$ over the

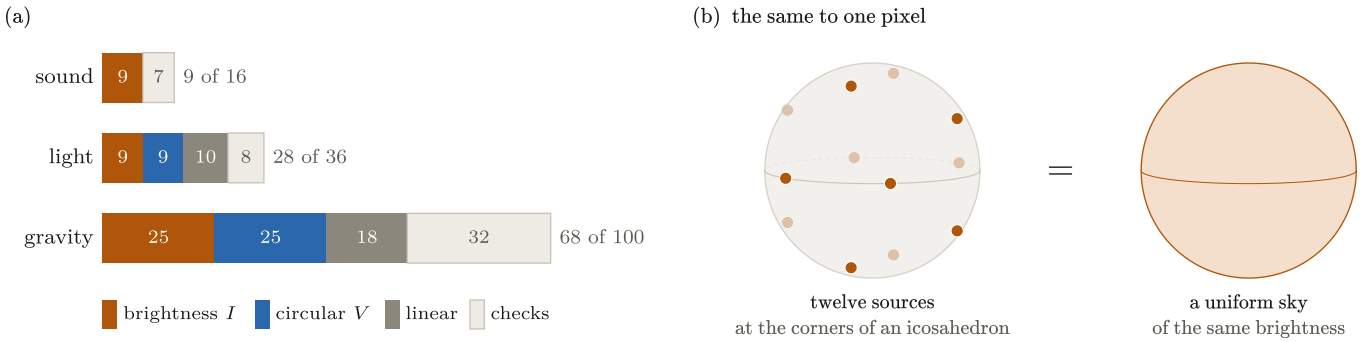


FIG. 25. What one pixel sees of the sky at one frequency. (a) Of the real numbers in the spectral matrix of a point sensor, those that carry the sky's brightness I, its circular polarization V and its linear polarization, and those that vanish for any sky of waves and serve as checks, Eq. (59), for sound (a pressure and a velocity), light and gravity. (b) What a pixel cannot see: twelve equal, unpolarized, independent sources at the corners of a regular icosahedron give it exactly the second moments of a uniform sky of the same total brightness, because those corners average every polynomial of degree five or less as the whole sphere does.

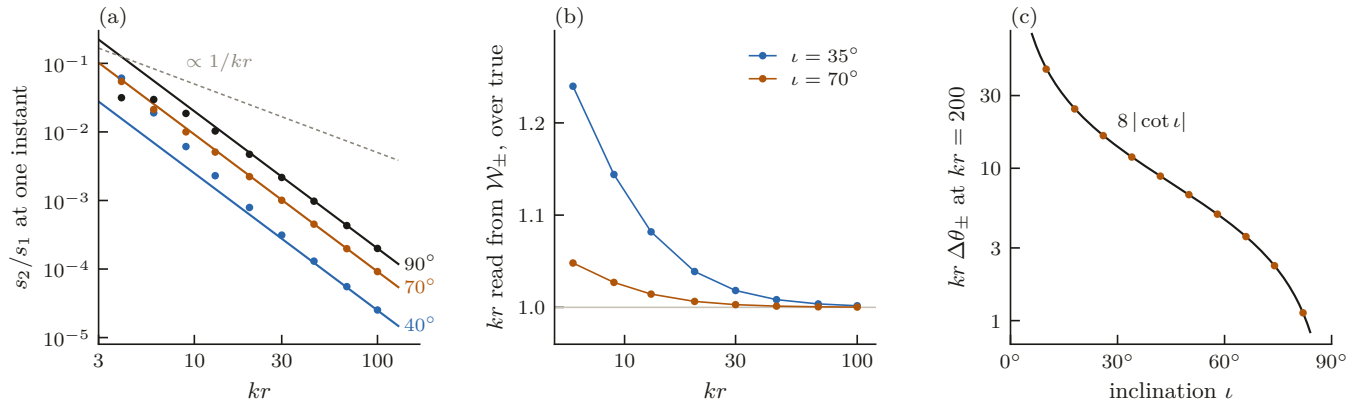


FIG. 26. Ranging a wave source from one pixel: the exact field of two equal masses turning in a circle, read at reduced distance kr and inclination ι (points), against the formulas (lines). (a) At one instant, at wave phase $\theta = 0$, the oscillating part of $\mathcal{W}$ departs from rank one by $C(\iota, 0)/(kr)^2$, Eqs. (61) and (62), not by $1/kr$ (dashed); the points approach the lines as the next order dies away. (b) Over a cycle, the distance read from the two frequency parts $\mathcal{W}_\pm$ alone, with no knowledge of the inclination, over the true distance. (c) The directions read from the two frequency parts differ by $8|\cot\iota|/kr$, Eq. (63), here at $kr = 200$.

columns of $\mathcal{E}$ and $\mathcal{B}$ turns Eq. (64) into a linear equation for $\mathbf{p} = (c/v_p)\hat{k}$,

$$\left(|\mathcal{E}|^2 - \mathcal{E}^2\right)\mathbf{p} = \textstyle\sum_j \mathbf{e}_j \times \mathbf{b}_j, \tag{65}$$

whose matrix is invertible whenever $\mathcal{E}$ has rank two or more; the residual $\mathcal{B} - [\mathbf{p}]_\times \mathcal{E}$, with $[\mathbf{p}]_\times$ the matrix of the cross product with $\mathbf{p}$, then tests that the reading is one wave. A purely longitudinal wave, $\mathcal{E} \propto \hat{k}\hat{k}$, has $\mathcal{B} = 0$, and its speed cannot be read at one point. In general relativity $v_p = c$ and only the two tensor polarizations appear. A massive graviton and a massive scalar differ even in sign: with $n = c/v_p$, the helicity-zero wave of a Fierz–Pauli graviton [96] has longitudinal and breathing amplitudes in the ratio $-2(1-n^2)$, a scalar wave $+(1-n^2)$ (Fig. 28). Testing general relativity this way at the level of present bounds would need extraordinary signal-to-noise ratios, but it needs only one point.

m. Matter at the pixel. Inside matter the pixel reads the density locally, whatever the matter is: in full, $\operatorname{tr}\mathcal{E} = 4\pi G[\rho + (p_1 + p_2 + p_3)/c^2]$, with p_a the principal stresses (so $3p$ for a fluid), less $2\Omega^2$ if the pixel's frame turns at Ω. The dark matter around the Sun, $0.4\,\mathrm{GeV\,cm^{-3}}$, gives $6 \times 10^{-31}\,\mathrm{s^{-2}}$, by its mass alone and with no other interaction. Between two plates a micrometre apart the Casimir energy density u is negative; the stress across the plates is $3u$ and the two along them $-u$ each, since the field has no trace, so the sum of stresses is u and the trace, $8\pi G u/c^2$, is $-8 \times 10^{-30}\,\mathrm{s^{-2}}$. The cosmological constant gives $-\Lambda c^2 = -1 \times 10^{-35}\,\mathrm{s^{-2}}$. Where radiation streams through with energy flux $\mathbf{F}$, as neutrinos from a supernova do, the trace is $8\pi G|\mathbf{F}|/c^3$ and the antisymmetric part of $\mathcal{B}$, $-(4\pi G/c^3)\,\epsilon_{ijk}F_k$, gives the flux as a vector (Section II), so that one reading inside the passing shell points back to the star, even when the collapse is perfectly spherical and sends out no waves at

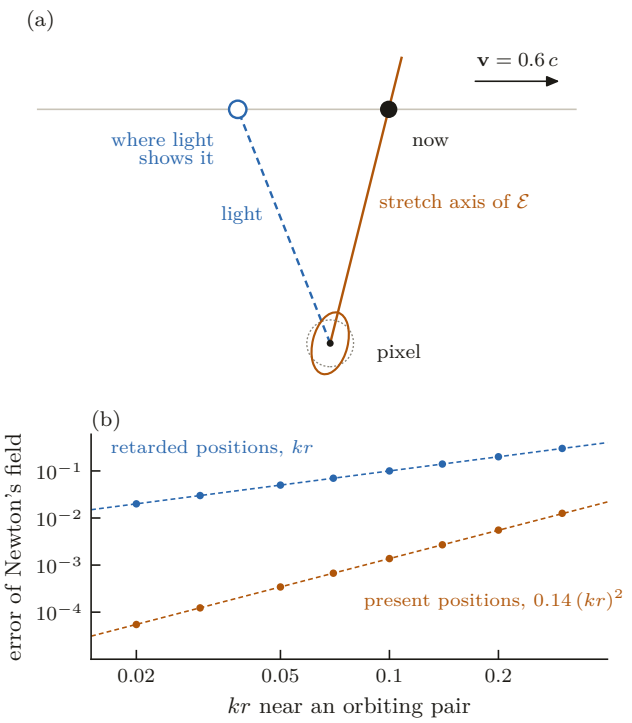


FIG. 27. The field of a moving mass points to its present position. (a) A mass passing a pixel at $0.6\,c$: the stretch axis of its exact field at the pixel (a ring of free masses, exaggerated) points at where the mass is now, while its light arrives from where it was a light-travel time ago. (b) Near two masses in orbit, at reduced distance kr, the changing part of the exact field against Newton's field of the masses at their present positions, which it matches to order $(kr)^2$, and at their retarded positions, which miss by kr.

all.

n. What no reading can tell. All of this assumes what kind of scene is in view. Without that assumption no finite amount of data at one event decides. Two masses, one with the tidal weight a along $\hat{y}$ and one with $2a$ along $\hat{z}$, give $\mathcal{E} = a\,\mathrm{diag}(3, 0, -3)$ and $\mathcal{B} = 0$; so do two equal waves crossing in opposite directions along $\hat{y}$, whose magnetic parts cancel. More is true. For every order N there is a positive shell of mass, whose field inside is exactly a constant $\mathcal{E}_0$, and a pair of counter-propagating pulses with the profile $f(u) = [1 - 2m(u/\tau)^{2m}]\, e^{-(u/\tau)^{2m}}$, $2m > N$, whose field and all its derivatives through order N agree with the shell's at one event; the pulses leave no lasting strain, since f and uf integrate to zero. What tells such scenes apart is a time record (the pulses pass), an aperture, or knowledge that the sources are compact and their waves outgoing. Nor does the algebraic type count bodies: two masses on a line make the same type D as one, and the reading with rows $(0, 0, 1)$, $(0, 0, i)$, $(1, i, 0)$ has both invariants zero, like a single wave, but rank two and $\mathcal{W}^3 = 0$: type III. The statements of this section are exact within the source classes they name.

o. One pixel and many. A single pixel already does part of a camera's work, as the paragraphs above show: it places one wave by Eq. (47), separates up to four from their time history, and sees the sky's brightness in its patterns of degree four and below. An array adds to this in two ways. Its size sharpens the image, Eq. (43). And it multiplies the number of sources that can be told apart: an array of N pixels, wherever they are placed and even along one line, has $5N$ independent steering vectors at each frequency and helicity, so subspace methods separate up to $5N - 1$ uncorrelated sources (one more, as above, if their circular polarizations differ), against $N - 1$ for scalar sensors and $3N - 1$ for sensors of light. The tensor nature of each pixel also removes the false images of a sparse array. Two scalar sensors far apart see a source equally well at any of the fringes of their pattern; two pixels D apart see the fringe at the source's true direction more strongly than its neighbours, because their response to two directions an angle ϑ apart is multiplied by $\cos^8(\vartheta/2)$. With a minimum-variance (Capon) estimator and a source at signal-to-noise ratio ρ, the true fringe stands above the nearest false one by the factor $1 + \rho^2[1 - \cos^8(\vartheta_1/2)]$, where ϑ_1 is the fringe spacing, λ/D for a source broadside to the pair and wider away from it, so that two pixels a hundred wavelengths apart form a telescope without ambiguity once ρ exceeds about a hundred (Fig. 29).

p. Variation across the array. A wave of wavelength λ changes across an array of width a by a fraction of order $2\pi a/\lambda$. The field of a mass at distance r, which falls as $1/r^3$, changes by a fraction of order $3a/r$. For a one-metre array, a wave at 100 Hz and a person three metres away, these are 2×10^{-6} and 1. Subtracting the average over the array therefore removes the wave and keeps the variation of the neighbourhood. The reverse is harder: the average itself contains the pull of everything nearby, and the person alone adds $3 \times 10^{-10}\,\mathrm{s}^{-2}$ to it, a million times the tidal field of the waves LIGO detects. To isolate the wave the camera must model the nearby masses from their variation and subtract them, which is how observatories plan to remove the changing pull of their surroundings [97, 98], or use the magnetic part, or compare two arrays far apart. With two arrays far apart the separation is cleaner still: a wave appears in both, with a delay that gives its direction, while a nearby mass appears in one.

q. Depth. The same variation measures distance. For an isolated mass the tidal field goes as M/r^3 and its gradient as M/r^4, so their ratio gives r, and then M: a pixel and its neighbours locate and weigh a body with no need to move the camera. This is the principle by which a calibration rotor's distance from a detector's mirror is found from the ratio of two of its multipoles [99]. A single pixel can range a moving mass without neighbours, but only with its magnetic part. The electric record alone cannot do it: the record of a mass M moving along $\mathbf{x}(t)$ is unchanged if the path is enlarged λ-fold and the mass λ^3-fold, while $\mathcal{B}$ grows λ-fold, because the speed of light supplies the scale. From Eq. (9), $\mathcal{B}\hat{n} = (3GM/cr^3)\,\hat{n} \times \mathbf{v}$

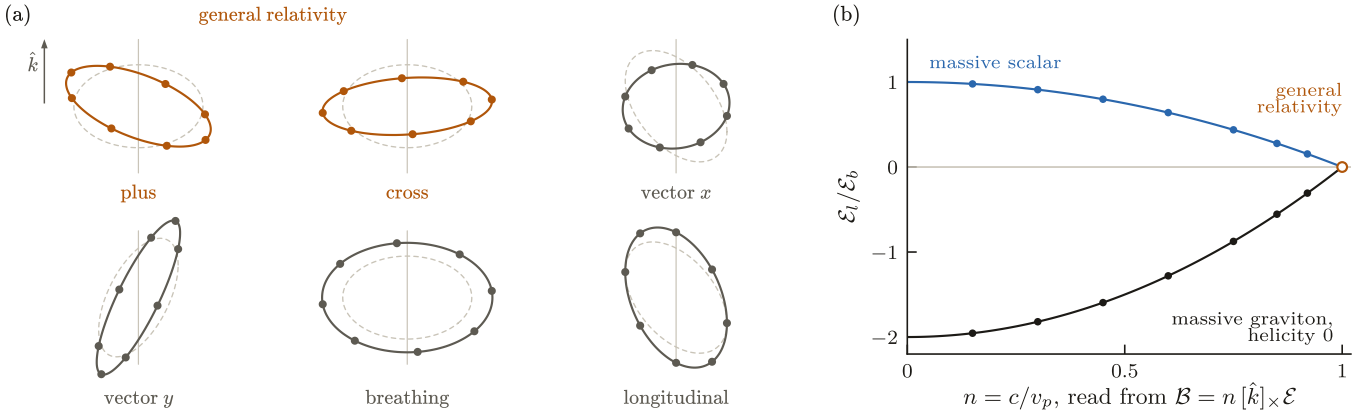


FIG. 28. Beyond general relativity in one reading. (a) The six polarizations a metric theory of gravity allows [95], each drawn as the distortion it makes of a ring of free particles in the plane where it acts (dashed: at rest; exaggerated), for a wave travelling along $\hat{k}$; general relativity has only the first two. One reading gives all six, with the direction and the phase speed, Eq. (64). (b) The ratio of the longitudinal to the breathing amplitude, and $n = c/v_p$, both read from one reading, for the helicity-zero wave of a massive graviton (black) and for a massive scalar (blue) (points: curvature computed from the metric), against $-2(1-n^2)$ and $+(1-n^2)$ (lines); general relativity is the open circle. The two differ in sign at every speed, and both ratios vanish as the speed approaches c.

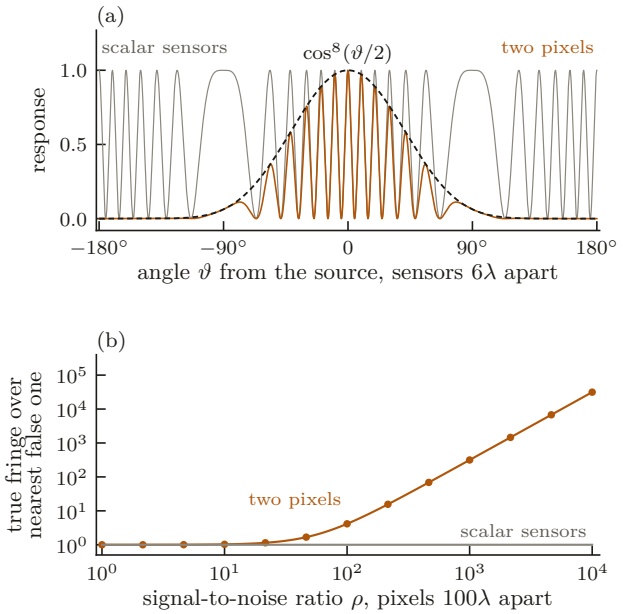


FIG. 29. Two pixels far apart. (a) The response of two sensors six wavelengths apart to one source, against the angle from it in the plane of their baseline: scalar sensors answer equally at every fringe, while for two pixels each fringe is weighed by $\cos^8(\vartheta/2)$, the overlap of their tensor responses to the two directions. (b) With a minimum-variance (Capon) estimator and two pixels a hundred wavelengths apart, the true fringe over the nearest false one, $1+\rho^2[1-\cos^8(\vartheta_1/2)]$ (line; points computed), against the signal-to-noise ratio, for a source 55° from broadside, where $\vartheta_1 = 1.8\,\lambda/D$; for scalar sensors the two are equal at any ρ.

and $P\dot{\mathcal{E}}\hat{n} = -(3GM/r^4)\,\mathbf{v}_\perp$, with $P = 1 - \hat{n}\hat{n}$, so that

$$\hat{n}\times(\mathcal{B}\hat{n}) = \frac{r}{c}\,P\dot{\mathcal{E}}\hat{n}, \qquad r = c\,\frac{|\mathcal{B}\hat{n}|}{|P\dot{\mathcal{E}}\hat{n}|}, \tag{66}$$

and then M from $\mathcal{E}$. The stretch axis of $\mathcal{E}$ gives $\hat{n}$ only up to sign; reversing it leaves the left side of the vector relation unchanged and reverses the right, so the sign that makes r positive fixes $\hat{n}$. Motion straight toward or away from the pixel gives no range, though it gives the time of arrival, Eq. (54); and the magnetic signal, smaller by v/c, sets the noise. For waves, range comes from the curvature of the wavefront, which across an array of width D amounts to a phase of order one at the distance D^2/λ; beyond it range is still measured, with a fractional error of order $\lambda r/\mathcal{R}D^2$ at signal-to-noise ratio $\mathcal{R}$. A single pixel also ranges a wave source, from how its field departs from that of a plane wave, Eq. (63).

r. Front and back. A flat array that records only the normal component $\mathcal{E}_{zz}$ cannot tell a mass in front of it from the mirror image of that mass behind it, because the two give the same $\mathcal{E}_{zz}$ on the plane. The shear components $\mathcal{E}_{xz}$ and $\mathcal{E}_{yz}$ change sign between the two, so the full tensor separates the half-spaces: a camera with no housing to block gravity can still ignore the photographer standing behind it.

s. Three dimensions. The pixels need not lie in a plane. A closed shell of pixels sees the whole sky at once and has no blind side; pixels filling a volume sample the field itself, although, as long as they stay outside the matter, the ambiguity of Section IV remains. And in the thermal regime the transparency of matter makes a further thing possible. Each image is then a set of line integrals, exactly the data of a medical tomograph. Images from several positions can be combined into a true three-dimensional map of emissivity, with nothing hidden

behind anything else.

t. How precisely. With white noise σ on each of the ten numbers, taken as the coefficients of $\mathcal{E}$ and $\mathcal{B}$ in an orthonormal basis of symmetric trace-free tensors ($e^A_{ij}e^B_{ij} = \delta^{AB}$, so that an off-diagonal entry carries $\sigma/\sqrt{2}$), and $\rho = |\mathcal{W}|/\sigma$, one pixel places one wave to within $1/\rho$ radian in each direction, against $\sqrt{2}/\rho$ for a sensor of light at the same signal-to-noise ratio; it reads its own velocity as given after Eq. (51); and it ranges a moving mass with the precision of Eq. (68) below. Table IV sets these counts beside those of a sensor of light.

How well each of these works against noise follows from the Cramér–Rao bounds of the same fields, compared in Fig. 30 with fits to simulated noisy readings; the details are collected in Appendix A.

u. Separation with noise. Take a wave at 100 Hz of strain 10^{-21} and, 3 m from the camera, a rotor of two 1 kg masses 12 cm apart turning 50 times a second, about the quadrupole of the rotor that calibrates LIGO by its pull [100]. Its changing tide has the wave's frequency and a hundred times its size. Shape alone tells an isolated wave from an isolated mass: the nearest wave to the field of a mass, and the nearest mass to a wave, lie at half the reading's size, so one reading of $\mathcal{E}$ puts the two $\rho/2$ standard deviations apart, with ρ here the size of $\mathcal{E}$ over its noise, and at $\rho = 12$ fewer than one reading in a hundred is taken for the other. A wave and a near field together are separated by the magnetic part, at a fixed price. Let the near field's $\mathcal{E}$ at the wave's frequency be anything at all, and its $\mathcal{B}$ below the noise. Fitting both then enlarges the error of the wave's amplitude by exactly $\sqrt{2}$, however strong the near field: the near field takes the wave's $\mathcal{E}$, and the wave is read from its $\mathcal{B}$, which carries half its signal. Ignored, the rotor would be read as a wave 35 times the true one; its own magnetic part, smaller than its $\mathcal{E}$ by about kr (the remark after Eq. (49)), leaks less than 10^{-4} of the wave. An array that reads only $\mathcal{E}$ must instead model the rotor from its variation, and pays more: the factor on the wave's error grows as r/b for neighbours at distance b, because a quadrupole's tide falls as r^{-5}, and is 2.2 for the rotor and an array a metre across, or 1.26 with $\mathcal{B}$ as well.

v. How well depth is measured. For one mass the field and its gradient give the range exactly, $r = \sqrt{15}\,|\mathcal{E}|/|\nabla\mathcal{E}|$ with norms over all components, and the Cramér–Rao bounds on range and mass are

$$\left(\frac{\sigma_r}{r}\right)^2 = \frac{1}{\rho_E^2} + \frac{1}{\rho_G^2}, \qquad \left(\frac{\sigma_M}{M}\right)^2 = \frac{16}{\rho_E^2} + \frac{9}{\rho_G^2}, \tag{67}$$

where ρ_E and ρ_G are the signal-to-noise ratios of the field and of its gradient, whatever the direction. A pixel with six neighbours at distance $b \ll r$ has $\rho_E = \sqrt{7}\,\rho$ and $\rho_G = \sqrt{30}\,\rho\, b/r$, so $\sigma_r/r \approx r/(\sqrt{30}\,\rho b)$. This rests on Euler's relation for a field homogeneous of degree $-N$ about its source, $(\mathbf{x}_s - \mathbf{x})\cdot\nabla f = Nf$, with $N = 3$ for the tide of a mass, by which geophysicists find the depth of buried sources from measured gradients [101, 102]. The magnetic part of one pixel, Eq. (66), ranges a moving mass with no neighbours to

$$\frac{\sigma_r}{r} = \frac{1}{\rho_B}, \tag{68}$$

ρ_B the signal-to-noise ratio of $\mathcal{B}$ alone, $\sqrt{3}\,v_\perp/c$ times that of $\mathcal{E}$ in each reading: for a person walking at $1.4\,\mathrm{m\,s^{-1}}$, a hundred million times worse than with neighbours. Depth along one line is the limit. For bodies on one line through the pixel every derivative of $\mathcal{E}$ there has the pattern of a single mass, so field and gradient see one body at $r_{\text{eff}} = \sum_i M_i r_i^{-3} / \sum_i M_i r_i^{-4}$, weighted toward the nearer: two equal masses Δ apart appear as one at $r - \Delta^2/r$, and a rod pointing at the camera as a point nearer than its centre. The spread of the depths shows first in the second derivatives, so two equal masses on one line are told from one only when Δ exceeds about $0.7\,(r^2/b)/\rho^{1/2}$: the square-root law that Section IV found for masses side by side. A round body of any size is a point, and its size is not measured at all.

At one point	Sound	Light	Gravity
Numbers recorded	4	6	10
Numbers no observer can change	–	2	4
Own velocity readable, components	–	2	3
Waves separated at one instant	1	1	2
Waves separated at one frequency	2	2	3
Waves separated over time	2	2	4
Sky numbers per frequency (of)	9 (16)	28 (36)	68 (100)
Direction of one wave, standard deviation	–	$\sqrt{2}/\rho$	$1/\rho$

TABLE IV. What a sensor at one point can measure, for sound (pressure and velocity), light (electric and magnetic fields) and gravity (the ten numbers of a pixel). Separation counts are for plane waves from distinct directions; over time the waveforms are arbitrary. A dash marks an entry that does not apply.

IX. A FIRST IMAGE

Because nothing absorbs or scatters, a thermal gravitational image is a line integral. Integrating Eq. (33) over frequency for constant η gives the energy emitted per unit volume and solid angle, $j_E = \alpha\sigma T^4/\pi$, where σ is the Stefan–Boltzmann constant. Dividing by the mean energy of a thermal quantum, $2.70\,k_{\mathrm{B}}T$, gives a number emissivity j_N, and the brightness of the pixel that looks along the unit vector $\hat{n}$ is

$$N(\hat{n}) = \int_0^\infty j_N\big(s\,\hat{n}\big)\,\mathrm{d}s, \tag{69}$$

in gravitons per second, per square metre of aperture, per steradian.

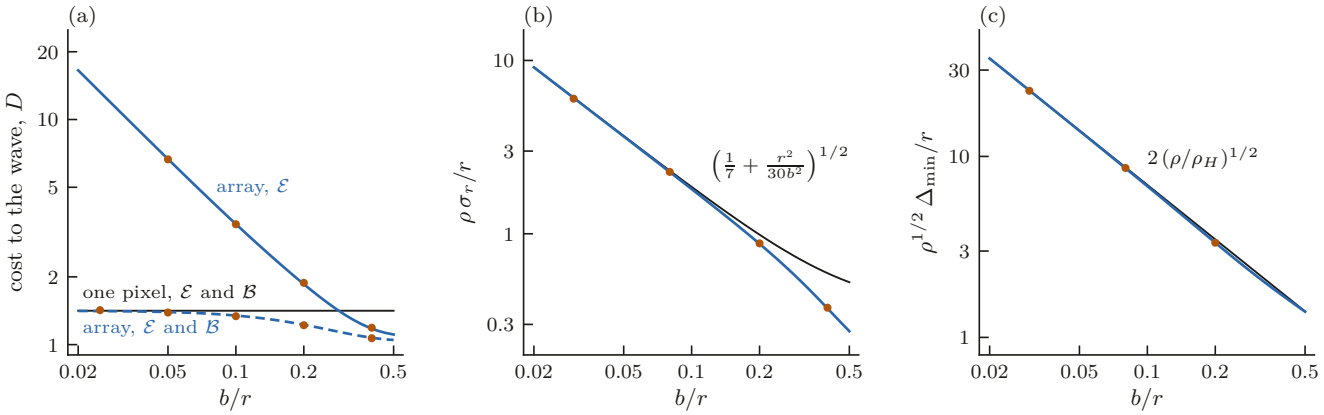


FIG. 30. Separation and depth with noise, against the distance b of a pixel's six neighbours over the distance r of the source. Blue: Cramér–Rao bounds of the full models; black: closed forms; dots: the spread of maximum-likelihood fits to simulated noisy readings (2000 readings for each point of (a), 10^4 in (b) and (c)). (a) The factor D by which fitting the rotor of the text enlarges the error of a wave's amplitude: at one pixel from $\mathcal{E}$ and $\mathcal{B}$, with any near field, $\sqrt{2}$ (the dot at left is a simulation with the rotor present); for the array, which fits the rotor as a point quadrupole of unknown moment and position, from $\mathcal{E}$ alone (solid) and from both (dashed). (b) The range of one mass, with ρ the signal-to-noise ratio of one pixel's reading, against Eq. (67). (c) The separation $\Delta_{\min}$ in depth at which two equal masses on one line are told from one at one standard deviation.

Figure 1 evaluates Eq. (69) for an observer on the night side of the Earth, at latitude 40° at local midnight. The Earth is modelled as five uniform shells with rounded textbook radii and temperatures, from a crust at 700 K to an inner core at 5500 K. Looking straight down, the line of sight runs through 12,700 km of rock and iron, and the expected brightness is at most 1.2×10^{-5} gravitons per second per square metre per steradian, each shell being given the most that its stiffness allows (below). Lines of sight that miss the core are fainter (Fig. 31). The Sun radiates of order 10^8 W in gravitational waves [10, 11, 103], about 4×10^{-16} W m^{-2} at the Earth: roughly one graviton per square metre per second, arriving from a patch of sky a tenth of a degree across. Its surface brightness, about 4×10^5 gravitons per second per square metre per steradian at the centre of the core in our model, is more than 10^{10} times that of the Earth's interior, so the Sun dominates the thermal gravitational sky by day and by night.

The Moon, in light the brightest thing in the night sky, is faint in thermal gravitational radiation: its centre is about eighty times fainter than the ground underfoot, because its interior is cooler, 1200–1700 K in our model, and a line of sight through it is a quarter as long.

The shells' radii and densities are rounded from the Preliminary Reference Earth Model [31]. Two assumptions carry most of the uncertainty. The Earth's internal friction at thermal frequencies is not known. Each shell is therefore given the most that its stiffness allows, Eq. (36), between 1.6 and 3.4×10^{-4} Pa s (see *What the Earth's materials allow*, below), so that every brightness of the Earth in this section is an upper bound. The Sun's emission is spread uniformly over the inner fifth of its radius, where the true profile is peaked toward the centre.

a. How faint. The image is an expectation value. Figure 33 sets the numbers of gravitons emitted side by side, and Table V the numbers a camera would receive in each of the scenes of this paper. The Sun delivers about one graviton per square metre per second. The whole Earth below delivers at most one every twenty hours, 3.6×10^4 per square metre in eighty years. That is a coarse picture: picking out features of ten per cent contrast at five standard deviations takes about 2500 counts each, so a lifetime's exposure resolves at most some fourteen picture elements. Everyday objects in a room take millions of years for a single graviton. These counts assume no other background. If the primordial glow of Section XI exists, its 3.6×10^{14} gravitons per second per square metre per steradian dwarf every one of them; but it is cold, and an ideal filter passing only frequencies above two terahertz leaves 4×10^{-43} of it, fainter than anything in this paper, while keeping 98 per cent of the gravitons from a body at room temperature, and more from hotter ones (with the friction taken as constant across the band). Its fluctuations, not its known mean, are what such a filter must remove.

b. Recovering the layers. A camera on the surface of a round planet needs no other viewpoint to see inside it. The line of sight at angle θ from straight down passes the centre at the distance $p = R\sin\theta$ and crosses the planet along the whole chord at that distance, so for an emissivity that depends only on the radius, Eq. (69) becomes

$$N(p) = 2\int_p^R \frac{j_N(r)\,r\,\mathrm{d}r}{\sqrt{r^2-p^2}}, \tag{70}$$

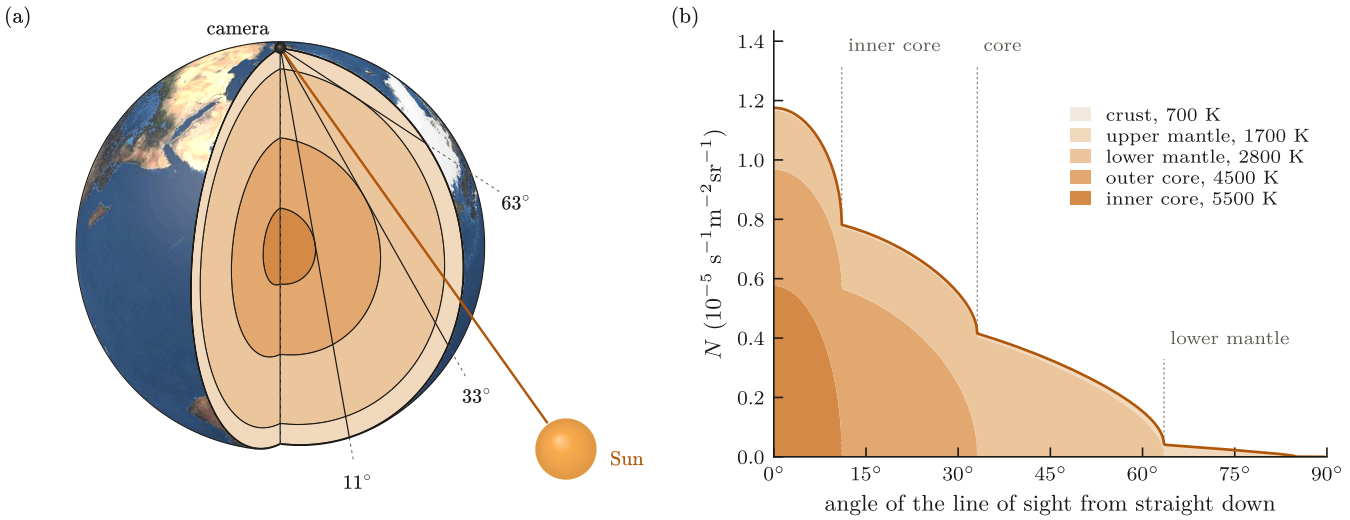


FIG. 31. The thermal glow of the Earth's interior seen from its surface. (a) The model's five shells, to scale, in a globe with a quarter cut away. Every line of sight starts at the camera on the surface; the three drawn graze the boundaries of the inner core, the core and the lower mantle, which they meet at $\arcsin(r/R)$ from straight down: 11°, 33° and 63°. The line to the Sun's core leaves 40° from straight down, as in Fig. 1, and crosses only the mantle. The Sun's size and distance are schematic; the surface is NASA's Blue Marble. (b) The brightness, Eq. (69), against the angle of the line of sight, with each shell's share shaded in its colour in (a). Its steps fall exactly at the grazing angles, so their places are a measurement of the radii that does not depend on the friction, here the most that each shell's stiffness allows, which sets only their heights.

the Abel transform of the profile $j_N(r)$, which can be inverted:

$$j_N(r) = -\frac{1}{\pi}\int_r^R \frac{\mathrm{d}N}{\mathrm{d}p}\,\frac{\mathrm{d}p}{\sqrt{p^2-r^2}}. \tag{71}$$

The planet's symmetry supplies the other viewpoints that tomography would need. For shells of uniform emissivity the inversion is a peeling. The line of sight that grazes the bottom of a shell crosses only that shell and those above it, so the crust's emissivity is read first and each deeper one in turn, as in the onion-peeling reconstructions of flames and plasmas [104]. Where the emissivity jumps, at a boundary of radius r, $\mathrm{d}N/\mathrm{d}p$ diverges as $(r-p)^{-1/2}$: the brightness has a kink at $\sin\theta = r/R$, and these kinks are the steps of Fig. 31. Their places are geometry, the radii of the boundaries; the friction, the temperatures and the exposure set only their heights.

The heights measure a product. From the definitions above,

$$j_N = \frac{16\,G\,\eta\,\sigma T^3}{2.70\,k_\mathrm{B}\,c^3}, \tag{72}$$

so counted gravitons give ηT^3 in each shell, and their energies give ηT^4. If the friction is flat across the thermal band, the two together give each shell's temperature, from the mean energy $2.70\,k_\mathrm{B}T$ of the gravitons it sends, and then its friction. The camera is then a thermometer for the deep Earth and a viscometer for its friction at terahertz frequencies, which no seismometer reaches. If the friction varies across the band, each shell's spectrum is $\alpha(\omega)$ times a Planck spectrum, Eq. (33), and the temperature trades off against the shape of α.

How well a lifetime does is shown in Fig. 32. It simulates eighty years of counts on a square metre that collects from every direction, about 3.6×10^4 gravitons with the shells at their bounds, with the Sun's path across the ground masked, and fits five shells to them by maximum likelihood, radii and emissivities together. In rings of one degree such a fit is expected, from the Fisher information of the model, to place the boundary of the core to within 29 km and the top of the lower mantle to within 5 km (one standard deviation), and to measure the emissivity of the lower mantle to 0.9 per cent, of the outer core to 1.8, of the upper mantle to 3, of the inner core, seen only within 11° of straight down, to 6, and of the thin crust hardly at all, to 56 per cent; with the temperatures known, these are also the errors of the friction. The errors scale as $1/\sqrt{\eta\tau}$ with the friction and the exposure time. The coarse picture of the previous paragraph, fourteen picture elements, is what a lifetime gives for a scene that is not known in advance. A planet known to be layered spends the same gravitons on nine numbers, as a simple scene does in the near field (Section IV). Departures from spherical symmetry, from the planet's flattening to the slabs and plumes of the mantle, would need cameras at several places, and are tomography proper.

c. What the Earth's materials allow. The placeholder of Section VI, 10^{-3} Pa s, would overstate the deep Earth. By Eq. (36), matching its count of gravitons needs 0.9 TPa of relaxing stiffness at 2800 K and 1.7 TPa at 5500 K, several times the shear stiffness of any shell. The

figures of this section grant each shell all of the shear stiffness at its base, and the core the weight of two free electrons per atom, 0.2 TPa, placed at the best frequency: 16 to 34% of the placeholder's count, shell by shell. That is the most the Earth can send, not an estimate of what it does; with the placeholder a lifetime would have brought 1.4×10^5 gravitons and found the boundary of the core to within 6 km. Real spectra fall further below. The mantle is an insulator whose vibrations end near 33 THz, twice that for pairs, while at 2800 K its glow would peak in number near 90 THz; and the electrons of the liquid iron core, with a resistivity of order a micro-ohm metre [105], collide every fraction of a femtosecond and spread their weight far beyond the band of heat, to about 3% of the placeholder's friction, a fifth of what the figures grant it. In counts the core may then hardly stand out from the mantle. In colour it does. The core's gravitons, from electrons whose friction is flat across the band, carry about $2.7\,k_BT \approx 1$ eV; the mantle's, confined below its highest vibrations, 0.09 to 0.17 eV. The boundary of the core, 33° from straight down, is a step in the colour of the glow by a factor of five to twelve, for any resistivity between half a micro-ohm metre and three. The steps of the figures fall at the same places whatever the friction.

d. Arrival and absorption. The counts of this section are of gravitons that arrive, and here the premise of an ideal pixel asks the most. A detector made of matter absorbs through the same friction by which matter glows, and the sum rule that caps the glow caps the catch (Section VI). Across the band of room-temperature heat, $k_BT/\hbar = 4\times10^{13}\,\mathrm{s}^{-1}$ wide, a metre of a solid with 30 GPa of relaxing stiffness stops no more than about 1.5×10^{-37} of what crosses it, and a metre of diamond not twenty times more. A cubic metre of such a detector, crossed by one graviton a second, would wait 2×10^{29} years for its first count. Dyson, and Rothman and Boughn, reached the same verdict for detectors of other kinds [106, 107]. The thermal pictures of this paper are pictures of what is there to be seen, not of what a detector made of matter could record.

e. Counting or recording. These budgets count gravitons, while the array of Section VII records the field at each pixel and combines the records afterwards. In the thermal regime the two are in tension. The radiation is so weak that each of its modes holds of order 10^{-30} gravitons on average, and any device that records both quadratures of a field at a pixel must add at least half a quantum of noise per mode [108]; recorded pixel by pixel, a thermal gravitational image would be buried in that noise. Counting avoids the noise but loses the phase that Eq. (42) needs. For weak thermal light the same tension is known: combining the pixels coherently before detection, as a lens does, extracts information in proportion to the occupation, whereas recording each pixel separately extracts it only in proportion to its square [109, 110]. A thermal gravitational camera therefore needs either pixels joined coherently into one quantum receiver, as quantum repeaters would join the stations of an optical interferometer [111], or a converter that turns each graviton into a photon travelling the same way, as a strong magnetic field does, so that ordinary optics can focus it [106]. The near field, a static field rather than radiation, is not affected.

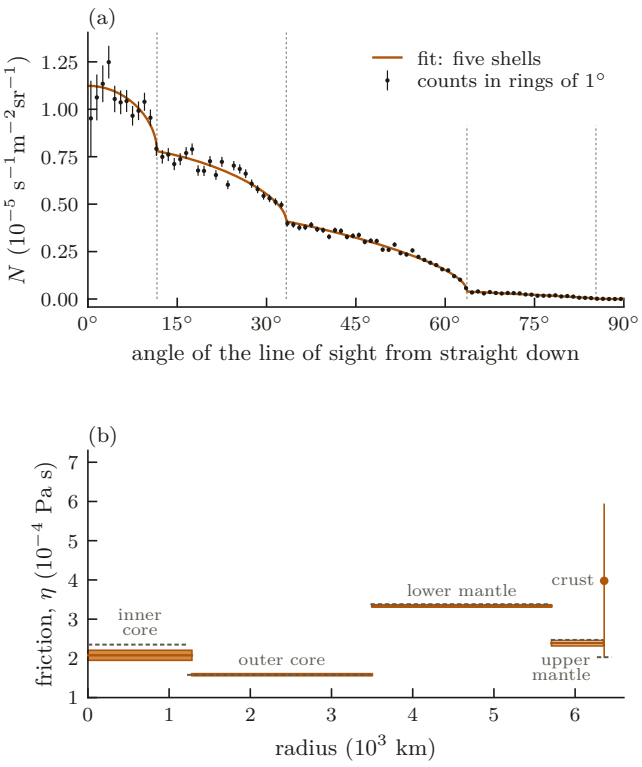


FIG. 32. The thermal Earth, inverted, in a simulation. (a) Eighty years of gravitons on a detector of one square metre that collects from every direction, pooled in rings of one degree about straight down (dots, with Poisson errors; 35,619 in all), and the maximum likelihood fit of five uniform shells, radii and emissivities together (line), Eq. (70). Dashed: the fitted boundaries, at $\arcsin(r/R)$. (b) Each shell's friction, read from its fitted emissivity at the model's temperature, Eq. (72), against radius. The boxes span the fitted radii and one standard deviation; the dashed grey lines are the frictions given to the model, each shell's bound (for the crust, too thin to draw, a short dash across its bar). The radii fitted to this simulated sample are 1281 ± 41, 3499 ± 28, 5709 ± 5 and 6350 ± 3 km, against the model's 1222, 3480, 5701 and 6346. The crust, 25 km thick, sends only about twelve of the gravitons.

A counting pixel still learns where each graviton came from. One graviton of helicity two from $\hat{n}$ excites the five local modes of its helicity in the state of Eq. (46), a coherent state of spin two [112], and the measurement made of all such states, equally weighted over the sky, is complete. It clicks at the angle γ from $\hat{n}$ with probability density $(5/4\pi)\cos^8(\gamma/2)$, and adds no noise: an empty mode never clicks. Each graviton then carries 1.17 bits about its direction, against 0.62 for a photon at a point sensor of light and none for a scalar, $\log_2(2s{+}1) - 2s/[(2s{+}1)\ln 2]$ for spin s, and Fisher information s about each

Scene, and what is counted	Regime	One graviton per square metre every
The Sun at midnight: the Sun's core	thermal	second
The Sun at midnight: the whole Earth below	thermal	20 hours, or more
The closed furnace: the hot iron, at 3.5 m	thermal	9×10^7 years
Which way it turns: one turning pair, at 4.5 m	waves	4×10^7 years
The other scenes	near field	none needed

TABLE V. The graviton budget of the scenes of this paper, for a detector of one square metre that collects from every direction. The thermal rates take for the Earth's shells the most their stiffness allows, and for the hot iron the estimate of Section VI. The turning pair is two steel balls of 33 kg, 0.44 m apart, turning once a second and seen along their axis; the rate is that of their far field, although at this distance the camera is deep inside their near zone. A flat detector facing the ground would collect each direction in proportion to the cosine of its angle from straight down, and would wait about 1.3 times as long for the Earth. The near field is a static field, not radiation: what limits it is noise, Eq. (21), not the number of gravitons.

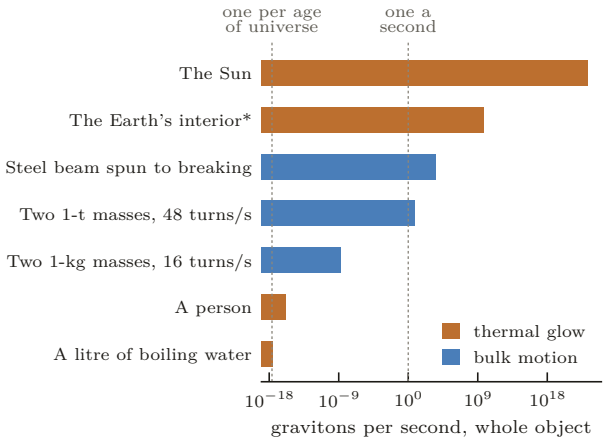


FIG. 33. Gravitons emitted per second by whole objects, on a logarithmic scale spanning forty powers of ten. The spinning masses radiate by bulk motion, Eq. (26); the others thermally, Eq. (33). The person, taken as seventy litres of water, and the litre of water have the friction of water (Section VI). The Earth's value (marked with an asterisk) depends on its assumed friction and is an upper estimate. The beam weighs 490 tonnes; the pairs of masses are of one tonne, two metres apart, and of one kilogram, a metre apart.

angle, half the quantum limit $2s$ for one angle alone. A square metre of such independent pixels finds the Sun's core through the Earth at midnight, at one graviton a second, to a degree in half an hour, with no coherent combination at all; it sees the sky only up to degree four, the twenty-five numbers of Section VIII, which is enough for a single bright source but not for an image.

X. WHAT THE CAMERA CAN DO THAT LIGHT CANNOT

Table VI collects what follows from the preceding sections for someone holding the camera.

The line of the table on what emits no light includes light itself. A beam of power P carries energy and an equal pressure along its length, and to a static observer beside it both gravitate: it pulls like a line of matter of $2P/c^3$ per metre, twice what its energy alone would suggest [113]. An infrared beam that no camera can see from the side is, for this one, a faint line; for a 100 kW beam, a change of five parts in 10^{25} of the tide of the room around it, visible only by subtracting the reading with the beam off. Its field has the form of a plane wave's rather than a mass's: beside the beam the tidal tensor has eigenvalues $(-1, 1, 0) \times 4GP/c^3b^2$ at distance b, a stretch along the line to the beam, a squeeze across both it and the beam, and nothing along the beam, and the magnetic part is just as large. Reversing the beam reverses the magnetic part and leaves the electric part alone, so the camera tells from the side which way an invisible beam is

The camera can	Because	Regime
See through anything	nothing absorbs or scatters gravity	near field, thermal
Find what is hidden	mass has one sign and no wall screens its pull, though its arrangement can be disguised	near field
Weigh by looking	the signal is set by mass, not by surface	near field
Ignore images	a reflection has no mass, and a screen's picture next to none	all
Read inside temperature	hot bodies are transparent to their own glow, given the material	thermal
Tell materials by their friction	emission follows the friction at the frequencies of heat	thermal
Read spin and its sense	polarization follows the motion of the source	waves
See flow inside a sealed body	the magnetic part of the field is made by moving mass, though opposite flows can cancel outside	near field
See what emits no light	all energy gravitates	near field
Read interiors by their tremor	the thermal motion of a body's mass, at a known temperature, gives its moments	near field

TABLE VI. What a gravitational camera affords, and why.

travelling; in a standing wave between two mirrors, as in an interferometer's arms, the magnetic part cancels.

The same reasoning tells what the camera cannot do. It cannot read a page, recognise a face by its colouring, or see a picture on a screen: the ink and the light carry mass-energy, but far too little against the page and the screen, and everything that light carries by reflection from surfaces is absent. The two kinds of camera are complementary, and a scene is best understood with both.

Within each channel there are also scenes that the camera cannot tell apart at any sensitivity. Table VII collects them, with what each channel does fix and what breaks each tie. The blind spots of one channel are covered by another: what the near field cannot place inside a body the glow can, what the glow cannot weigh the near field can, and what does not radiate is still felt as a pull. The camera's full set of channels leaves little hidden; any one of them alone leaves a great deal.

XI. ASTROPHYSICAL AND COSMOLOGICAL SCENES

The scenes so far are rooms and planets. This section follows the same equations to astrophysical scales, in problems that have exact or closed-form solutions.

a. A pair of black holes, from the near zone to the wave zone. Outside any compact source, linearized gravity has an exact solution organised by multipoles [114]. Kept to the order of the mass quadrupole I_{ij}, with $u = t - r/c$ and $\hat{n}$ the direction from the source, the trace-reversed perturbation in harmonic gauge is

$$\begin{aligned} \bar{h}^{00} &= \frac{4G}{c^2}\Big[\frac{M}{r} + \frac{1}{2}\,\partial_i\partial_j \frac{I_{ij}(u)}{r}\Big], \\ \bar{h}^{0i} &= \frac{2G}{c^3}\Big[\frac{\dot{I}_{ij}(u)\,\hat{n}_j}{r^2} + \frac{\ddot{I}_{ij}(u)\,\hat{n}_j}{c\,r} + \frac{(\mathbf{J}\times\mathbf{x})_i}{r^3}\Big], \\ \bar{h}^{ij} &= \frac{2G}{c^4}\,\frac{\ddot{I}_{ij}(u)}{r}, \end{aligned} \tag{73}$$

with M the mass, $\mathbf{J}$ the angular momentum and $I_{ij} = \int \rho\, x_i x_j \,\mathrm{d}^3x$ the second moment of the mass. For a circular orbit its trace is constant, and then it changes only the gauge outside the source, not the curvature; for a source whose trace varies, I_{ij} should be its trace-free part. It satisfies the gauge condition exactly, and its curvature gives the tidal field in every zone at once [115]: exactly, within linearized gravity and this truncation of the multipoles. Figure 34 shows it in the plane of an orbit, for two black holes of thirty solar masses each about ten seconds before they merge, when they are 2200 km apart and move at a tenth of the speed of light; their waves are 35,000 km long. Within a reduced wavelength, $\lambda/2\pi$, the changing part of the field is Newton's pull of two masses, turning rigidly with them and falling as r^{-5}. Beyond it the pattern winds into a two-armed spiral whose strength falls only as r^{-1}: the waves. The two meet where $G\,\Delta I/r^5 \approx G\,\Delta I\,\omega^4/c^4 r$, that is at $r \approx c/\omega = \lambda/2\pi$.

This marks a crossover between the two ways the camera sees, not a sharp edge. Well inside it the near-field imaging of Section IV applies, and an array could resolve the pair as two bodies, if its signal-to-noise ratio and width meet the blur law there; well outside it, Eq. (27) holds and the pair is a point whose polarization tells the axis and sense of its orbit. Being within about a sixth of a wavelength is needed to see two black holes as two, but it is not enough by itself. The field of Eq. (73) becomes Newton's field of the two masses near them, with an error falling as $(d/r)^2$, and the quadrupole wave far away, with an error falling as λ/r; it is the curvature of vacuum, with $|\mathcal{B}| = |\mathcal{E}|$ in the waves.

One pixel on the axis of the orbit follows the crossover in its four principal null directions. There the reading is the pair's static tide plus the wave, $\mathcal{W} = (GM/r^3)\,\mathrm{diag}(1,1,-2) + w\,\mathbf{m}_0\mathbf{m}_0^T$ with $\mathbf{m}_0 = (1,i,0)$, and Eq. (48) factors: $\mathbf{m}^T\mathcal{W}\mathbf{m} = 4z^2(wz^2 - 3GM/r^3)$. Two of them lie on the direction of the wave from the start; the other two, at $z = \pm(3GM/r^3 w)^{1/2}$, turn about the line of sight in step with the orbit and move out to join them as the wave outgrows the pull, so the type goes from D through II to N. They cross the sky's equator where $|w| = 3GM/r^3$, the wave's stretch one and a half times the static stretch along the line of sight, which is not at $\lambda/2\pi$: the static tide of the whole mass exceeds the changing quadrupole there by $(c/v)^2$, and the wave overtakes it only near $(\lambda/2\pi)(c/v)$, ten times farther for the pair of Fig. 34. The magnetic part has no tide of the mass, only that of the spin, GJ/cr^4, and its crossover from the one to the wave falls at $\lambda/2\pi$ whatever the speed.

b. Memory. Radiation that escapes to infinity carries away mass, and a camera it passes is left permanently deformed: the memory [116–118]. For energy radiated with angular distribution $\mathrm{d}E/\mathrm{d}\Omega'$, at nearly the speed of light, the change in strain seen from direction $\hat{N}$ at distance r is [118, 119]

$$\Delta h_{ij}^{\mathrm{TT}} = \frac{4G}{c^4 r}\int \frac{\mathrm{d}E}{\mathrm{d}\Omega'}\left[\frac{n'_i n'_j}{1-\hat{n}'\cdot\hat{N}}\right]^{\mathrm{TT}} \mathrm{d}\Omega'. \tag{74}$$

Applied to the waves of a merger themselves, whose power goes as $(1+\cos^2\iota)^2/4 + \cos^2\iota$, it gives

$$\Delta h_+ = \frac{G\,\Delta E}{24\,c^4 r}\,\sin^2\iota\,\big(17+\cos^2\iota\big), \tag{75}$$

the shape found by Wiseman and Will [120, 121]. It is largest seen edge-on, where the oscillating wave is weakest (Fig. 35). A camera that records the field, not the strain, sees the memory as a burst of $\mathcal{E}$ whose second time integral does not return to zero. The memory has a partner of the other parity, the spin memory [122, 123]: a lasting offset not in the strain but in its time integral, the third integral of the field. For a pair that does not precess its pattern goes as $\sin^2\iota\cos\iota$: it vanishes seen face-on and edge-on, peaks at $\cos\iota = \pm 1/\sqrt{3}$, and changes sign between the two sides of the orbit. The displacement memory, even under $\iota \to \pi - \iota$, cannot tell which way the pair turned; the spin memory records it.

Channel	Fixes	Cannot tell apart	Broken by
Near field, electric part, outside the matter	the harmonic part of the density	a nugget, a flush and a skin; a shell and a ball; every round body and a uniform ball	spin, through the moment of inertia and the moments like it; heat, through the tremor's moments; the glow; a pixel inside, $\operatorname{tr}\mathcal{E} = 4\pi G\rho$
Near field, magnetic part, outside the matter	at most the corresponding part of the flow of mass	a ball and a shell turning in opposite senses with no total angular momentum; spherical bodies of equal angular momentum; any confined flow that is the same all round an axis and turns in its meridian planes	a pixel inside, $\mathcal{B}_{[ij]} \propto \epsilon_{ijk}\rho v_k$
Waves	the stress transverse to the line of sight, on the light cone	steady motion in a straight line; spherical pulsation; pressure; a body turning steadily about an axis of symmetry	the near field of the same motion, except for a spherical pulsation, which changes nothing outside the body
Thermal glow	line integrals of ηT^3 (counts) and ηT^4 (energy)	friction from temperature, without the spectrum; mass, which does not glow; dark matter without collisions, which has no friction	the spectrum; the near field
Every local channel	curvature	a straight cosmic string and empty space	what lies behind it: double images, a step in a background's temperature
One pixel	the sky's harmonics of degree four and below	twelve sources at the corners of an icosahedron and a uniform sky	an array

TABLE VII. What each channel of the camera fixes, what it cannot tell apart at any sensitivity, and what breaks the tie, collected from Sections IV to IX and, for the string, Section XI. The harmonic part of the density is that of Eq. (11); the nugget, the flush and the skin are those of Fig. 6.

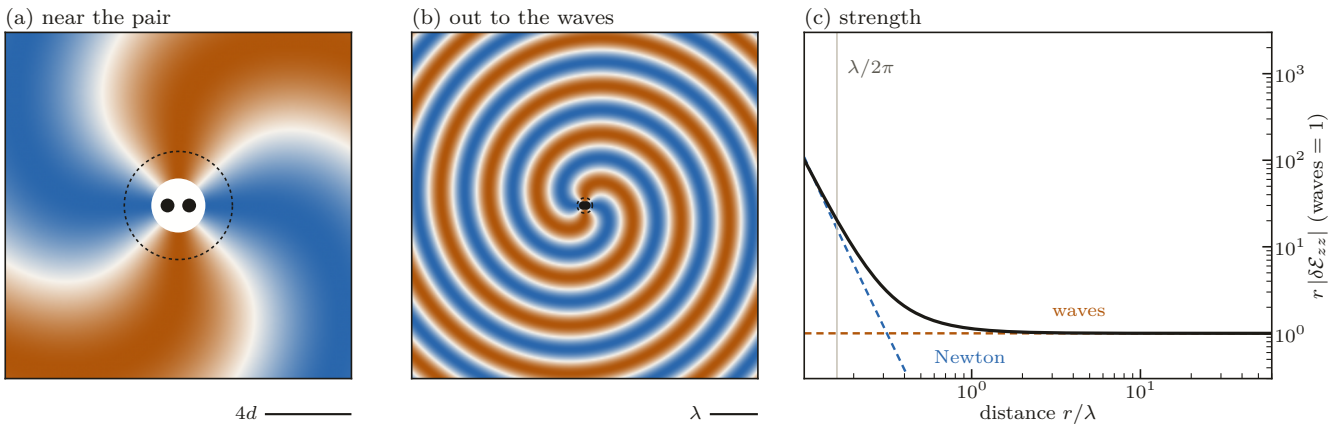


FIG. 34. Two black holes of thirty solar masses, ten seconds before they merge, in the plane of their orbit: the changing part of the tidal field $\mathcal{E}_{zz}$ (across the plane), from the linearized solution of Eq. (73), exact within that model. Colour gives the phase, orange for stretch and blue for squeeze, scaled at each place by the local strength. (a) Near the pair, whose separation is d, the pattern turns rigidly with it; beyond the dashed circle, $r = \lambda/2\pi$, it begins to wind. (b) Farther out it is the spiral of the waves. (c) The strength along a line in the plane, times r: Newton's r^{-5} near the pair and the waves' r^{-1} far from it, the two laws crossing at $0.3\,\lambda$, twice the radius of the dashed circle. The field is an exact solution of linearized gravity truncated at the mass quadrupole, which this close to a merger is a guide to the full solution, not a substitute for it.

c. An exploding star. A spherical collapse or explosion radiates nothing: by Birkhoff's theorem the field outside a spherical body is that of a point mass, whatever happens within. It does change once. A core collapse sends out some 3×10^{46} J in neutrinos, a sixth of a solar mass, as a thin shell moving at nearly the speed of light, and outside the shell the field is that of the original mass, inside it that of the remnant [124]. A near-field camera sees the star lose the neutrinos' mass at the moment the shell passes the camera, not before: it weighs the burst as it arrives. While the shell passes, the camera also feels the neutrinos themselves. Their flux of energy, $F = L/4\pi r^2$ at luminosity L, enters the Ricci part of the curvature and squeezes the camera evenly across their direction of travel, $\mathcal{E}_{ij} = (GL/c^3r^2)(\delta_{ij} - \hat{n}_i\hat{n}_j)$, while $\mathcal{B}$ gains the antisymmetric part of Section II, set by their flow, so that one pixel points to the star although the explosion is spherical. From ten kiloparsecs this squeeze, while it lasts, is some 10^{11} times the change of pull it leaves behind. If the neutrinos leave unevenly the explosion also leaves memory [119, 125]. A narrow jet of energy E leaves $\Delta h = (2GE/c^4r)(1 + \cos\theta)$ at angle θ from it, largest just off the line it travels along (exactly on that line symmetry allows none, and a jet of finite width turns the memory off within its own width of the axis); two opposite jets leave the same $2GE/c^4r$ in every direction off their axis; a sphere leaves nothing (Fig. 35). Only the quadrupole and higher parts of the pattern count: the radiation of a burst that is merely brighter on one side, a pure dipole, leaves no memory at all. It does push the star the other way, and the recoiling remnant leaves a memory of its own, second order in the small recoil [121]. A burst stronger along an axis than across it, in proportion to $1 + q\,P_2(\cos\theta')$, leaves

$$\Delta h = \frac{q\,GE}{2\,c^4 r}\,\sin^2\theta. \tag{76}$$

For a supernova ten kiloparsecs away and $q = 0.01$ this is 4×10^{-21} seen from the side.

d. The Milky Way. Tens of millions of close pairs of white dwarfs radiate at millihertz frequencies; together they make a foreground that will dominate the sky of the planned space detectors below a few millihertz [126]. They trace the Galaxy's stars, and averaged over time and over orientations, which we take to be random, each radiates the same in every direction; so their brightness on the sky is the column integral of Eq. (69) over a model of the stellar mass, here two exponential discs and a central bulge with masses and sizes from Bland-Hawthorn and Gerhard [127]. Light from the same stars passes through a thin disc of dust, which in this model dims the light of the Galactic centre by about thirty magnitudes, at the low end of the thirty to fifty inferred from the infrared [128]. Figure 36 shows both on one scale. In light the centre is hardly brighter than the opposite side of the sky; in gravitational waves it is a hundred times brighter, and the map is a map of where the Galaxy's stars are. Seeing it this sharply as a smooth glow would take a camera

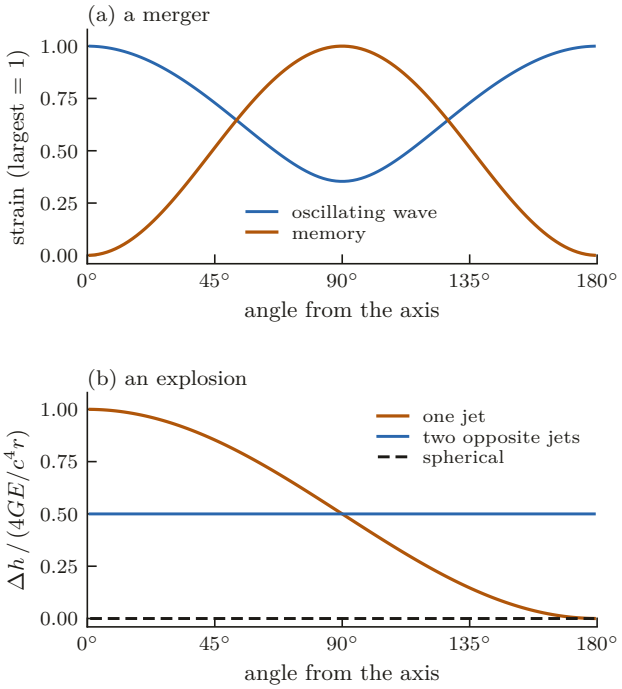


FIG. 35. The memory, Eq. (74), against the direction of the camera. (a) A merger: the oscillating wave is strongest along the orbit's axis, the memory, Eq. (75), in its plane. (b) An explosion whose energy leaves in one jet, in two opposite jets, or evenly in all directions, in units of $4GE/c^4r$.

some 50 AU across, since at three millihertz the waves are two-thirds of an astronomical unit long. The pairs are not a glow, though: after years of observation thousands of the brightest, above a few millihertz, would each sit alone in its own frequency bin, and a single pixel could place each of them by Eq. (47), breaking the smooth map into points.

e. A primordial graviton background. Gravitons stop interacting near the Planck temperature. If the early universe was ever that hot, they were then in equilibrium and have kept a black-body spectrum ever since. Every species that later annihilated heated the photons but not them, so by conservation of entropy their temperature today is [129]

$$T_g = \left(\frac{3.91}{106.75}\right)^{1/3} T_\gamma = 0.905\,\mathrm{K}, \tag{77}$$

with $T_\gamma = 2.7255\,\mathrm{K}$ [130] and the particles of the Standard Model; more particles would make it colder. Whether this background exists is a test of inflation, which would have diluted it away [131]. Its energy density counts as 0.05 of an extra species of neutrino, within present bounds.

If it exists, it carries more energy than any other background in the gravitational sky: 7×10^{-7} of the critical density, against about 10^{-8} for the background found by pulsar timing at nanohertz frequencies [132]. At high frequencies it outshines everything else in this

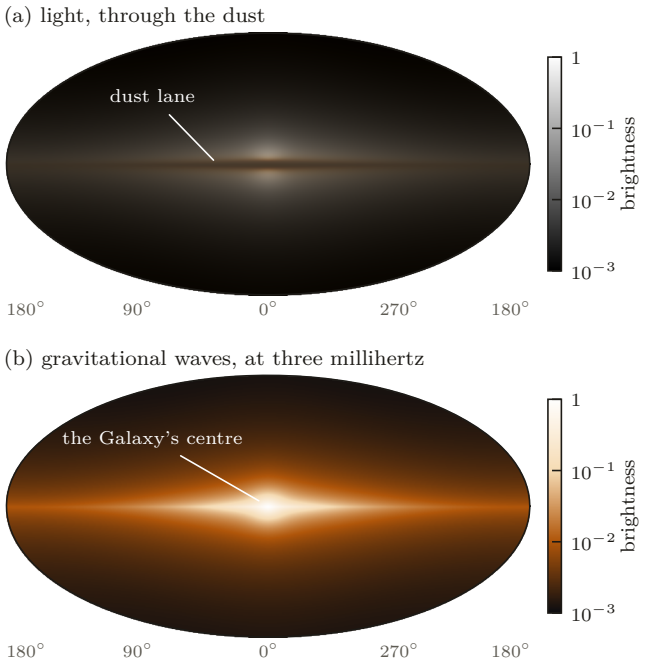


FIG. 36. The Milky Way from the Sun, over the whole sky, centred on the Galaxy's centre with Galactic longitude, marked beneath each map, increasing to the left, both on one logarithmic scale of brightness. (a) Light from the model's stars, dimmed and reddened by its dust. (b) Gravitational waves from white-dwarf pairs that trace the same stars, as an ideal camera about 50 AU across would see them at three millihertz. Without its dust, (a) would be identical to (b) in brightness.

paper. A black body of two polarizations sends $N = 4\zeta(3)(k_BT/h)^3/c^2$ quanta per second per square metre per steradian: 3.6×10^{14} at 0.905 K, against at most 1.2×10^{-5} for the Earth's interior and 4×10^5 for the Sun's core (Section IX). It is also the easiest to image. Its gravitons are about a centimetre long, so an aperture of a metre resolves a degree. The following properties follow from what is already known.

- *It has a dipole from our motion.* We move at 370 km/s relative to the frame in which the microwave background is isotropic [133]. If the graviton background is isotropic in the same frame, our motion makes it hotter by $v/c = 1.2 \times 10^{-3}$ of its temperature in the direction in which we move, exactly as for the microwave background.

- *On large scales it shares the microwave background's spots.* On scales larger than the horizon at the time the microwave background was released, the Boltzmann equation of any massless species reduces to $\dot\Theta = -\dot\Phi$ (Θ the fractional change of temperature, Φ that of the spatial metric, $g_{ij} = a^2(1 + 2\Phi)\delta_{ij}$), the same for gravitons streaming freely as for photons held in the plasma. With the same adiabatic start, the two arrive at that time with the same temperature perturbation, and from then on travel together through the same potentials. To this approximation the graviton sky shares the large spots of the microwave sky, from a surface only 2% farther away; how closely, scale by scale, is a question for a cross-correlation of the two. The same redshift was found for the gravitons that inflation makes [134]. It differs below a degree or so, where it has no acoustic peaks, its gravitons never having moved with the plasma, and it is not smoothed by the diffusion that blurs the microwave sky below a few arcminutes, since its gravitons never scattered [135].

- *Lensing leaves its uniform part unchanged.* Bending conserves surface brightness, so a uniform background stays uniform however its rays are bent; only its departures from uniformity, the dipole of our motion and the spots, are moved about.

- *Only black holes cast shadows on it.* Nothing else absorbs appreciably across a broad band (Section VII). Seen against this background, the sky is a uniform glow at 0.905 K, warmer in the direction of our motion, with a black disc wherever a black hole stands.

Figure 37 computes one such view by exact rays of the Schwarzschild metric [136–138]. The camera is at rest $40\,GM/c^2$ from a black hole that lies just above the Galaxy's centre. In light, the Milky Way bends around the hole into a ring, with a second image above it. In primordial gravitons the background is uniform except for the dipole of our motion, so all that shows is the shadow, of angular radius $\sin^{-1}[\sqrt{27}\,(GM/c^2r)\sqrt{1 - 2GM/c^2r}] = 7.3°$, and the dipole folded around it. The whole sky is 2.6% warmer than far from the hole, $T_g/\sqrt{1 - 2GM/c^2r}$, so the camera's thermometer also reads how deep it sits in the hole's potential.

A black hole is dark against this background only because it is colder. Its Hawking temperature, $\hbar c^3/8\pi GMk_B$, equals 0.905 K for a mass of 1.36×10^{23} kg, nearly two masses of the Moon. A heavier hole casts a shadow; a lighter one glows against the sky; and one of just this mass, in balance with the graviton background (though not with the warmer microwave one), returns in every mode exactly what it receives, and against a uniform sky at that temperature it cannot be seen in gravitons at all (it still lenses the sky's spots and anything behind it). Spin changes this too. A spinning hole amplifies the waves that turn with it, by up to 138% for the most favoured mode of a hole spinning near its limit [79], so at wavelengths comparable to its size it would return more of the background than it receives on that side, and appear brighter than the sky there rather than dark.

Mode by mode the bookkeeping is exact. A wave of angular degree l and frequency ω that reaches the hole is absorbed with probability $\Gamma_l(\omega)$ and otherwise scattered back, and the hole emits in the same proportion, so what the camera receives from it in that mode differs from

the sky's occupation $n_{\rm bg}$ by $\Gamma_l\,(n_H - n_{\rm bg})$, with n_H the occupation at the hole's temperature. For a spinning hole n_H is taken at $\omega - m\Omega_H$, Ω_H the angular velocity of its horizon, and in the modes that turn with it but more slowly than it, $\omega < m\Omega_H$, both factors change sign: whatever the temperatures, those modes come out brighter than the sky. For a hole that does not spin we have computed Γ_l for every mode from the Regge–Wheeler equation. The shadow is then less deep than the black disc of the geometric cross-section $27\pi G^2M^2/c^4$ suggests, because the sky's gravitons are not short compared with the hole: against the 0.905 K background, a hole ten times the equilibrium mass is 93% as dark as that disc, three times, 54%, and twice, 29%; only above about a hundred times, 10^{25} kg, is it black. The computed Γ_l conserve flux in every mode and reach Page's limit for long waves, $\Gamma_2 \to (256/225)(GM\omega/c^3)^6$ [139], and the geometric cross-section for short ones.

f. A freely falling camera. A camera at rest near a hole must hover, and the thrust that holds it grows without limit as it nears the horizon; a camera falling freely from far away crosses it without noticing. Falling straight in, it reads the same tide as one at rest at the same radius, $\mathcal{W} = (GM/r^3)\,\mathrm{diag}(1, 1, -2)$, with no magnetic part, because a boost along the line to the hole leaves a field of type D unchanged, and nothing marks the horizon. Its view of the sky does change. Passing the hovering camera inward at $v = (2GM/r)^{1/2}$, it sees the shadow shrunk by aberration: at $40\,GM/c^2$, 5.8° instead of 7.3°; at the photon sphere, 35.3° instead of a whole hemisphere; and at the horizon, where the hovering camera would see the shadow fill almost the whole sky, $\cos\alpha = 23/31$, 42.1°, less than 13% of it. The rest of the sky, the primordial glow among it, crowds toward the edge of the shadow, bluer there and redder behind.

g. Through a room at nearly the speed of light. Fly a pixel through a still room at speed βc. The reading is the room's, carried by a boost: its invariants do not change and its eigenvalues stay real, so the pixel can tell that the scene is still; but the magnetic part grows to match the electric, $|\mathcal{B}|/|\mathcal{E}| \to 1$, and the four principal null directions, which mark directions of travel, all crowd toward the way behind, within angles of it that shrink as $1/\gamma$ (flying along the axis of the tide's middle eigenvalue, onto one cone of half-angle $\arccos\beta$ about it; a field of type D flown along its own axis is the exception, and does not change). Every piece of furniture then looks, to one pixel, like a wave coming from in front, a gravitational shock of the kind Aichelburg and Sexl found for a mass moving at the speed of light [140], and only the unchanged invariants say otherwise.

h. Counting coincidences. Pixels that only count can still tell skies apart, by how their counts arrive together, as Hanbury Brown and Twiss measured stars. Gravitons from one mode of a coherent source, such as a cloud of light bosons about a spinning hole, arrive independently, $g^{(2)} = 1$, where $g^{(2)}$ is the rate of coincident counts over that of independent arrivals; from a thermal sky, such as the 0.905 K glow, they bunch, $g^{(2)} = 2$. Inflation leaves neither: it makes gravitons in pairs of opposite momentum, a two-mode squeezed state [141], in which each direction alone looks thermal while counts in opposite directions coincide with $g^{(2)} = 2 + 1/\bar{n}$ for $\bar{n}$ gravitons per mode, more than any two classical fields allow. Two counting pixels looking in opposite directions would tell a sky born hot from one born in inflation; intensity interferometry of primordial gravitons has been proposed for the purpose [142].

i. A cosmic string. Space around a straight cosmic string is flat: a wedge of angle $8\pi G\mu/c^2$ is missing around it, μ its mass per length, and outside its core every pixel reads zero [143]. A string a metre from the camera is invisible to the near field however heavy it is. It shows only against what lies behind it: the missing wedge makes double images of sources beyond it, and a string moving across the line of sight at speed v cuts a background into two halves whose temperatures differ by up to $8\pi G\mu\gamma v/c^3$ [144]; against the primordial glow, a string with $G\mu/c^2 = 10^{-6}$ moving at half the speed of light makes a step of 1.5×10^{-5} of its temperature.

j. The transparent Sun as a lens. Gravitational waves pass through the Sun and, where geometric optics holds, are bent by the mass inside the cylinder of their impact parameter, $\alpha(b) = 4GM_{\rm cyl}(b)/c^2b$. For Eddington's standard model of the Sun the bending peaks at 4.2″ for rays passing 0.27 of a radius from the centre, more than twice the 1.75″ of rays that graze it (Fig. 38). Rays through the centre come to a focus first, $c^2/4\pi G\Sigma(0) = 34$ AU behind the Sun, where Σ is the column density; Patla and Nemiroff found 23.5 AU for the denser core of the standard solar model [77]. From farther away a compact source directly behind the Sun appears as a ring inside the solar disc, at the impact parameter whose focus lies at the camera. A uniform background, such as the primordial one, is not changed.

Geometric optics needs more than a wavelength shorter than the Sun. A lens of mass M delays a wave by about $4GM/c^3$, twenty microseconds for the Sun, and it focuses only if that delay spans a radian or more of the wave's phase, that is above $c^3/8\pi GM = 8$ kHz for the Sun, whatever its size. Below, diffraction erases the focus: even a point of the Sun's mass raises the intensity on its axis only by the factor $\pi w/(1 - e^{-\pi w})$, with $w = 8\pi GMf/c^3$, which is 1.02 at 100 Hz. The transparent Sun is a lens for thermal and primordial gravitons, not for the waves of orbiting or merging bodies.

Wave optics joins the two regimes. For a source directly behind the Sun the amplitude on the axis, a distance d behind it, is the Fresnel integral over the plane of the Sun of $e^{ik[b^2/2d - \Phi(b)]}$, where $\Phi' = \alpha$ is the extra path through its field. Outside the disc Φ is a point mass's, and that part of the integral is an incomplete gamma function; inside it is smooth, and we integrate it numerically. On Earth's orbit the Sun never raises the intensity by more than the 6% of the central ray's geometric focusing, $(1 - d/f_0)^{-2}$ with $f_0 = 33.7$ AU, which it reaches only above about

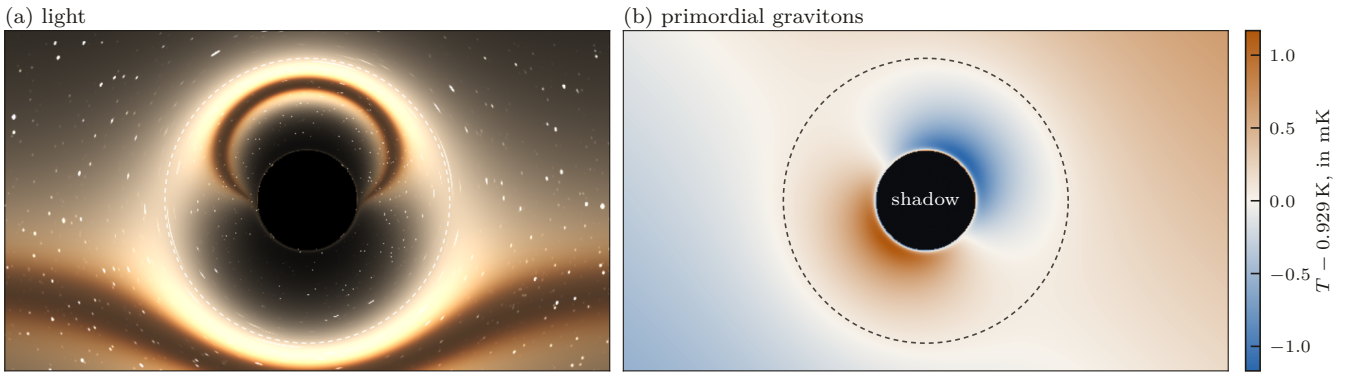


FIG. 37. A black hole seen from rest $40\,GM/c^2$ away, through exact Schwarzschild rays, with the Galaxy's centre 9° below the hole. (a) Light: the model Milky Way of Fig. 36, with stars added for orientation. (b) The primordial graviton background, Eq. (77), warmed to 0.929 K by the depth of the potential and hotter toward our direction of motion; the colour shows its departure from the mean, folded around the shadow by the bending. The two skies differ, but the rays that carry them are the same: dashed, in both panels, is the Einstein ring, 20° in radius, where the sky straight behind the hole is seen. The Galaxy's bulge, which reaches up to that line, is drawn out around it into the bright ring of (a). Inside the ring each side of the sky appears on the opposite side of the hole: the band of the Milky Way below the hole appears again as the arc above it in (a), and the background's dipole turns over in (b). Nothing else in a gravitational image casts a shadow.

10 kHz. Beyond the central focus a ring of rays from inside the Sun converges on the axis, and the gain there grows in proportion to the frequency: at 50 AU it is 3.4 at 10 kHz, 44 at 100 kHz and 480 at 1 MHz, from 0.9 to 1.2 times that of a point of the Sun's mass, πw, and equal to it at 550 AU, where the converging rays graze the limb. At the frequencies of thermal gravitons, near 10^{13} Hz, the same proportion gives some 5×10^9. The integral reproduces the point mass's closed form, and both limits: long waves, which see only the Sun's whole mass, and short ones, which follow the rays.

k. Scattering, earthquakes and tails. A scene cannot be illuminated with gravitational waves. To light a scene and see what it reflects, matter would have to scatter gravitational waves, and the cross-section of a body of mass m is of order $(Gm/c^2)^2$ [145], $3 \times 10^{-51}\,\mathrm{m}^2$ for a person: every picture in this paper is made by what the scene itself emits, how it pulls, or, in the near field, how it yields to a pull (Section IV). An earthquake shows in two parts of the field. Compressional waves change the density of the rock they cross, and with it $\mathcal{E}$; that is the prompt signal already recorded [6]. Shear waves in a uniform medium do not change its density, but they move mass, and so appear in $\mathcal{B}$, through Eq. (10). In curved space a burst does not arrive all at once. Huygens's principle fails: waves scatter off the curvature they cross and arrive followed by a tail inside the light cone [146], an echo whose size records the mass between the source and the camera; for a binary it shifts the phase of the wave by an amount set by the system's total mass [147].

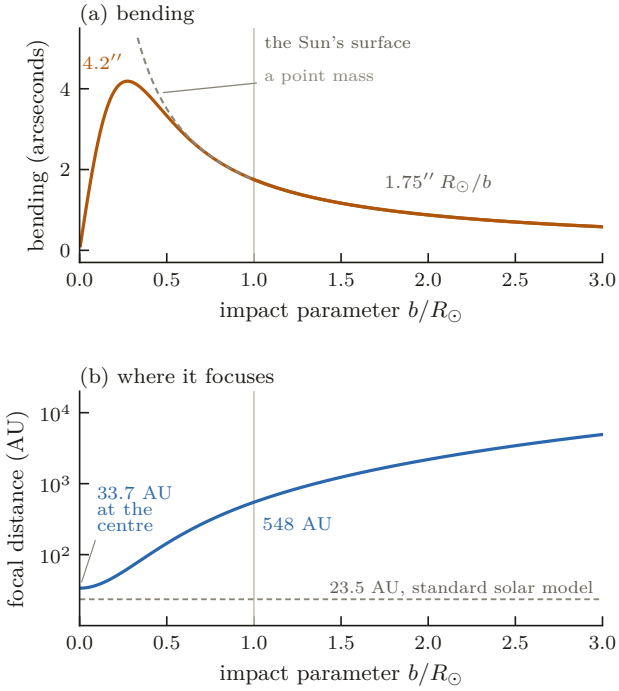


FIG. 38. The transparent Sun as a lens for gravitational waves, in Eddington's standard model. (a) Bending against the impact parameter: inside the Sun it rises to 4.2″ and falls to zero at the centre; the dashed curve is what a point mass would give. (b) The distance behind the Sun at which the rays at each impact parameter cross the axis: 34 AU through the centre, 548 AU at the surface. The dashed line marks the 23.5 AU found for the standard solar model.

XII. THE EXTERIOR FIELD AND THE INTERIOR: GRAVITATIONAL HAIR

The limits of the near field were met one at a time in Section IV: an ambiguity, a blur, a count of bits, a tie broken by heat. They are one subject, and its natural name is hair: what the field outside a body fixes of its interior. This section puts them together, in the form that quantum mechanics gives them, and compares a black hole with an ordinary body.

a. The field at one time. Outside a body, with no waves coming in from elsewhere, the field at one time is built from the moments $Q_h = \int \rho\, h \,\mathrm{d}V$ of its mass against the functions h that are harmonic in it, and from the like moments of its flow. A density that has none of these moments, $\nabla^2\chi/4\pi G$, has no effect on a camera outside (Eq. (11)). This generalizes Newton's shell theorem. In general relativity still less is fixed at one time. To first order the constraints fix to the matter its total energy, momentum and angular momentum and its centre of mass, and the fields of its higher moments can be cancelled, on that one slice, by a free field added to them [148]; in the full theory vacuum data inside a large enough ball can be joined, across a shell, to a slice of the field of a black hole, spinning and in general moving, outside it [149]. The statements of this paper suppose that no such field has been added (Section VIII).

b. The field at two times. A second reading, a moment later, does not repeat the first, because the moments change. For matter whose forces do not depend on velocity, with $Q_h = \sum_a m_a h(\mathbf{x}_a)$ and its rate of change $\dot{Q}_g = \frac{1}{2}\sum_a (\mathbf{p}_a \cdot \nabla g + \nabla g \cdot \mathbf{p}_a)$, where $\mathbf{p}_a$ are the momenta, the two do not commute:

$$[\, Q_h,\, \dot{Q}_g \,] = i\hbar \int \rho\, \nabla h \cdot \nabla g \,\mathrm{d}V, \tag{78}$$

and the Poisson bracket of classical mechanics has the same form. The right-hand side appears in three results. In classical thermal equilibrium $\langle \dot{Q}_h \dot{Q}_g \rangle$ is $k_B T$ times it, Eq. (13). It is the whole weight of the response to an applied tide, Eq. (15). And far above every frequency at which the body can respond, the moment Q_h follows a tide that acts on Q_g as

$$\chi_{hg}(\omega) \to -\frac{1}{\omega^2} \int \rho\, \nabla h \cdot \nabla g \,\mathrm{d}V, \tag{79}$$

which is the response of dust: driven faster than its bonds can act, every body responds as a cloud of free mass, as every atom responds to an X-ray as a cloud of free electrons.

The right-hand side is not a harmonic moment. For h and g harmonic it is the moment of the density against $\nabla h \cdot \nabla g$, and such products are enough to build any function. Take $h_\pm = e^{\boldsymbol{\zeta}_\pm \cdot \mathbf{x}}$ with $\boldsymbol{\zeta}_\pm = \frac{1}{2}(i\boldsymbol{\xi} \pm \boldsymbol{\eta})$, where $\boldsymbol{\eta}$ is perpendicular to $\boldsymbol{\xi}$ and as long. Both are harmonic, since $\boldsymbol{\zeta}_\pm \cdot \boldsymbol{\zeta}_\pm = 0$, and

$$\int \rho\, \nabla h_+ \cdot \nabla h_- \,\mathrm{d}V = -\tfrac{1}{2}\,|\boldsymbol{\xi}|^2 \int \rho\, e^{i\boldsymbol{\xi}\cdot\mathbf{x}} \,\mathrm{d}V : \tag{80}$$

the data at two times are the Fourier transform of the density. This is Calderón's argument [32], made for the problem of finding the conductivity inside a body from currents and voltages at its surface. The present problem is that one in its linearized form, with density in place of conductivity, and here, in Newton's theory, the linear form is exact. The null space of Eq. (11) is therefore a property of a reading at one time, not of gravity. The nugget, its flush and its skin (Fig. 6) have the same exterior field at any instant, and are told apart as soon as they are warm or a tide is applied.

c. Stability. Each of $h_\pm$ grows to $e^{|\boldsymbol{\xi}|a/2}$ across a body of radius a, and the camera must build them from multipoles that reach it weakened by $(a/r)^\ell$ at each degree, so detail of size $2\pi/|\boldsymbol{\xi}|$ costs exponentially in sensitivity, as in Eq. (17). This is a known property of Calderón's problem, whose stability, for conductivities bounded beforehand, is logarithmic and cannot be better [150, 151]. Readings at two times remove the ambiguity and keep the blur.

d. The number of bits. Read on a sphere of radius R_c about a body of radius a, the multipole of degree ℓ is weaker than the monopole by $(a/R_c)^\ell$, and there are $2\ell+1$ of each. If the monopole is read at the signal-to-noise ratio SNR, the argument that gave Eq. (24) gives, for the whole body at one time,

$$H \approx \frac{1}{\ln 2}\left[\frac{L^3}{3\Lambda^2} + \frac{L^2}{2\Lambda}\right], \qquad L = \ln \mathrm{SNR}, \quad \Lambda = \ln\frac{R_c}{a} \tag{81}$$

bits, whose leading term is that of Eq. (24) for a camera close to the surface. From a distance of three of its radii, a camera with SNR $= 10^6$ reads 1,200 bits of a body, and at the heuristic ceiling of Section IV, 10^{70}, it reads 1.7×10^6: two hundred kilobytes, for a person watched for the age of the universe. A black hole has less. All the moments of its field are fixed by its mass and its spin [152], which with its place make seven numbers in the frame in which it is at rest (its velocity adds three, as any body's does): at most $7 \log_2 \mathrm{SNR}$ bits, 140 at 10^6 and 1,600 at 10^{70}, whatever its size. A neutron star is nearly as bald, its moment of inertia, its quadrupole and its yielding to a tide being tied to one another, to about one per cent, whatever it is made of [153]. Having no hair is the end of a scale on which every body lies, and the scale is short. Between a person and a black hole there is a factor of nine in what gravity can tell at SNR $= 10^6$, and of a thousand at that ceiling (Fig. 39b).

e. Response of a black hole to a tide. A black hole responds to a tide as no ordinary body does. Its Love numbers are zero [154, 155], with spin as without [156]: a steady tide raises no moment on a hole that does not turn, and on one that turns it raises one by friction only, since a tide that is not symmetric about the axis of spin is not steady to the turning horizon. The response is that of the horizon, and it is purely dissipative. In a tide that changes slowly a hole of mass M and Schwarzschild

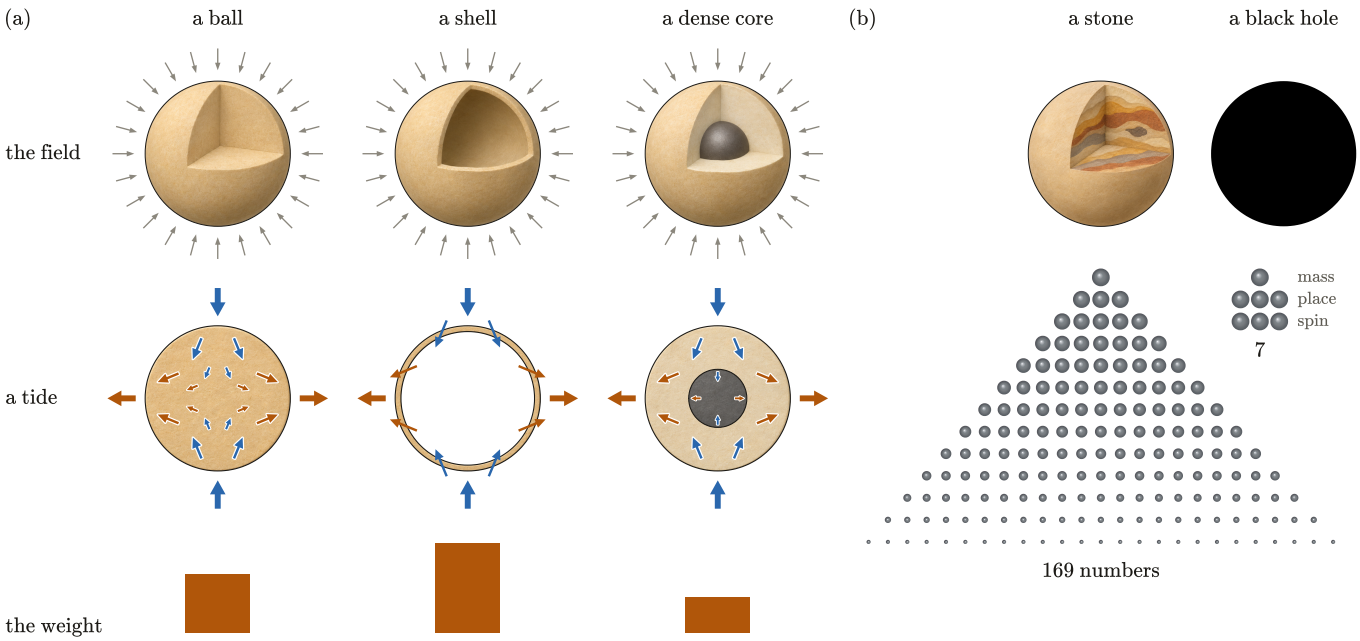


FIG. 39. What the exterior field determines. (a) Three bodies of one size and one mass: a uniform ball, a shell whose skin is eight per cent of its radius thick, and a ball of light rock whose core, of 0.4 of its radius, holds half the mass. The field: outside, the pull of the three is the same at any one time (grey arrows). A tide: an impulsive tide of potential proportional to $x^2 - y^2$ gives each part an impulse along $(x, -y)$ and in proportion to its distance from the z axis, outward near one axis (orange) and inward near the other (blue), drawn on sections of the three. The weight: the energy each gains, Eq. (86), is proportional to its $\int \rho\, r^2\, \mathrm{d}V$, which is 0.60, 0.92 and 0.37 Ma^2 (bars). (b) The numbers that the field outside carries, a bead for each. A stone read at SNR $= 10^6$ from three of its radii shows the 169 moments of degree twelve and below, the $2\ell + 1$ of each degree in a row, each bead's area in proportion to the bits it holds, about 1,200 in all (Eq. (81)); a black hole at rest shows seven. The cutaway bodies and the stone's layers are pictures; the sections, the directions of the impulses, the bars and the beads are exact.

radius r_s, not turning, absorbs energy at the rate [157]

$$\frac{\mathrm{d}E}{\mathrm{d}t} = \nu\,(\dot{\mathcal{E}}_{ij}\dot{\mathcal{E}}_{ij} + \dot{\mathcal{B}}_{ij}\dot{\mathcal{B}}_{ij}),$$
$$\nu = \frac{16}{45}\,\frac{G^5M^6}{c^{13}} = \frac{Mr_s^5}{90\,c^3}, \tag{82}$$

so that its response has a dissipative part and no elastic part: a quadrupole Q_{ij} with the energy $Q_{ij}\mathcal{E}_{ij}$ in a tide (half of Newton's $\int \rho\,(x_ix_j - \frac{1}{3}r^2\delta_{ij})\,\mathrm{d}V$) and $\mathrm{Im}\,\chi = \nu\omega$ [158]. This is the absorption of long gravitons, seen in the near field: through that coupling and its magnetic counterpart, which the horizon answers with the same friction, the limit of Section XI for the absorption of a quadrupole wave is $(16/5)\,G\nu\,\omega^6/c^5$ [159].

f. Fluctuations of a black hole's quadrupole. For a hole formed by collapse and left alone, that quadrupole also fluctuates, at frequencies far below c/r_s, with a flat spectrum [159]:

$$\langle Q_{ij}(t)\,Q_{kl}(0)\rangle = \Pi_{ijkl}\int S_Q\,e^{-i\omega t}\,\frac{\mathrm{d}\omega}{2\pi},$$
$$S_Q = \frac{\hbar\,r_s^5}{360\pi G}, \tag{83}$$

with $\Pi_{ijkl} = \frac{1}{2}(\delta_{ik}\delta_{jl} + \delta_{il}\delta_{jk}) - \frac{1}{3}\delta_{ij}\delta_{kl}$. The spectrum was found by matching to Hawking's radiation, for which at these frequencies the chance of emitting a quantum and the chance of absorbing one are both the classical absorption times $k_BT/\hbar\omega$. Inserting Eqs. (82) and (83) into the thermometer of Eq. (16) gives

$$T = \frac{S_Q}{2k_B\,\nu} = \frac{\hbar c^3}{8\pi GMk_B}, \tag{84}$$

the Hawking temperature. The result is not independent, the noise having been fixed by matching to radiation at that temperature; what it confirms is that the friction, found from the growth of the horizon, and the absorption, found from the scattering of waves, are the same number. A hole's near field therefore obeys the rule of every warm body, noise equal to friction at its own temperature, so that a camera beside it reads that temperature from the field that does not radiate, without absorbing any quantum of the radiation. The signal is far beyond reach, like most in this paper: for the hole as warm as the graviton sky, 0.905 K, it is $4 \times 10^{-32}\,\mathrm{s}^{-2}$ in a second, a metre away, where the hole's steady tide is $2 \times 10^{13}\,\mathrm{s}^{-2}$. The tremor carries nothing else. A stone's tremor carries $\int \rho\,\nabla h\cdot\nabla g\,\mathrm{d}V$ for every pair of harmonic functions, and so the whole of its interior; a hole's carries M again (Table VIII).

g. What gravity cannot decohere. The null space has a meaning in quantum mechanics. Put a body into a

	A stone, a planet, a star	A black hole
The field at one time	the harmonic moments of its mass and its flow	at rest, mass, place and spin: seven numbers
Bits, at SNR	$[L^3/3\Lambda^2 + L^2/2\Lambda]/\ln 2$	$7\log_2 \mathrm{SNR}$
A steady tide	its Love numbers	nothing, if it does not turn
A changing tide	when fast, $-\omega^{-2}\int \rho\,\nabla h\cdot\nabla g\,\mathrm{d}V$: the density	when slow, friction, ν
Its tremor	$\langle \dot{Q}_h \dot{Q}_g\rangle = k_B T\int \rho\,\nabla h\cdot\nabla g\,\mathrm{d}V$: the density, at a known temperature	$S_Q = 2k_BT\nu$ at low frequencies: the temperature
Its weight, after a tide	after an impulsive one, $\frac{1}{2}\epsilon^2\int \rho\,\lvert\nabla g\rvert^2\,\mathrm{d}V$ more: the density	after a slow one, $\nu\int(\dot{\mathcal{E}}_{ij}\dot{\mathcal{E}}_{ij} + \dot{\mathcal{B}}_{ij}\dot{\mathcal{B}}_{ij})\,\mathrm{d}t$ more: its mass

TABLE VIII. What the field outside a body determines of its interior, for ordinary matter and for a black hole. $L = \ln \mathrm{SNR}$ and $\Lambda = \ln(R_c/a)$ are those of Eq. (81); h and g are harmonic functions; ν is the horizon's friction, Eq. (82); in the last line the stone's entry is Eq. (86), and the hole's holds for a tide that changes slowly beside r_s/c.

superposition of two arrangements of its mass that have the same field outside: a ball and a shell, the nugget and its skin, or two stages of any motion that keeps a body round. At any one time the field outside is the same in both branches. It holds no record of which, and nothing outside that touches the body through its field alone can learn which from a reading at one time; if the superposition is made by a motion that leaves the field outside unchanged throughout, as a round motion does, no graviton is emitted in making it. To the outside the branches differ only in readings at two times, in their tremor and in their response to a tide, Eq. (79). Yet they differ at once in the measure by which Diósi and Penrose proposed that gravity itself ends superpositions [160, 161], the gravitational self-energy of the difference of the two densities:

$$E_G = \frac{1}{8\pi G}\int |\mathbf{g}_1 - \mathbf{g}_2|^2\,\mathrm{d}V = \frac{GM^2}{10R} \tag{85}$$

for a ball and a shell of mass M and radius R, whose fields $\mathbf{g}_{1,2}$ differ only inside (the numerical factor in front of E_G is a matter of convention). For the mass and size of a glass bead a micron in radius, $\hbar/E_G$ is a fifth of a second; a real bead cannot move its mass to its surface, and if it only breathes, by a part δ/R of its radius, $E_G = \frac{9}{10}(\delta/R)^2 GM^2/R$ and the time is longer by $R^2/9\delta^2$. Such a pair would separate the two ideas cleanly: the ordinary way in which gravity ends a superposition, by carrying away a record of it [46, 47], is closed (save for tides from outside, which the branches answer differently, Eq. (79), at second order in the coupling), and a collapse of Diósi's and Penrose's kind is not (in its simplest form, with no free length, it has since been excluded by experiment [162]). A spherical disturbance with no change of mass has been noted, for dark matter, to be the kind most robust against decoherence by gravity [163].

h. An impulsive tide and a weighing. The second reading can be of a single number. Let a tide act on the body impulsively: masses outside make, for an instant, the potential $-\epsilon\, g(\mathbf{x})\,\delta(t)$, with g harmonic in the body, and each part of it, of mass m, receives the impulse $\epsilon m\nabla g$ where it stands. For matter whose forces do not depend on velocity the energy gained is

$$\Delta E = \epsilon\,\dot{Q}_g + \frac{\epsilon^2}{2}\int \rho\,|\nabla g|^2\,\mathrm{d}V, \tag{86}$$

exactly in Newton's mechanics, with no further terms; it is the sum rule of Eq. (15) in time instead of frequency, and it holds of the operators of quantum mechanics, where the impulse is $e^{i\epsilon Q_g/\hbar}$. Energy has weight: the mass that the monopole of the body's field reports rises by $\Delta E/c^2$, and an isolated body keeps the gain until it is read. Impulses of both signs, given to two copies of the body prepared alike, and two weighings therefore give $\int \rho\,|\nabla g|^2\,\mathrm{d}V$ and, separately, $\dot{Q}_g$. The first, with the impulses taken in pairs, is the left-hand side of Eq. (80): sixteen weighings for each Fourier component of the density. The second then gives the motion. For a body of N parts the gradients of harmonic functions at their N places can be chosen at will, so that, once the places are known from the density, enough impulses give every momentum (Appendix B). A ball and a shell of the same weight and the same exterior field gain energy from the same quadrupolar impulsive tide in the ratio three to five (Fig. 39a, where the shell has some thickness). Only the weight has been read, the one number that Gauss's law carries to any distance.

The pair $h_\pm$ of Eq. (80) varies in two directions only. Each is the profile of a wave with flat fronts that travels along the third, and in general relativity such a wave, arriving all at once with any profile that is harmonic across its front, is an exact solution; the field of a particle without mass is one [140]. What a pair of them reads is the Fourier transform, at $\boldsymbol{\xi}$, of the density summed along the wave's path: a projection, as in X-ray tomography, and the body is reconstructed from its projections in the same way.

The measurement is far beyond reach. An impulse that changes velocities by Δv raises the weight by about $\frac{1}{2}(\Delta v/c)^2$ of itself, five parts in 10^{41} for $\Delta v = 3\times10^{-12}\,\mathrm{m\,s^{-1}}$, which the tide of a tonne a metre away gives the edge of a body a metre across in fifty microseconds, far less time than any such mass could be brought up and taken away in; fine detail costs exponentially in sensitivity, as before; the impulse must be over before the body can respond, which requires that the body's own

motions be slow compared with light; and Eq. (86) is the first order in $1/c^2$, not the whole theory.

i. The algebra of the moments and the energy. The result can be stated algebraically. A quantity whose Poisson bracket with every harmonic moment vanishes does not depend on the momenta, and if its bracket with the energy vanishes too it is a constant (Appendix B). In this sense the moments and the weight, all of them measured outside, generate all that can be determined of the body; the moments alone leave every function of position undetermined. In general relativity, where the energy is itself a term at the boundary, the corresponding statement was made by Marolf [164], who noted that it does not by itself let a classical observer determine the interior from the boundary: J_z is the bracket of J_x and J_y, yet the values of those two do not determine J_z. This holds for an observer who only measures the field. An observer who can apply a tide measures brackets, since the bracket of two quantities is the response of the first to an impulse generated by the second, and Eq. (86) is such a response taken twice. If the body is warm no tide need be applied: its thermal motion supplies the impulses, and in the classical tremor, $\langle \dot{Q}_h \dot{Q}_g \rangle = k_B T \int \rho \nabla h \cdot \nabla g \, \mathrm{d}V$, the temperature stands exactly where $\hbar$ stands in Eq. (78). In quantum mechanics the zero-point motion supplies them at any temperature, which is why the correlations of a quantum state contain its commutators, and those of a cold classical body do not.

j. Black holes and the classical limit. For ordinary matter, then, the exterior field determines the interior, with a precision that grows as the logarithm of the sensitivity. For a black hole it gives seven numbers at one time, in the frame in which it is at rest, and a temperature at two; a hole subjected to a slow tide and then weighed has gained $\nu \int (\dot{\mathcal{E}}_{ij} \dot{\mathcal{E}}_{ij} + \dot{\mathcal{B}}_{ij} \dot{\mathcal{B}}_{ij}) \, \mathrm{d}t$, which gives its mass again, and whatever the tide, what it gains is set by its mass and spin alone. Whether the exterior field holds more is the question of the fate of what falls in. It has been argued that in quantum gravity it does: that everything massless particles will carry out to infinity can be learnt there before they arrive, from correlations of the energy with the waves [165]; that observers at the boundary of an asymptotically anti-de Sitter space can find the state within by simple operations there and a measurement of the energy [166]; and that quantum corrections to the field outside an ordinary body depend on its density profile where the classical field does not [167]. The first two are said by their authors to have no classical counterpart, and for a reading at one time they have none, by Newton's shell theorem. An impulsive tide followed by a weighing is what remains of them without $\hbar$: an operation made from outside and then a reading of the energy. Its differences from the quantum results show what in them is quantum. It needs time, for the tide to reach the body and the change of mass to be read, where they need next to none. It gives a density and a motion, not a state. It is not peculiar to gravity, since the work done by any applied force can be measured, and charges obey the analogue of Eq. (86) with the square of the charge over the mass in place of the mass; what is peculiar to gravity is that no part of a body can be shielded from the tide, that the quantity read is the mass itself, and that the result remains in the field outside. On a black hole the method fails. A hole's tremor is of order $\hbar$, its temperature in Eq. (84) being proportional to it: without $\hbar$ a hole is at zero temperature and has no tremor, and under a tide it gives only its mass. Whatever more the exterior field holds of a hole is of order $\hbar$, beyond the classical account given here.

XIII. CONCLUSION

Nearly all of the results of this paper follow from the spin of gravity and the two small numbers of Section III. Gravity has spin two, so a reading at a single point holds ten numbers: four principal null directions and a rest frame, and a record of them over time separates four waves. Matter is slow, so everything near us is near field: seen at once, where it is now, through any wall, and never sharply. Matter is tenuous, so nothing bends, reflects or stops a wave: warm matter glows all the way through, too faintly for anything made of matter to detect, and every image is a computation.

Each channel has scenes that it cannot tell apart, and they can be stated as exactly as what it sees: the harmonic part of the density and nothing more, the swirl of a flow and not its rolls, the shear of a stress and not its pressure, friction times a power of the temperature and not either alone, sixty-eight numbers of the sky and not a sixty-ninth. The ambiguities are removed across channels: by spin, by heat, by an applied tide, by a second pixel. The most important of them, which hides the interior of a body from its exterior field, holds for a reading at one time only. A body that is warm, or to which a tide can be applied, reveals in time where all its mass is; a black hole does not (Section XII).

The field of light at a point is a vector and that of gravity a square. From that difference a pixel reads its own velocity through an unknown room, detects whether anything in the room is moving, and separates four waves where a sensor of light separates two. The blur of a near-field image does not limit the precision of a measurement. A near-field picture holds few bits, tens to hundreds at signal-to-noise ratios between a thousand and a million, for each patch of the scene as wide as it is far, and a scene that is simple, or merely positive, spends them all on a few numbers: the readings that could never draw a face place a mass to within a millimetre.

The camera of this paper cannot be built, but parts of it exist. Gradiometers already map what is buried [1], a satellite has flown one around the Earth [24], and every gravitational-wave observatory models the pull of its surroundings in order to remove it [97]. That pull is the near-field signal described here.

XIV. OPEN PROBLEMS

Two calculations would complete Section XI. Both have their methods in the literature; neither is made here. The first is the graviton background's spots scale by scale: its angular power spectrum and its cross-correlation with the microwave sky, which on large scales it should follow and below a degree should not [134, 135]. That needs the Boltzmann equation of a species streaming freely from the Planck time, integrated through the same potentials as the photons. The second is the greybody factors of a spinning black hole, from Teukolsky's equation [168], which would say mode by mode how much brighter than the sky a hole's co-rotating modes appear; for a hole that does not spin they are computed here. Neither would change what the camera is, or what it can and cannot see.

Four further problems are open in the near field and the glow. Heat and a push fix a body's interior in principle, with no null space and through the same logarithm as the static field (Section XII); how much of a real body, the Earth for one, a finite record at finite sensitivity over a finite band actually recovers has not been worked out. The pair of arrangements that gravity cannot tell apart at one time, Eq. (85), is a test of gravitational collapse that is described here and not designed. The reading of a body by an impulsive tide and a weighing, Eq. (86), is exact in Newton's theory with the weight of energy added; its statement in the full theory, with waves for the tides and the mass read at infinity for the weight, has not been made. And the friction of real materials at the frequencies of heat, on which every thermal count in this paper rests, deserves a microscopic calculation for at least one crystal, phonon by phonon, of the kind already made for absorption by crystal detectors [56], and for the deep Earth at its temperatures and pressures.

USE OF AI

This work was carried out with Claude (Anthropic; the models Claude Opus 5.5 and Claude Fable 5.2), used throughout as a research assistant. Under the author's direction it drafted and revised the text, carried out and checked derivations, searched the literature and checked the references against their sources, and wrote the reference implementation and its tests, the code that draws the figures, and the interactive version of the scenes. The question, the choice of problems and of what the paper says, and the judgment of the results are the author's, who takes responsibility for every statement in it. The illustrated objects in Figs. 17 and 39 (the person, door, furnace and camera, and the cutaway bodies and the stone) were drawn with an image model, OpenAI's GPT Image, and are marked as illustrations in their captions; every mark that carries a number is drawn by code from the computed results.

Appendix A: Details of the numerical examples

The main text quotes the results of several numerical examples; their details are collected here.

a. Separation with noise. The wave and rotor are those of Section VIII. With $\mathcal{E}$ and $\mathcal{B}$ at one pixel the near field pays the same $\sqrt{2}$ as the wave in the two components it shares with the wave, and nothing in the other three. An array that reads only $\mathcal{E}$ fits the rotor as a point quadrupole of unknown moment and position; for a pixel and six neighbours at distance b along three axes and $b \ll r$, the factor on the wave's error lies between about $0.2\,r/b$ and $0.7\,r/b$, depending on the directions of the wave and of the rotor's axis, and the array overtakes the magnetic part beyond $b = 0.29\,r$. In return the wave costs the rotor's moment and position factors of 1.5 and 1.3 from $\mathcal{E}$ alone, and 1.07 and 1.04 with $\mathcal{B}$ too. Modelling the rotor as a point leaves a false wave of 0.005 of the true one, from its next multipole, which matters only above $\rho \approx 270$; ignored altogether, the rotor is read as 70 times the wave by the array.

b. Depth with noise. For a person 3 m away and neighbours 0.5 m out, the Cramér–Rao bound of the full model on σ_r/r is between $0.90/\rho$ and $1.08/\rho$, depending on direction, against $1.16/\rho$ from the closed form of Eq. (67) (Fig. 30b): wider stencils gain from the curvature of the field across them. For a person walking at $1.4\,\mathrm{m\,s^{-1}}$ the magnetic bound is $\sigma_r/r = 1.2 \times 10^8/\rho$. Bodies on one line: a rod of length L pointing at the camera appears as a point $L^2/3r$ nearer than its centre; the spread s of the depths enters the second derivatives as a share s^2/r^2, which the seven pixels read to $1/\rho_H$, with ρ_H between 8.1 and 10.5 times $\rho\,(b/r)^2$ depending on direction, so that two equal masses, $s = \Delta/2$, are told from one when $\Delta > 2r/\rho_H^{1/2}$, between 0.62 and 0.70 times $(r^2/b)/\rho^{1/2}$.

c. The worked inversion. The array of Section IV's worked case is a square a metre across, of 11×11 pixels 10 cm apart, centred on the camera and facing the safes; the noise on each component is set by $\mathrm{SNR} = 2Gm/z^2\sigma a$ for $m = 324$ kg, $z = 3.5$ m and spacing a. The image is the Gaussian posterior on point masses at the nodes of a grid 25 cm apart, 5 m × 2.5 m, in the plane of the safes, each with prior standard deviation equal to the gold's mass; it is computed through the singular values of the design matrix, which stays exact at any noise. A safe's mass is the sum over the cells of its footprint, 0.9 m wide. Gold 0.2 m farther back and 14% heavier, so as to pull as hard on the array's centre, is told apart at $\mathrm{SNR} \approx 10^3$, from the way the field changes across the array. The posterior uncertainty is ±730 kg at $\mathrm{SNR} = 10^3$ and ±490 kg at 10^6 for the metre-wide array, and ±350 kg at 10^6 for one six metres across; these belong to the array and the noise, not to the data. Tilting changes nothing in principle, since each pixel reads the whole tensor wherever it points: turned through 70°, the metre-wide array tells the two safes apart 9% better, and the six-metre one, whose near edge then comes within 0.7 m of the safes, thirty times better. The positive reconstruction is non-negative least

squares on the same grid, with no prior, over forty draws of the noise.

d. The trembling lattice. The ball and the shell of Fig. 8 are the sites of a simple cubic lattice of unit spacing within a radius of six spacings, less the one at the centre, the shell keeping only those beyond four, each site joined to its six nearest neighbours by springs of unit stiffness and to its twelve next-nearest by springs half as stiff, which makes a stable elastic solid. The masses are equal within each body and add to the same total in both. The normal modes give the response of every moment directly: a mode of frequency ω_n moves q_h by c_n per unit of its mass-weighted amplitude, and in equilibrium $\langle \dot{q}_h^2 \rangle = k_B T \sum_n c_n^2$ and $\langle q_h^2 \rangle = k_B T \sum_n c_n^2/\omega_n^2$. The first sum equals $k_B T \int \rho \, |\nabla h|^2 \, \mathrm{d}V$ to rounding error for any stiffnesses, as Eq. (13) requires; for $h = x$ all of it lies in the free translation, the Brownian motion of Eq. (14) with $\ell = 1$. The steel ball's numbers use Rayleigh's method with the displacement $\mathbf{u} = (q/R)(-x/2, -y/2, z)$, which has no divergence, so that it changes the density nowhere and moves mass only at the surface: effective mass $3M/10$, stiffness $3\mu V/R^2$, a quadrupole $\frac{1}{5} M R q \, \mathrm{diag}(-1, -1, 2)$ and so a tide $36GMRq/5r^5$ on its axis. Rayleigh's method overestimates the frequency; these are estimates, not the exact modes of a steel sphere.

For a quantum system the jitter is no longer $k_B T \chi(0)$. With the static compliance χ_0 and the sum A of Eq. (15) both finite, the measure $(2/\pi\chi_0) \, \mathrm{Im}\, \chi(\omega) \, \mathrm{d}\omega/\omega$ has unit weight and mean square frequency A/χ_0, and the quantum fluctuation–dissipation theorem gives the jitter as its average of $\frac{1}{2} \hbar \chi_0 \, \omega \coth(\hbar\omega/2k_BT)$. Since $\sqrt{x} \coth(b\sqrt{x})$ is concave in x,

$$k_B T \chi_0 \le \langle \delta q^2 \rangle \le \frac{\hbar}{2} \sqrt{A\chi_0} \, \coth\Big(\frac{\hbar}{2k_BT} \sqrt{\frac{A}{\chi_0}} \Big), \quad \text{(A1)}$$

with the upper bound reached by a single mode. The shell drive of Eq. (16) has no monopole or dipole, interacts with point masses outside it exactly as $-f\,D : \mathcal{E}$, and makes the field $6GfD/a^5$ at its centre.

Appendix B: Three short proofs

Two statements of Section VIII and one of Section XII are exact, and their proofs are short enough to give in full.

a. The principal null directions of a moving body. In the body's rest frame its field is static, $\mathcal{W} = (GM/R_*^3)(1 - 3\,\hat{n}_0 \hat{n}_0^T)$, with $\hat{n}_0$ the direction of the body from the pixel and R_* its distance. For a null $\mathbf{m}$, Eq. (48) is then $(\mathbf{m} \cdot \hat{n}_0)^2 = 0$: the principal null directions are the two directions $\pm\hat{n}_0$ along the line through the body, each counted twice. Let the pixel move through that frame with velocity $c\boldsymbol{\beta}$, and write $\gamma = (1-\beta^2)^{-1/2}$, $a = \boldsymbol{\beta} \cdot \hat{n}_0$ and $\hat{n}_0 = (a/\beta)\hat{\beta} + \mathbf{n}_\perp$. A ray that runs along $\hat{k}$ in the body's frame runs, for the pixel, along $[\hat{k}_\perp + \gamma(\hat{k}_\parallel - \boldsymbol{\beta})]/\gamma(1 - \boldsymbol{\beta}\cdot\hat{k})$, the aberration of light, with the parts of $\hat{k}$ along and across $\boldsymbol{\beta}$. The two pairs are therefore at

$$\hat{p}_\pm = \frac{\pm\mathbf{n}_\perp + \gamma(\pm a/\beta - \beta)\,\hat{\beta}}{\gamma(1 \mp a)}, \quad \text{(B1)}$$

and their half sum and half difference are

$$\begin{aligned} \tfrac{1}{2}(\hat{p}_+ + \hat{p}_-) &= \frac{a^2 - \beta^2}{\beta(1-a^2)}\,\hat{\beta} + \frac{a}{\gamma(1-a^2)}\,\mathbf{n}_\perp, \\ \tfrac{1}{2}(\hat{p}_+ - \hat{p}_-) &= \frac{(a/\gamma\beta)\,\hat{\beta} + \mathbf{n}_\perp}{\gamma(1-a^2)}. \end{aligned} \quad \text{(B2)}$$

For the pixel the body moves with velocity $\mathbf{v} = -c\boldsymbol{\beta}$. Transforming its worldline to the pixel's frame, at the instant of the reading it is at $\mathbf{r} = R_*[(a/\gamma\beta)\,\hat{\beta} + \mathbf{n}_\perp]$, at the distance $r = R_*(1-a^2)^{1/2}$. The half difference is therefore $\hat{n}/\gamma(1-a^2)^{1/2}$, with $\hat{n} = \mathbf{r}/r$: it lies along the line to where the body is now. Removing from $\mathbf{v}/c$ its part along $\hat{n}$ leaves exactly the half sum, which is Eq. (52); and since $\hat{p}_\pm$ are unit vectors, the half difference has the length $(1 - v_\perp^2/c^2)^{1/2}$. The same $\mathbf{r}$ gives $R_*^2 = \gamma^2(r^2 - |\mathbf{v}\times\mathbf{r}|^2/c^2)$, the distance used in Eq. (53).

b. The count of waves. In the coordinate z of Eq. (48) the $2s+1$ independent components of a reading of N waves are, up to a fixed linear map, the moments $y_j = \sum_a c_a z_a^j$, $j = 0, \dots, 2s$. Let $p(z) = \prod_a (z - z_a) = \sum_{k=0}^N p_k z^k$, with $p_N = 1$. Then

$$\sum_{k=0}^{N} p_k \, y_{j+k} = \sum_a c_a z_a^j \, p(z_a) = 0, \qquad j = 0, \dots, 2s - N, \quad \text{(B3)}$$

in every snapshot, whatever the amplitudes: $L(2s-N+1)$ linear equations for the N unknown coefficients of p. They fix p, and with it the directions, when $L(2s - N + 1) \ge N$ and the stacked matrix of the y_{j+k} has rank N; the amplitudes then follow from a linear system. The first condition is Eq. (57). No method does better, because N waves have N directions and LN amplitudes, $N(L+1)$ complex unknowns, against the $L(2s+1)$ complex numbers recorded. The second condition is what "generically" means there.

c. The moments and the weight. Let a body be N masses m_a at different places $\mathbf{x}_a$, with momenta $\mathbf{p}_a$ and the energy $H = \sum_a p_a^2/2m_a + V(\mathbf{x}_1, \dots, \mathbf{x}_N)$. First, the gradients of harmonic functions at the N places take every value in $\mathbb{R}^{3N}$. If they did not, there would be vectors $\mathbf{w}_a$, not all zero, with $\sum_a \mathbf{w}_a \cdot \nabla g(\mathbf{x}_a) = 0$ for every g harmonic in the body. Take $g = 1/|\mathbf{x} - \mathbf{y}|$ with $\mathbf{y}$ outside it. The sum is then the potential at $\mathbf{y}$ of dipoles $\mathbf{w}_a$ set at the $\mathbf{x}_a$. It would vanish everywhere outside, and so, being harmonic wherever there is no dipole, everywhere else; but the potential of a dipole is unbounded at its place unless the dipole is zero. So every $\mathbf{w}_a = 0$. Now let a function F of the places and momenta have a vanishing Poisson bracket with every harmonic moment, $\{F, Q_h\} = -\sum_a m_a \nabla h(\mathbf{x}_a) \cdot \partial F/\partial \mathbf{p}_a = 0$. By the first step every $\partial F/\partial \mathbf{p}_a$ vanishes, and F depends on the places alone. If its bracket with the energy vanishes

too, $\{F, H\} = \sum_a (\mathbf{p}_a/m_a) \cdot \partial F/\partial \mathbf{x}_a = 0$ for all momenta, then F is a constant. The same first step gives the momenta from the pushes of Eq. (86): its odd part is $\sum_a \mathbf{p}_a \cdot \nabla g(\mathbf{x}_a)$, and $3N$ suitable g make of these a system of full rank for the $\mathbf{p}_a$. For the functions that commute with the moments alone, which are all functions of the places, the second step is what the energy adds.

Appendix C: Where each result is checked

Every number in this paper is produced by the reference implementation, a Python package (`reference/gravcam`), and is tested there. Table IX says where. An interactive version of the scenes also exists; its images are drawn by separate code and are tested against the reference implementation. A check of this kind shows that a formula agrees with an independent calculation of the same model, for instance with the curvature of a metric taken by finite differences; it does not show that the model is the right one. Where the text says that a result is exact, it rests on an argument, and the number quoted beside it is the accuracy of the check.

[1] B. Stray *et al.*, Quantum sensing for gravity cartography, Nature **602**, 590 (2022).

[2] R. P. Middlemiss, A. Samarelli, D. J. Paul, J. Hough, S. Rowan, and G. D. Hammond, Measurement of the Earth tides with a MEMS gravimeter, Nature **531**, 614 (2016).

[3] A. Prasad, R. P. Middlemiss, A. Noack, K. Anastasiou, S. G. Bramsiepe, K. Toland, P. R. Utting, D. J. Paul, and G. D. Hammond, A 19 day earth tide measurement with a MEMS gravimeter, Sci. Rep. **12**, 13091 (2022), arXiv:2109.13715.

[4] A. N. Jordan and J. C. Howell, Method for scanning an object using a gravimeter, U.S. Patent 10,983,244 B2 (2021), filed 21 December 2018, granted 20 April 2021.

[5] K. S. Thorne and C. J. Winstein, Human gravity-gradient noise in interferometric gravitational-wave detectors, Physical Review D **60**, 082001 (1999), arXiv:gr-qc/9810016.

[6] M. Vallée *et al.*, Observations and modeling of the elastogravity signals preceding direct seismic waves, Science **358**, 1164 (2017).

[7] B. Kirkendall, Y. Li, and D. Oldenburg, Imaging cargo containers using gravity gradiometry, IEEE Transactions on Geoscience and Remote Sensing **45**, 1786 (2007).

[8] L. Wu and J. Tian, Automated gravity gradient tensor inversion for underwater object detection, Journal of Geophysics and Engineering **7**, 410 (2010).

[9] L. Boyle and U.-L. Pen, Pulsar timing arrays as imaging gravitational wave telescopes: Angular resolution and source (de)confusion, Phys. Rev. D **86**, 124028 (2012), arXiv:1010.4337.

[10] C. García-Cely and A. Ringwald, Complete gravitational-wave spectrum of the Sun, Physical Review Letters **135**, 061001 (2025), arXiv:2407.18297.

[11] A. M. Steane, Gravitational bremsstrahlung in plasmas and clusters, Physical Review D **109**, 063032 (2024), arXiv:2309.06972.

[12] D. A. Nichols *et al.*, Visualizing spacetime curvature via frame-drag vortexes and tidal tendexes: General theory and weak-gravity applications, Physical Review D **84**, 124014 (2011), arXiv:1108.5486.

[13] L. F. O. Costa, L. Wylleman, and J. Natário, Gravitomagnetism and the significance of the curvature scalar invariants, Phys. Rev. D **104**, 084081 (2021), arXiv:1603.03143.

[14] R. Maartens and B. A. Bassett, Gravito-electromagnetism, Class. Quantum Grav. **15**, 705 (1998), arXiv:gr-qc/9704059.

[15] Y. N. Obukhov and D. Puetzfeld, Measuring the gravitational field in General Relativity: From deviation equations and the gravitational compass to relativistic clock gradiometry, in *Relativistic Geodesy: Foundations and Applications*, Fundam. Theor. Phys., Vol. 196, edited by D. Puetzfeld and C. Lämmerzahl (Springer, Cham, 2019) pp. 87–130, arXiv:1811.10474.

[16] S. M. Merkowitz and W. W. Johnson, Spherical gravitational wave antennas and the truncated icosahedral arrangement, Phys. Rev. D **51**, 2546 (1995).

[17] P. Bruno, Majorana's stellar representation for the local polarization of harmonic electromagnetic and gravitational waves (2019), arXiv:1903.08166 [physics.class-ph].

[18] F. A. E. Pirani, On the physical significance of the Riemann tensor, Acta Phys. Polon. **15**, 389 (1956), reprinted in Gen. Relativ. Gravit. **41**, 1215 (2009).

[19] P. Szekeres, The gravitational compass, J. Math. Phys. **6**, 1387 (1965).

[20] R. L. Forward, Multidirectional, multipolarization antennas for scalar and tensor gravitational radiation, Gen. Relativ. Gravit. **2**, 149 (1971).

[21] R. V. Wagoner and H. J. Paik, in *Experimental Gravitation: Proceedings of the International Symposium, Pavia, 1976* (Accademia Nazionale dei Lincei, Rome, 1977) p. 257.

[22] H. J. Paik, C. E. Griggs, M. V. Moody, K. Venkateswara, *et al.*, Low-frequency terrestrial tensor gravitational-wave detector, Classical and Quantum Gravity **33**, 075003 (2016).

[23] M. V. Moody, H. J. Paik, and E. R. Canavan, Three-axis superconducting gravity gradiometer for sensitive gravity experiments, Rev. Sci. Instrum. **73**, 3957 (2002).

[24] R. Rummel, W. Yi, and C. Stummer, GOCE gravitational gradiometry, J. Geod. **85**, 777 (2011).

[25] V. B. Braginsky, C. M. Caves, and K. S. Thorne, Laboratory experiments to test relativistic gravity, Phys. Rev. D **15**, 2047 (1977).

[26] B. Mashhoon, H. J. Paik, and C. M. Will, Detection of the gravitomagnetic field using an orbiting superconducting gravity gradiometer. Theoretical principles,

Result	Section	Module	Tests
The tidal field of a scene and its trace inside matter	II	`tidal`	`test_tidal`
The magnetic part of moving and spinning bodies; the current column	IV	`gravitomagnetic`, `currents`	`test_gravitomagnetic`, `test_currents`
Same outside, different inside; the Earth from outside; silent flows; the shear zeros of a buried pair	IV	`nullspace`	`test_nullspace`, `test_silent_flows`
The thermal tremor, the sum rule, the thermometer, the jitter bounds	IV, A	`response`	`test_response`
The resolution law and Table II	IV	`resolution`	`test_resolution`
The information in a near-field image	IV	`capacity`	`test_capacity`
The worked inversion, with and without positivity	IV, A	`inversion`	`test_inversion`
A rotor's waves, their power and polarization; a source larger than its wave	V	`waves`, `wavezone`	`test_waves`, `test_wavezone`
Absorption, emission and the graviton budgets	VI, IX	`emission`	`test_emission`
The friction and glow of materials, Table III; the bound on the glow	VI	`materials`, `glowbounds`	`test_materials`, `test_glow_skies`
The bound on optics; surface and volume glow; a black hole as a lens	VI, VII	`optics`, `lens`	`test_optics`, `test_lens`
One pixel: the square, the types, the principal null directions, the pixel's own velocity, the separation of waves, the sky's numbers, ranging	VIII	`pixel`, `onepixel`, `identify`	`test_pixel`, `test_one_pixel`, `test_identify`, `test_single_pixel_bandlimit`
The absence of aberration; other theories of gravity	VIII	`present`, `beyond`	`test_present`, `test_beyond`
Separation and depth with noise	VIII, A	`separation_noise`	`test_separation_noise`
The thermal Earth and its inversion	IX	`abel`	`test_abel`
A pair of black holes; memory; the Sun as a lens	XI	`binary`, `memory`, `sunlens`, `sunwave`	`test_binary`, `test_memory_sunlens`, `test_sunwave`
The Milky Way, the primordial background, a black hole and its modes	XI	`galaxy`, `primordial`, `schwarzschild`, `bhmodes`, `skies`	`test_vistas`, `test_bhmodes`, `test_glow_skies`
Hair: the field at two times, the count of bits, a black hole's friction and tremor, pushing and weighing, what gravity cannot decohere	XII	`hair`, `bhmodes`	`test_hair`
The interactive version's images against the reference	IX	`export_fixtures`	`test_fixtures`, and its own tests

TABLE IX. Where each result is checked. Modules are files of `reference/gravcam`, tests are files of `reference/tests`; the name of each test says what it checks.

Phys. Rev. D **39**, 2825 (1989).

[27] J. Frauendiener, Gravitational waves and the Sagnac effect, Class. Quantum Grav. **37**, 05LT01 (2020), arXiv:1808.08653.

[28] D. Baskaran and L. P. Grishchuk, Components of the gravitational force in the field of a gravitational wave, Class. Quantum Grav. **21**, 4041 (2004), arXiv:gr-qc/0309058.

[29] U. Yurtsever, C. Marzban, and M. Meila, On the gravitational inverse problem (2010), arXiv:1004.4939 [math-ph].

[30] V. Isakov, *Inverse Source Problems*, Mathematical Surveys and Monographs, Vol. 34 (American Mathematical Society, Providence, RI, 1990).

[31] A. M. Dziewonski and D. L. Anderson, Preliminary reference Earth model, Phys. Earth Planet. Inter. **25**, 297 (1981).

[32] A. P. Calderón, On an inverse boundary value problem, Comput. Appl. Math. **25**, 133 (2006), reprint of the 1980 original in *Seminar on Numerical Analysis and its Applications to Continuum Physics* (Soc. Brasil. Mat., Rio de Janeiro).

[33] A. J. Devaney, The inverse problem for random sources, J. Math. Phys. **20**, 1687 (1979).

[34] R. L. Weaver and O. I. Lobkis, Ultrasonics without a source: thermal fluctuation correlations at MHz frequen-

cies, Phys. Rev. Lett. **87**, 134301 (2001).
[35] H. B. Callen and T. A. Welton, Irreversibility and generalized noise, Phys. Rev. **83**, 34 (1951).
[36] E. Lipparini and S. Stringari, Sum rules and giant resonances in nuclei, Phys. Rep. **175**, 103 (1989).
[37] A. E. H. Love, The yielding of the earth to disturbing forces, Proc. R. Soc. Lond. A **82**, 73 (1909).
[38] Y. Levin, Internal thermal noise in the LIGO test masses: A direct approach, Phys. Rev. D **57**, 659 (1998), arXiv:gr-qc/9707013.
[39] G. K. C. Clarke, Optimum second-derivative and downward-continuation filters, Geophysics **34**, 424 (1969).
[40] R. L. Parker, The rapid calculation of potential anomalies, Geophys. J. R. Astron. Soc. **31**, 447 (1973).
[41] J. D. Maynard, E. G. Williams, and Y. Lee, Nearfield acoustic holography: I. Theory of generalized holography and the development of NAH, J. Acoust. Soc. Am. **78**, 1395 (1985).
[42] J. M. Brockmann, T. Schubert, and W.-D. Schuh, An improved model of the Earth's static gravity field solely derived from reprocessed GOCE data, Surv. Geophys. **42**, 277 (2021).
[43] A. Kvas, J. M. Brockmann, S. Krauss, T. Schubert, T. Gruber, U. Meyer, T. Mayer-Gürr, W.-D. Schuh, A. Jäggi, and R. Pail, GOCO06s – a satellite-only global gravity field model, Earth Syst. Sci. Data **13**, 99 (2021).
[44] D. L. Donoho, Superresolution via sparsity constraints, SIAM J. Math. Anal. **23**, 1309 (1992).
[45] E. J. Candès and C. Fernandez-Granda, Towards a mathematical theory of super-resolution, Commun. Pure Appl. Math. **67**, 906 (2014), arXiv:1203.5871.
[46] A. Belenchia, R. M. Wald, F. Giacomini, E. Castro-Ruiz, Č. Brukner, and M. Aspelmeyer, Quantum superposition of massive objects and the quantization of gravity, Phys. Rev. D **98**, 126009 (2018), arXiv:1807.07015.
[47] D. L. Danielson, G. Satishchandran, and R. M. Wald, Gravitationally mediated entanglement: Newtonian field versus gravitons, Phys. Rev. D **105**, 086001 (2022), arXiv:2112.10798.
[48] C. E. Shannon, A mathematical theory of communication, Bell System Technical Journal **27**, 379 (1948).
[49] S. W. Hawking, Perturbations of an expanding universe, Astrophysical Journal **145**, 544 (1966).
[50] J. Ghiglieri and M. Laine, Gravitational wave background from standard model physics: qualitative features, Journal of Cosmology and Astroparticle Physics **2015** (07), 022, arXiv:1504.02569.
[51] R. C. Tolman, On the weight of heat and thermal equilibrium in general relativity, Phys. Rev. **35**, 904 (1930).
[52] G. Baym, S. P. Patil, and C. J. Pethick, Damping of gravitational waves by matter, Phys. Rev. D **96**, 084033 (2017), arXiv:1707.05192.
[53] Y. N. Srivastava, A. Widom, and G. Pizzella, Electronic enhancements in the detection of gravitational waves by metallic antennae (2003), arXiv:gr-qc/0302024 [gr-qc].
[54] T. Hirayama, Empirical formulae of electrical and thermal conductivities of elemental metals at room temperature ranges (2011), arXiv:1108.6141 [cond-mat.mtrl-sci].
[55] D. S. P. Tanner, C. A. Broderick, A. C. Kirwan, S. Schulz, and E. P. O'Reilly, Fully analytic valence force fields for the relaxation of group-IV semiconductor alloys: elastic properties of group-IV materials calculated from first principles (2021), arXiv:2110.11888 [cond-mat.mtrl-sci].
[56] Y. Kahn, J. Schütte-Engel, and T. Trickle, Searching for high-frequency gravitational waves with phonons, Phys. Rev. D **109**, 096023 (2024), arXiv:2311.17147.
[57] A. Lemaître and C. Maloney, Sum rules for the quasi-static and visco-elastic response of disordered solids at zero temperature, J. Stat. Phys. **123**, 415 (2006), arXiv:cond-mat/0410592.
[58] T. Damart, A. Tanguy, and D. Rodney, Theory of harmonic dissipation in disordered solids, Phys. Rev. B **95**, 054203 (2017), arXiv:1611.06041.
[59] F. Léonforte, A. Tanguy, J. P. Wittmer, and J.-L. Barrat, Inhomogeneous elastic response of silica glass, Phys. Rev. Lett. **97**, 055501 (2006), arXiv:cond-mat/0605380.
[60] J. C. F. Schulz, A. Schlaich, M. Heyden, R. R. Netz, and J. Kappler, Molecular interpretation of the non-Newtonian viscoelastic behavior of liquid water at high frequencies, Phys. Rev. Fluids **5**, 103301 (2020), arXiv:2003.08309.
[61] P. Duthil, Material properties at low temperature, in *CAS–CERN Accelerator School: Superconductivity for accelerators*, CERN Yellow Report CERN-2014-005 (CERN, Geneva, 2014) pp. 77–95, arXiv:1501.07100.
[62] S. Lim, Y. Kim, G. Maeng, and Y. Lee, Validation of constant mean free path and relaxation time approximations for metal resistivity: explicit treatment of electron–phonon interactions, J. Phys.: Condens. Matter **38**, 015503 (2026), arXiv:2603.06146.
[63] X. Sha and R. E. Cohen, First-principles studies of electrical resistivity of iron under pressure, J. Phys.: Condens. Matter **23**, 075401 (2011), arXiv:1007.3423.
[64] J. Camassel, L. A. Falkovsky, and N. Planes, Strain effect in silicon-on-insulator materials: Investigation with optical phonons, Phys. Rev. B **63**, 035309 (2000), arXiv:cond-mat/0009459.
[65] G. Stoikos and E. Granados, Influence of phonon harmonicity on spectrally pure resonant Stokes fields, Phys. Rev. A **106**, 023504 (2022), arXiv:2204.11255.
[66] C. W. Misner, K. S. Thorne, and J. A. Wheeler, *Gravitation* (W. H. Freeman, San Francisco, 1973).
[67] G. Schäfer and H. Dehnen, Gravitational radiation by the thermal phonons of a solid, Physical Review D **23**, 2129 (1981).
[68] G. Schäfer and H. Dehnen, Erratum: Gravitational radiation by the thermal phonons of a solid, Phys. Rev. D **24**, 3352 (1981), erratum to Phys. Rev. D 23, 2129 (1981), doi:10.1103/PhysRevD.23.2129.
[69] H. Dehnen, F. Romero, and G. Schäfer, Gravitational radiation of an isotropic elastic sphere, Classical and Quantum Gravity **1**, 305 (1984).
[70] F. J. Dyson, Seismic response of the Earth to a gravitational wave in the 1-Hz band, Astrophys. J. **156**, 529 (1969).
[71] P. C. Peters, Index of refraction for scalar, electromagnetic, and gravitational waves in weak gravitational fields, Physical Review D **9**, 2207 (1974).
[72] W. H. Press, On gravitational conductors, waveguides, and circuits, Gen. Relativ. Gravit. **11**, 105 (1979).
[73] R. Flauger and S. Weinberg, Gravitational waves in cold dark matter, Phys. Rev. D **97**, 123506 (2018), arXiv:1801.00386.
[74] L. Smolin, The thermodynamics of gravitational radiation, Gen. Relativ. Gravit. **16**, 205 (1984).
[75] L. Smolin, On the intrinsic entropy of the gravitational field, Gen. Relativ. Gravit. **17**, 417 (1985).

[76] A. Loeb, Upper limit on the dissipation of gravitational waves in gravitationally bound systems, Astrophys. J. Lett. **890**, L16 (2020), arXiv:2001.01730.

[77] B. Patla and R. J. Nemiroff, Gravitational lensing characteristics of the transparent Sun, Astrophys. J. **685**, 1297 (2008), arXiv:0711.4811.

[78] B. McKernan, K. E. S. Ford, B. Kocsis, and Z. Haiman, Stars as resonant absorbers of gravitational waves, Mon. Not. R. Astron. Soc. **445**, L74 (2014), arXiv:1405.1414.

[79] S. A. Teukolsky and W. H. Press, Perturbations of a rotating black hole. III. Interaction of the hole with gravitational and electromagnetic radiation, Astrophys. J. **193**, 443 (1974).

[80] J. B. Pendry, Negative refraction makes a perfect lens, Physical Review Letters **85**, 3966 (2000).

[81] A. Z. Petrov, The classification of spaces defining gravitational fields, General Relativity and Gravitation **32**, 1665 (2000), translation of the 1954 original.

[82] R. Penrose, A spinor approach to general relativity, Annals of Physics **10**, 171 (1960).

[83] R. P. Kerr, Gravitational field of a spinning mass as an example of algebraically special metrics, Physical Review Letters **11**, 237 (1963).

[84] J. J. Sylvester, On a remarkable discovery in the theory of canonical forms and of hyperdeterminants, The London, Edinburgh, and Dublin Philosophical Magazine and Journal of Science 4, **2**, 391 (1851).

[85] S. Kunis, T. Peter, T. Römer, and U. von der Ohe, A multivariate generalization of Prony's method, Linear Algebra Appl. **490**, 31 (2016), arXiv:1506.00450.

[86] A. Nehorai and E. Paldi, Vector-sensor array processing for electromagnetic source localization, IEEE Transactions on Signal Processing **42**, 376 (1994).

[87] B. Hochwald and A. Nehorai, Identifiability in array processing models with vector-sensor applications, IEEE Transactions on Signal Processing **44**, 83 (1996).

[88] B. Allen and A. C. Ottewill, Detection of anisotropies in the gravitational-wave stochastic background, Phys. Rev. D **56**, 545 (1997), arXiv:gr-qc/9607068.

[89] N. Seto and A. Cooray, LISA measurement of gravitational wave background anisotropy: Hexadecapole moment via a correlation analysis, Phys. Rev. D **70**, 123005 (2004), arXiv:astro-ph/0403259.

[90] N. Seto and A. Taruya, Measuring a parity-violation signature in the early universe via ground-based laser interferometers, Physical Review Letters **99**, 121101 (2007).

[91] O. Giraud, P. Braun, and D. Braun, Classicality of spin states, Phys. Rev. A **78**, 042112 (2008), arXiv:0805.2592.

[92] P. Delsarte, J. M. Goethals, and J. J. Seidel, Spherical codes and designs, Geometriae Dedicata **6**, 363 (1977).

[93] R. K. Sachs, Gravitational waves in general relativity VIII. Waves in asymptotically flat space-time, Proceedings of the Royal Society of London A **270**, 103 (1962).

[94] S. Carlip, Aberration and the speed of gravity, Physics Letters A **267**, 81 (2000).

[95] D. M. Eardley, D. L. Lee, and A. P. Lightman, Gravitational-wave observations as a tool for testing relativistic gravity, Physical Review D **8**, 3308 (1973).

[96] M. Fierz and W. Pauli, On relativistic wave equations for particles of arbitrary spin in an electromagnetic field, Proceedings of the Royal Society of London A **173**, 211 (1939).

[97] J. Harms, Terrestrial gravity fluctuations, Living Rev. Relativ. **22**, 6 (2019).

[98] W. Chaibi *et al.*, Low frequency gravitational wave detection with ground-based atom interferometer arrays, Physical Review D **93**, 021101 (2016), arXiv:1601.00417.

[99] Y. Inoue *et al.*, Improving the absolute accuracy of the gravitational wave detectors by combining the photon pressure and gravity field calibrators, Physical Review D **98**, 022005 (2018), arXiv:1804.08249.

[100] M. P. Ross *et al.*, Initial results from the LIGO Newtonian calibrator, Physical Review D **104**, 082006 (2021), arXiv:2107.00141.

[101] D. T. Thompson, EULDPH: A new technique for making computer-assisted depth estimates from magnetic data, Geophysics **47**, 31 (1982).

[102] A. B. Reid, J. M. Allsop, H. Granser, A. J. Millett, and I. W. Somerton, Magnetic interpretation in three dimensions using Euler deconvolution, Geophysics **55**, 80 (1990).

[103] S. Weinberg, Infrared photons and gravitons, Phys. Rev. **140**, B516 (1965).

[104] C. J. Dasch, One-dimensional tomography: a comparison of Abel, onion-peeling, and filtered backprojection methods, Applied Optics **31**, 1146 (1992).

[105] M. Pozzo, C. Davies, D. Gubbins, and D. Alfè, Thermal and electrical conductivity of iron at Earth's core conditions, Nature **485**, 355 (2012).

[106] F. J. Dyson, Is a graviton detectable?, Int. J. Mod. Phys. A **28**, 1330041 (2013).

[107] T. Rothman and S. Boughn, Can gravitons be detected?, Found. Phys. **36**, 1801 (2006), arXiv:gr-qc/0601043.

[108] C. M. Caves, Quantum limits on noise in linear amplifiers, Phys. Rev. D **26**, 1817 (1982).

[109] M. Tsang, Quantum nonlocality in weak-thermal-light interferometry, Phys. Rev. Lett. **107**, 270402 (2011), arXiv:1108.1829.

[110] D. Carney, V. Domcke, and N. L. Rodd, Graviton detection and the quantization of gravity, Phys. Rev. D **109**, 044009 (2024), arXiv:2308.12988.

[111] D. Gottesman, T. Jennewein, and S. Croke, Longer-baseline telescopes using quantum repeaters, Phys. Rev. Lett. **109**, 070503 (2012), arXiv:1107.2939.

[112] F. T. Arecchi, E. Courtens, R. Gilmore, and H. Thomas, Atomic coherent states in quantum optics, Phys. Rev. A **6**, 2211 (1972).

[113] R. C. Tolman, P. Ehrenfest, and B. Podolsky, On the gravitational field produced by light, Physical Review **37**, 602 (1931).

[114] K. S. Thorne, Multipole expansions of gravitational radiation, Reviews of Modern Physics **52**, 299 (1980).

[115] S. A. Teukolsky, Linearized quadrupole waves in general relativity and the motion of test particles, Physical Review D **26**, 745 (1982).

[116] Y. B. Zel'dovich and A. G. Polnarev, Radiation of gravitational waves by a cluster of superdense stars, Sov. Astron. **18**, 17 (1974), [Astron. Zh. 51, 30 (1974)].

[117] D. Christodoulou, Nonlinear nature of gravitation and gravitational-wave experiments, Phys. Rev. Lett. **67**, 1486 (1991).

[118] K. S. Thorne, Gravitational-wave bursts with memory: The Christodoulou effect, Physical Review D **45**, 520 (1992).

[119] R. Epstein, The generation of gravitational radiation by escaping supernova neutrinos, The Astrophysical Journal **223**, 1037 (1978).

[120] A. G. Wiseman and C. M. Will, Christodoulou's nonlinear gravitational-wave memory: Evaluation in the quadrupole approximation, Physical Review D **44**, R2945 (1991).

[121] M. Favata, Nonlinear gravitational-wave memory from binary black hole mergers, The Astrophysical Journal Letters **696**, L159 (2009).

[122] S. Pasterski, A. Strominger, and A. Zhiboedov, New gravitational memories, J. High Energy Phys. **2016** (12), 053, arXiv:1502.06120.

[123] D. A. Nichols, Spin memory effect for compact binaries in the post-Newtonian approximation, Phys. Rev. D **95**, 084048 (2017), arXiv:1702.03300.

[124] P. C. Vaidya, The gravitational field of a radiating star, Proceedings of the Indian Academy of Sciences, Section A **33**, 264 (1951).

[125] M. S. Turner, Gravitational radiation from supernova neutrino bursts, Nature **274**, 565 (1978).

[126] G. Nelemans, L. R. Yungelson, and S. F. Portegies Zwart, The gravitational wave signal from the galactic disk population of binaries containing two compact objects, Astronomy & Astrophysics **375**, 890 (2001).

[127] J. Bland-Hawthorn and O. Gerhard, The galaxy in context: Structural, kinematic, and integrated properties, Annual Review of Astronomy and Astrophysics **54**, 529 (2016).

[128] T. K. Fritz, S. Gillessen, K. Dodds-Eden, D. Lutz, R. Genzel, W. Raab, T. Ott, O. Pfuhl, F. Eisenhauer, and F. Yusef-Zadeh, Line derived infrared extinction toward the Galactic Center, Astrophys. J. **737**, 73 (2011).

[129] E. W. Kolb and M. S. Turner, *The Early Universe* (Addison-Wesley, Redwood City, 1990).

[130] D. J. Fixsen, The temperature of the cosmic microwave background, The Astrophysical Journal **707**, 916 (2009).

[131] S. Vagnozzi and A. Loeb, The challenge of ruling out inflation via the primordial graviton background, The Astrophysical Journal Letters **939**, L22 (2022).

[132] G. Agazie *et al.*, The NANOGrav 15 yr data set: Evidence for a gravitational-wave background, The Astrophysical Journal Letters **951**, L8 (2023).

[133] Planck Collaboration, Planck 2018 results. I. Overview and the cosmological legacy of Planck, Astronomy & Astrophysics **641**, A1 (2020).

[134] V. Alba and J. Maldacena, Primordial gravity wave background anisotropies, J. High Energy Phys. **2016** (03), 115, arXiv:1512.01531.

[135] N. Bartolo, D. Bertacca, S. Matarrese, M. Peloso, A. Ricciardone, A. Riotto, and G. Tasinato, Anisotropies and non-Gaussianity of the cosmological gravitational wave background, Physical Review D **100**, 121501 (2019).

[136] C. G. Darwin, The gravity field of a particle, Proceedings of the Royal Society of London A **249**, 180 (1959).

[137] J. L. Synge, The escape of photons from gravitationally intense stars, Monthly Notices of the Royal Astronomical Society **131**, 463 (1966).

[138] J.-P. Luminet, Image of a spherical black hole with thin accretion disk, Astronomy & Astrophysics **75**, 228 (1979).

[139] D. N. Page, Particle emission rates from a black hole: Massless particles from an uncharged, nonrotating hole, Phys. Rev. D **13**, 198 (1976).

[140] P. C. Aichelburg and R. U. Sexl, On the gravitational field of a massless particle, Gen. Relativ. Gravit. **2**, 303 (1971).

[141] L. P. Grishchuk and Y. V. Sidorov, Squeezed quantum states of relic gravitons and primordial density fluctuations, Phys. Rev. D **42**, 3413 (1990).

[142] S. Kanno and J. Soda, Detecting nonclassical primordial gravitational waves with Hanbury-Brown–Twiss interferometry, Phys. Rev. D **99**, 084010 (2019), arXiv:1810.07604.

[143] A. Vilenkin, Gravitational field of vacuum domain walls and strings, Phys. Rev. D **23**, 852 (1981).

[144] N. Kaiser and A. Stebbins, Microwave anisotropy due to cosmic strings, Nature **310**, 391 (1984).

[145] P. C. Peters, Differential cross sections for weak-field gravitational scattering, Phys. Rev. D **13**, 775 (1976).

[146] B. S. DeWitt and R. W. Brehme, Radiation damping in a gravitational field, Ann. Phys. **9**, 220 (1960).

[147] L. Blanchet and T. Damour, Hereditary effects in gravitational radiation, Phys. Rev. D **46**, 4304 (1992).

[148] W. Donnelly and S. B. Giddings, How is quantum information localized in gravity?, Phys. Rev. D **96**, 086013 (2017), arXiv:1706.03104.

[149] J. Corvino and R. M. Schoen, On the asymptotics for the vacuum Einstein constraint equations, J. Differential Geom. **73**, 185 (2006), arXiv:gr-qc/0301071.

[150] G. Alessandrini, Stable determination of conductivity by boundary measurements, Appl. Anal. **27**, 153 (1988).

[151] N. Mandache, Exponential instability in an inverse problem for the Schrödinger equation, Inverse Probl. **17**, 1435 (2001).

[152] R. O. Hansen, Multipole moments of stationary spacetimes, J. Math. Phys. **15**, 46 (1974).

[153] K. Yagi and N. Yunes, I-Love-Q: unexpected universal relations for neutron stars and quark stars, Science **341**, 365 (2013).

[154] T. Binnington and E. Poisson, Relativistic theory of tidal Love numbers, Phys. Rev. D **80**, 084018 (2009), arXiv:0906.1366.

[155] T. Damour and A. Nagar, Relativistic tidal properties of neutron stars, Phys. Rev. D **80**, 084035 (2009), arXiv:0906.0096.

[156] P. Charalambous, S. Dubovsky, and M. M. Ivanov, On the vanishing of Love numbers for Kerr black holes, J. High Energy Phys. **2021** (05), 038, arXiv:2102.08917.

[157] E. Poisson, Absorption of mass and angular momentum by a black hole: time-domain formalisms for gravitational perturbations, and the small-hole/slow-motion approximation, Phys. Rev. D **70**, 084044 (2004), arXiv:gr-qc/0407050.

[158] W. D. Goldberger and I. Z. Rothstein, Dissipative effects in the worldline approach to black hole dynamics, Phys. Rev. D **73**, 104030 (2006), arXiv:hep-th/0511133.

[159] W. D. Goldberger and I. Z. Rothstein, Virtual Hawking radiation, Phys. Rev. Lett. **125**, 211301 (2020), arXiv:2007.00726.

[160] L. Diósi, A universal master equation for the gravitational violation of quantum mechanics, Phys. Lett. A **120**, 377 (1987).

[161] R. Penrose, On gravity's role in quantum state reduction, Gen. Relativ. Gravit. **28**, 581 (1996).

[162] S. Donadi, K. Piscicchia, C. Curceanu, L. Diósi, M. Laubenstein, and A. Bassi, Underground test of gravity-related wave function collapse, Nature Phys. **17**, 74 (2021), arXiv:2111.13490.

[163] I. Allali and M. P. Hertzberg, Gravitational decoherence of dark matter, J. Cosmol. Astropart. Phys. **2020** (07),

056, arXiv:2005.12287.

[164] D. Marolf, Unitarity and holography in gravitational physics, Phys. Rev. D **79**, 044010 (2009), arXiv:0808.2842.

[165] A. Laddha, S. G. Prabhu, S. Raju, and P. Shrivastava, The holographic nature of null infinity, SciPost Phys. **10**, 041 (2021), arXiv:2002.02448.

[166] C. Chowdhury, O. Papadoulaki, and S. Raju, A physical protocol for observers near the boundary to obtain bulk information in quantum gravity, SciPost Phys. **10**, 106 (2021), arXiv:2008.01740.

[167] X. Calmet, R. Casadio, S. D. H. Hsu, and F. Kuipers, Quantum hair from gravity, Phys. Rev. Lett. **128**, 111301 (2022), arXiv:2110.09386.

[168] D. N. Page, Particle emission rates from a black hole. II. Massless particles from a rotating hole, Phys. Rev. D **14**, 3260 (1976).